

Electronic Thesis and Dissertation Repository

8-4-2022 12:30 PM

Co-gasification of Plastic and Biomass Waste

Joshua J. Cullen, *The University of Western Ontario*

Supervisor: Klinghoffer, Naomi, *The University of Western Ontario*

A thesis submitted in partial fulfillment of the requirements for the Master of Engineering
Science degree in Chemical and Biochemical Engineering

© Joshua J. Cullen 2022

Follow this and additional works at: <https://ir.lib.uwo.ca/etd>

Recommended Citation

Cullen, Joshua J., "Co-gasification of Plastic and Biomass Waste" (2022). *Electronic Thesis and Dissertation Repository*. 8842.
<https://ir.lib.uwo.ca/etd/8842>

This Dissertation/Thesis is brought to you for free and open access by Scholarship@Western. It has been accepted for inclusion in Electronic Thesis and Dissertation Repository by an authorized administrator of Scholarship@Western. For more information, please contact wlsadmin@uwo.ca.

Abstract

Gasification technologies have been considered as viable avenues for diverting mixed non-recycled plastic waste landfilling. The main objective of this work was to investigate CO₂ assisted air gasification with mixed plastic and biomass. High-density polyethylene was co-gasified with Douglas fir in different volumes of CO₂ in a semi-batch updraft gasifier. These tests were done in a thermogravimetric analyzer (TGA) to compare the gas, tar and char products of the gasifier with the TGA data. The injection of 10 and 20% CO₂ in air gasification with an air to fuel ratio of 0.3 improved carbon conversion from the tar to the gas phase by 20 and 28 carbon wt% respectively. Injecting CO₂ was an effective moderator for the H₂/CO ratio, beneficial for tar reduction and a key contributor to the energy density of the syngas. From these tests, synergies from the mixed feedstock were identified and discussed for future work.

Keywords

Co-gasification, Air gasification, Thermal Decomposition, Carbon Dioxide Utilization, Carbon Dioxide, Plastics

Summary for Lay Audience

The extensive pollution of mixed plastics in landfilling has garnered considerable attention over the last twenty years and as a result, how to reduce this waste has become a prominent issue. In 2018, the United States alone landfilled 24 million tonnes of plastic waste while only recycling 2.8 million tonnes (8% of all waste plastics) [1]. Alternative approaches to managing non-recycled plastics which would otherwise accumulate in landfills and oceans, need to be researched and developed. Various methods have been investigated to address this problem such as incineration, mechanical, chemical, and thermochemical recycling. The complex composition of these mixed plastic wastes and the consequential environmental effects resulting from some of these proposed solutions have caused greater interest in thermochemical processes such as gasification and pyrolysis. Furthermore, landfilled non-recycled plastics are commonly mixed with biomass residues that decompose into greenhouse gases such as carbon dioxide (CO₂) and methane (CH₄). Therefore, conversion processes that can accept mixed plastic and biomass wastes would be considered as highly advantageous. While gasification technologies are traditionally used for converting biomass feedstocks into fuels with air, there has been some deliberation whether these technologies could be used with mixed waste biomass and plastic feeds in carbon dioxide (CO₂). This work will look to address the possibility of CO₂ assisted air gasification of waste plastics with biomass. This is beneficial because it presents an opportunity to utilize CO₂, plastic and biomass wastes and convert them into valuable products. Gasification is a high temperature process that can address all of these needs, by converting waste streams into adaptable syngas (synthesis gas), mainly comprised of hydrogen and carbon monoxide (H₂ and CO), which can be used for chemical and fuel synthesis. Therefore, the proposed process has the potential to convert plastic, biomass and carbon dioxide waste into valuable fuels and chemicals in a single tunable conversion process. The flexibility of the technology could potentially divert mixed waste plastics from the present archaic waste management infrastructure and carbon dioxide away from current emission pollution.

Acknowledgements

Firstly, this work would not be possible without the support, mentorship, guidance and instruction of my supervisor Dr Naomi Klinghoffer. I would like to wholeheartedly thank her for her patience and encouragement over the last two years. I am beyond appreciative of this opportunity, and the time that she spent helping me develop as an academic and a person.

I would like to give my sincerest gratitude to Dr Kang for his friendship and teachings. I can recall so many occasions, where he went out of his way to help me throughout my time spent at ICFAR. I consider him a true friend and wish him all the best in his future endeavors.

I would also like to take this opportunity to thank professors Dr Berutti and Dr Pjontek for allowing me to work with their students and equipment.

I would like to thank all the people that I had the pleasure of meeting and working with at ICFAR. The work being done around me was inspiring and motivated me to continue with this thesis. I would like to give my special thanks to Islam Elghamrawy and Alex Frainetti,

To my family, words do not describe the endless love that they have provided. I would like to thank my father, mother and brother for the past 23 years of support and inspiration.

Last but not least, I would like to thank my significant other Michaela Richardson. We have worked side by side to complete our graduate degrees. I cannot begin to describe how proud and thankful I am to have her in my life.

Thank you all

Table of Contents

<i>Abstract</i>	<i>i</i>
<i>Keywords</i>	<i>ii</i>
<i>Summary for Lay Audience</i>	<i>iii</i>
<i>Acknowledgements</i>	<i>iv</i>
<i>List of Figures</i>	<i>vii</i>
<i>List of Tables</i>	<i>x</i>
1 Introduction and Literature Review	1
1.1 Research Motivation and Objectives	1
1.1.1 Research Motivations	1
1.1.2 General Introduction	3
1.2 Review of Gasification Technology Literature	5
1.2.1 Background Information	5
1.2.2 Feedstock Characterization	8
1.2.3 Current Technology and Reactor Designs	9
1.2.4 Gasification Chemistry	11
1. Temperature.....	12
2. Residence time	13
3. Catalyst.....	13
4. Gasification Agent	14
1.2.5 Pre/Post Treatment	16
1.2.6 Reported Synergistic Non-linear Trends.....	17
1.2.7 Mechanisms for feedstock synergy.....	21
1.2.8 Value of Current Research and Objectives	22
2 Experimental Methods and Materials	24
2.1 Feedstock Preparation and Characterization	24
2.1.1 Feedstock Selection and Preparation	24
2.1.2 Ultimate Analysis	25
2.1.3 Proximate Analysis	26
2.2 Experimental Setup	27
2.2.1 Thermogravimetric Analysis	27
2.2.2 Micro Fixed Bed Gasifier	28
2.3 Experimental Method	30
2.3.1 Thermogravimetric Analysis	30
2.3.2 Updraft Micro-Gasifier.....	31
2.3.3 CHNSO Analysis.....	32
2.3.4 Micro-Gas Chromatography	32
3 Experimental Results and Discussion	34

3.1	Synergies between blended feedstocks in N₂ and CO₂ environments.....	34
3.1.1	<i>Experimental Plan</i>	34
3.1.2	<i>Temperature Phases and Mass Loss</i>	34
3.2	Influence of CO₂ injections at Equivalence Ratio of 0.3	39
3.2.1	<i>Experimental Plan</i>	39
3.2.2	<i>Adding CO₂ to Air Gasification (ER=0.3), TGA and Micro-Gasifier Analysis</i>	40
3.2.3	<i>TGA Final Char/ Residue Analysis</i>	42
3.2.4	<i>Fixed Bed Micro Gasifier Gas Composition and Yields</i>	44
3.2.5	<i>Fixed Bed Micro Gasifier Char Composition and Yields</i>	49
3.2.6	<i>Influence of CO₂ in Fixed Bed Micro Gasifier</i>	51
3.3	Influence of CO₂ injection at Equivalence Ratio of 0.2.....	54
3.3.1	<i>Experimental Test Plan.....</i>	54
3.3.2	<i>Adding CO₂ to Air Gasification (ER=0.2), TGA and Micro-Gasifier Analysis</i>	55
3.3.3	<i>TGA Final Char/ Residue Analysis</i>	57
3.3.4	<i>Fixed Bed Micro Gasifier Gas Composition and Yields</i>	58
3.3.5	<i>Fixed Bed Micro Gasifier Char Composition and Yields</i>	63
3.3.6	<i>Influence of CO₂ in Fixed Bed Micro Gasifier</i>	65
4	<i>Conclusions and Recommendations</i>	69
4.1	Conclusions.....	69
4.2	Recommendations.....	70
	<i>References.....</i>	72
5.	<i>Appendices</i>	78
	Appendix A: Supplementary Data Tables and Figures	78
	<i>Curriculum Vitae</i>	84

List of Figures

Figure 1-1: Illustration of plastic waste handling in Canada adapted from [5].....	2
Figure 1-2: Illustration of the co-gasification process adapted from [30]	5
Figure 1-3: Possible mechanisms of CO₂ influence on biomass and plastic pyrolysis/gasification adapted from [32].....	19
Figure 2-1: Collected feedstocks of HDPE (A) and Douglas fir (B)	24
Figure 2-2: Ground and sieved Douglas fir and HDPE.....	25
Figure 2-3: Mass loss graph of Douglas fir (Proximate analysis).....	27
Figure 2-4: Picture of thermogravimetric analyzer setup used, a nearly fully automated system with air cooling, touch screen and blending gas delivery module (GDM).	27
Figure 2-5: Updraft (fixed bed) micro-gasifier diagram	28
Figure 2-6: Main reactor setup of updraft micro-gasifier	29
Figure 3-1 Comparison of individual and mixed feedstock decomposition up to 700°C in N₂ environment.....	35
Figure 3-2: Comparison of individual, mixed and calculated feeds up to 700°C with 20% CO₂ injected	37
Figure 3-3: Comparison of Heating Rates (°C/min) TGA Curves in 20 vol% CO₂ environments	38
Figure 3-4: Mass loss curves of HDPE and Douglas fir (1:1) over temperature in air and CO₂	41
Figure 3-5: Mass loss curves of HDPE and Douglas fir (1:1) over time in air and CO₂	41
Figure 3-6: DTG curves of all TGA runs with air (ER=0.3) and injections of CO₂	42
Figure 3-7: The final char residues recorded after dwell in air gasification with increasing percentages of CO₂ (HDPE and DGFIR mix at 850°C)	43
Figure 3-8: Comparison of final char after ramp to 850°C and after 10-minute dwell at 850°C	43
Figure 3-9: Evolution of hydrogen gas with increasing input flow of CO₂	45
Figure 3-10: Evolution of methane gas with increasing CO₂ input flow	45
Figure 3-11: Evolution of carbon monoxide gas with increasing CO₂ input flow	46
Figure 3-12: Evolution of pentane gas with increasing CO₂ input flow.....	47
Figure 3-13: Evolution of CO₂ gas with increasing CO₂ input flow.....	48

Figure 3-14: Flowrates output of CO₂ gas with increasing input flow of CO₂.....	48
Figure 3-15: Final char mass in MG with increasing input flow of CO₂.....	50
Figure 3-16: Comparison of final char masses in TGA and MG	50
Figure 3-17: Elemental compositions of chars from MG with increasing input flow of CO₂	51
Figure 3-18: Combined energy of syngas at different temperature with increasing input flow of CO₂.....	53
Figure 3-19: Changes in molar hydrogen and carbon monoxide ratio of syngas (H₂/CO)..	53
Figure 3-20: Mass loss curves of HDPE and Douglas fir (1:1) over temperature.....	56
Figure 3-21: Mass loss curves of HDPE and Douglas fir (1:1) over time	56
Figure 3-22: The final char residues recorded in air gasification with increasing percentages of CO₂.....	57
Figure 3-23: Comparison of final char after ramp to 850°C versus after 10-minute dwell.	58
Figure 3-24: Evolution of hydrogen gas with increasing input flow CO₂.....	59
Figure 3-25: Evolution of methane gas with increasing CO₂ input flow	60
Figure 3-26: Evolution of carbon monoxide gas with increasing CO₂ input flow	61
Figure 3-27: Evolution of pentane gas with increasing CO₂ input flow.....	61
Figure 3-28: Evolution of CO₂ gas with increasing CO₂ input flow.....	62
Figure 3-29: Output flow rates of CO₂ gas with increasing injection volume of CO₂.....	63
Figure 3-30: Final char mass in MG with increasing input flow of CO₂.....	64
Figure 3-31: Comparison of final char masses in TGA and MG	65
Figure 3-32: Elemental compositions of chars with increasing input flow of CO₂.....	65
Figure 3-33: Combined energy of syngas at different temperature with increasing input flow of CO₂.....	67
Figure 3-34: Changes in molar hydrogen and carbon monoxide ratio of syngas	68
Figure 5-1: Evolution of gases with air (ER 0.3)	78
Figure 5-2: Evolution of gases with air and 10% CO₂ (ER 0.3)	78
Figure 5-3: Evolution of gases with air and 20% CO₂ (ER 0.3)	79
Figure 5-4: Evolution of gases with air and 40% CO₂ (ER 0.3)	79
Figure 5-5: ER 0.3 carbon conversion chart with CO₂.....	80
Figure 5-6: Evolution of gases with air (ER 0.2)	81

Figure 5-7: Evolution of gases with air and 10% CO₂ (ER 0.2) 81
Figure 5-8: Evolution of gases with air and 20% CO₂ (ER 0.2) 82
Figure 5-9: Evolution of gases with air and 40% CO₂ (ER 0.2) 82
Figure 5-10: ER 0.2 carbon conversion chart with CO₂..... 83

List of Tables

Table 1-1: Comparison of fuels calorific values (MJ/kg), adapted from [35]	7
Table 1-2: Biomass Waste Types adapted from [9]	8
Table 1-3: Breakdown of most notable gasifier configurations adapted from [9]	9
Table 1-4: Primary Gasification Reactions adapted from [13]	12
Table 1-5: Reactions with oxygen adopted from [13]	14
Table 1-6: Reactions influenced by steam adopted from [13]	15
Table 1-7: Reactions influenced by carbon dioxide adopted from [13]	16
Table 2-1: Ultimate Analysis (wt%, dry basis) of HDPE and Douglas fir	25
Table 2-2: Proximate analysis (wt%) of HDPE and Douglas fir	26
Table 2-3: Legend for micro gasifier parts	28
Table 2-4: Example of input flows for tests in ER of 0.3	31
Table 3-1: Conditions for all TGA tests done in this section	34
Table 3-2: Final Mass in TGA of mixed HDPE and DGFIR (50:50) in N₂	35
Table 3-3: Final Mass percentages of heating rate TGA runs	37
Table 3-4: TGA tests with 0.3 ER	39
Table 3-5: Micro-gasifier tests with 0.3 ER	39
Table 3-6: Input flowrates of air (O₂ and N₂) and CO₂ for each MG run	45
Table 3-7: Overall change in CO₂ flow based on input flow	49
Table 3-8: Carbon Balance of MG Gasifier Runs with ER 0.3	52
Table 3-9: Total energy of syngas (CO and H₂) ER 0.3	52
Table 3-10: Conditions for TGA runs for equivalence ratio 0.2	54
Table 3-11: Completed runs in gasifier for equivalence ratio 0.2	55
Table 3-12: Input flowrates of air (O₂ and N₂) and CO₂ for each MG run	59
Table 3-13: Overall change in CO₂ flow based on input flow (ER= 0.2)	63
Table 3-14: Carbon balance of MG runs with ER 0.2	66
Table 3-15: Total energy of syngas (CO and H₂) ER 0.2	67

1 Introduction and Literature Review

1.1 Research Motivation and Objectives

1.1.1 Research Motivations

Over the last century, humanity's energy dependence has propelled technologies that extract and exploit fossil fuel resources to the forefront of industry. Petroleum, natural gas, coal and oil sands are some of the leading examples of non-renewables that have pervaded the global chemical, fuel and energy sectors. Consequently, overconsumption of these resources has raised universal concerns regarding the anthropogenic effects of their by-products. In Canada, 710 mega tonnes of carbon equivalent (Mt CO₂ eq) greenhouse gas emissions (GHG's) were expelled into the atmosphere in 2010, and this value grew annually to 740 Mt of CO₂ eq by 2018 [2]. In 2020, 672 dioxide Mt of CO₂ eq were released, and Ontario accounted for 150 Mt of CO₂ eq [2]. This excessive volume of GHG emissions, especially the largest being CO₂, has led to growing concerns of global climate change [3]. The largest sources of CO₂ emissions were flue gas from fossil fuel combustion powerplants, transportation, and the manufacturing industries [4].

In terms of plastic waste, it was documented in 2016 that out of all plastic waste in Canada, only 9% is recycled annually [5]. 4% is incinerated for energy recovery, leaving 87% of all plastics in Canada ending up in landfills [5]. This equates to 2.8 mega tonnes of plastic landfilled annually. Due to the low degradability of plastics in the environment, this poses as a significant challenge for effective waste management. Figure 1-1 illustrates this breakdown of virgin plastic resins to plastic waste in Canada. In 2018, the Canadian Council of Ministers of the Environment adopted the Canada-wide Strategy on Zero Plastic Waste [6]. The objective outlined in the strategy was to provide a framework for implementing a life cycle and circular economy approach to non-recycled plastics. Phase two of the report outlines key areas of development to achieve this goal, and scientific research was stated as one of the imperative drivers for innovation to diversify traditional energy production and waste management infrastructure [6].

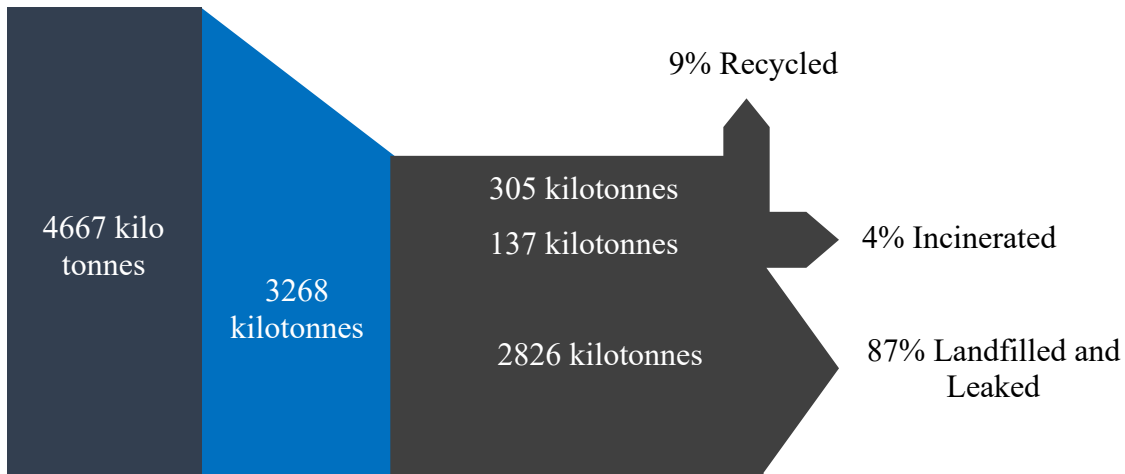


Figure 1-1: Illustration of plastic waste handling in Canada adapted from [5]

The Canadian political climate is shifting to prioritize waste mitigation strategies for diverting plastic waste from landfills. This work aims to address this research need by investigating gasification technology and its flexibility with waste non-recycled plastics and biomass. This work will also look to address the possibility of CO₂ assisted air gasification of waste plastics with biomass. Therefore, if this technology could be used to divert waste plastic, biomass and CO₂ streams into fuels and chemicals, this technology would be considered as a carbon dioxide utilization technology (CDU) and negative emissions technology (NET) [4]. This would not only support a circular economy, but also possibly displace some of the importation of non-renewable raw materials for local and renewable energy and chemicals. If there are markets in the pharmaceutical, chemical, polymer, and automotive industries that CO₂ gasification can disrupt, this would ultimately promote the implementation of carbon capture technologies [7]. [6]

1.1.2 General Introduction

The global emergence of SARS-Cov-2, better known as Covid-19, has led to several serious health and safety concerns. One of these that had developed unknowingly surrounds the buildup of medical, one-time use plastic waste. All around the world, medical and health workers have been using a substantial amount of one time use medical plastics to effectively contain the Covid-19 virus. This includes personal protective equipment (PPE), covid testing packages, hand sanitizer bottles and other goods [8]. This has also led to an enormous increase in medical plastic waste that requires effective waste treatment. These products cannot be landfilled since they are classified as hazardous biomedical waste. At the beginning of the pandemic, in the Wuhan region of China, the production of hazardous medical plastic waste peaked at 240 tons/day [8]. The infrastructure in place had a capacity 40 tons/day [8]. The waste management infrastructure in place could not handle this increase in medical plastic waste, and therefore needed new means to address this issue [8]. This was a more recent example that highlights the rigidity of landfilling and therefore new flexible waste mitigation strategies are needed.

To reduce the volume of waste sent to landfills, variations of different repurposing methods have become attractive pathways for research [9]. Methods such as incineration, mechanical, chemical and thermochemical recycling are some of the alternatives that have been proposed and investigated. Gasification has been one of the thermochemical methods that has emerged as a potential avenue for diverting fossil fuel energy [4], [10], [11]. It has gained attention in recent years because of its potential as a carbon neutral or even carbon negative solution [4]. In addition, its reducing environment lowers the concentrations of harmful emissions in the producer gas while promoting the formation of syngas [12]. One of the objectives for the application of this technology would be for feedstocks that are heavily mixed and as a result are difficult and costly to separate or recycle mechanically and chemically. If this is the case, there is some potential to reduce the extent of pre-treatment separation units and their associated costs. This would be a substantial advantage for this technology [9].

Gasification provides a pathway for the utilization of waste materials and the production of renewable fuels and chemicals using locally available feedstocks. In addition, there also have been recent studies evaluating the efficiency of gasification technology with carbon dioxide

utilization [10], by using carbon dioxide as a gasification agent [13]–[15]. Therefore, some see this technology as a potential avenue for consuming carbon dioxide through the heterogeneous gasification reactions of the solid and liquid/vapor products [16]. Ultimately, this technology has the potential to not only consume carbon dioxide, but also convert waste into high value fuels and chemicals.

As many plastic waste streams are mixed with other wastes, it would be useful to understand the gasification behaviour of mixed feedstocks. Recently, there has been a surge in research investigating co-gasification for this reason. There has been an increase in the number of research papers that have documented non-linear synergies when investigating co-gasification of mixed feedstocks. There have been reports that co-gasification produces higher gas yields of hydrogen, lower tar and lower char yields compared to the sum of the individual feedstocks [10], [13], [17]–[21]. There has been some research into CO₂ co-gasification and CO₂ assisted air co-gasification [17], [22]–[29]. Most of these investigations have focused on common polyolefins such as high-density polyethylene and therefore will be a focus for this review. In addition, there will be some discussion of the proposed mechanisms for these non-linear synergies with respect to CO₂ as a gasifying agent.

1.2 Review of Gasification Technology Literature

1.2.1 Background Information

Gasification is a thermochemical conversion method where solid carbonaceous feedstocks are partially oxidized into gaseous products. This process operates at high temperatures, mostly between 700-1400°C, with sub-stoichiometric amounts of a gasifying reagent [12]. Co-reactants such as air, enriched oxygen, steam, carbon dioxide or mixtures of these components are introduced in order to thermochemically break down the solid feedstocks into syngas (CO + H₂), and other small hydrocarbons [12]. While the primary product is the gas phase product, [30] gasification technologies generate a distribution of products among different phases (gaseous, liquid and solid). Some of the stored energy is converted into lesser value by-product's such as tars, char, ash, water and other gaseous compounds [9]. Figure 1-2 illustrates a summary of the co-gasification process with plastic and biomass feeds with a co-reactant or gas mixture.

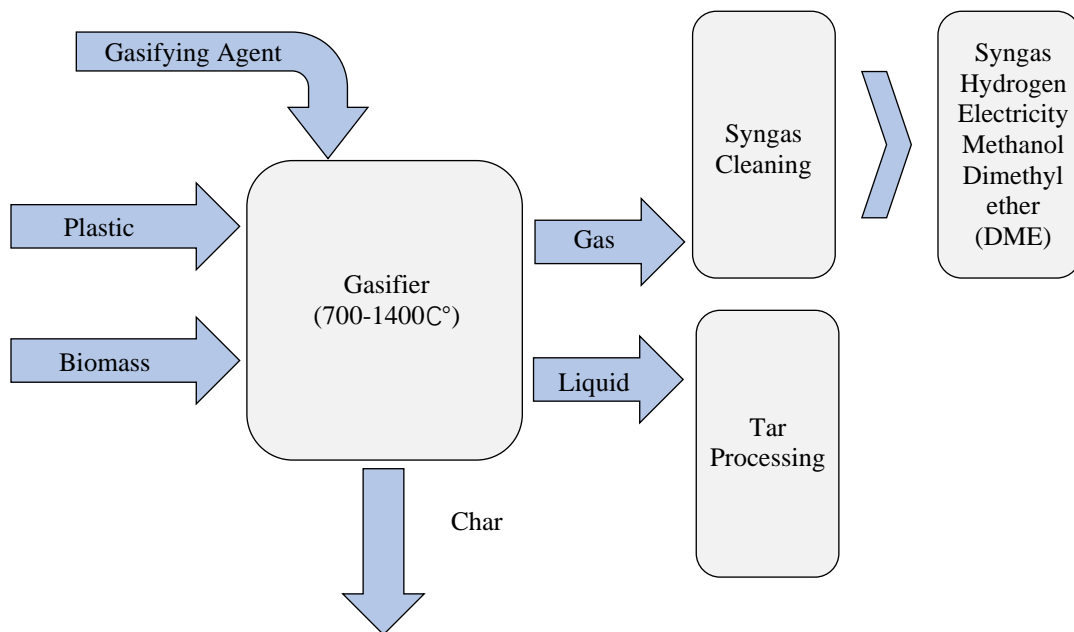


Figure 1-2: Illustration of the co-gasification process adapted from [30]

An alternative approach to valorization of waste is pyrolysis. The difference in the distribution of products between gasification and pyrolysis is caused by the presence of a gaseous secondary reagent such as air, and the fact that pyrolysis takes place at lower temperatures than gasification [31]. For many pyrolysis systems, nitrogen is used as an inert medium to remove gaseous

volatiles during the breakdown of the feed into mainly bio-oils and char [32]. When adding air or steam as a co-reactant, the reactive compound (O_2 , H_2O or CO_2) participates in reforming, cracking and heterogeneous gasification reactions [12]. Therefore, the yield of solid chars and condensable liquid tars is decreased [12], while promoting the formation of higher value gases such as hydrogen, carbon monoxide, methane, and other hydrocarbons [9].

The utility and application of the output gas is dependent on its overall quality, energy content, and composition. Syngas can be utilized in a variety of applications such as for electricity generation, hydrogen production, Fischer-Tropsch liquid fuels and chemicals production, methanol and dimethyl ether (DME) production [4], [10], [12]. It can be characterized by the molar hydrogen to carbon monoxide ratio and the lower heating value (LHV), the minimum available energy for usage [12]. Syngas with a lower LHV and H_2/CO ratio would be used for electricity and power generation, while it has been found that a ratio of H_2/CO over 2 would be suitable for producing ammonia [33]. The flexibility of this technology is of high interest. Depending on a variety of chosen variables such as the reactor design, feedstocks, reactor conditions, catalysts and downstream units, the producer gas could be utilized for the production of many different fuels and chemicals [34]. One challenge that has prevented the commercialization of gasification technologies is the production of low value by-products, which results in a need for downstream treatment to produce high quality syngas. This increases the capital and operating costs and increases complexity of the process [12]. If the syngas is not properly cleaned up, the presence of by-products can reduce the LHV of the output gas and therefore overall energy efficiency of the process [30].

Gasification technologies are traditionally utilized with biomass or coal feedstocks for direct fuel conversion. There has been a considerable amount of research on traditional gasification technologies with biomass and coal feedstocks [20]. Therefore, the technology and market implications are well developed and understood. The most significant drawback of biomass feeds when compared to fossil fuels, is that they have a much lower energy density by mass and volume [9], [15]. To compare, Table 1-1 illustrates the values for plastics, mixed plastics and common fossil fuels. Gasoline, coal, fuel oil and even plastic wastes have energy densities ranging from 30 to 45 MJ/kg [35], while for many biomass feedstocks, the calorific value is

often close to or lower than 20 MJ/kg [36]. One of the proposed solutions has been to mix biomass with other feedstocks such as coal or plastics. Among the studies reviewed, it has been found that there are many operational and process advantages when mixing the feedstocks [9], [11]. Biomass and plastic mixed feeds have been found to address the other's main issues [20].

Table 1-1: Comparison of fuels calorific values (MJ/kg), adapted from [35]

Fuel	Calorific Value (MJ/kg)
Methane	53
Gasoline	46
Fuel Oil	43
Coal	30
Polyethylene	43
Mixed Plastics	30-40
Municipal solid waste	10
Pine Wood	21

In addition to having higher calorific value than biomass, plastic feedstocks can produce higher hydrogen content in the syngas and have higher availabilities at lower costs [11]. Biomass sources are generally much more unreliable for annual operation, because of their seasonality and regionality [9]. Not only does adding plastics into biomass feedstocks increases the overall energy density but it also lowers the overall volume of feed by a significant margin. This ultimately lowers many of the associated costs for pre-treatment stages such as transportation, feed storage and harvesting [9]. Furthermore, there have been many reports of significant operational problems when gasifying plastic without co-feeding other materials [20]. Plastics that can be used for gasification are thermoplastic and therefore have a much higher volatility compared to biomass which has some fixed carbon [20]. They also generally have much lower ash, moisture and oxygen contents as opposed to common biomass sources [11]. Thermoplastics will soften when introduced continuously to higher temperature systems, causing upstream feeding and downstream processing issues [11]. The plastics become viscous and form a melt phase by which they tend to stick to the sides of reactor walls, feeding tubes and downstream units. These have been seen as large black clumps which causing feeding issues and downstream blockages due to clogging. This ultimately requires more downtime for cleaning and maintenance [20]. It has been found that adding biomass to plastic feedstocks greatly reduces or

eliminates the operational clogging by [20] preventing the melt phase from agglomerating [11], [15], [20], [37].

The benefits of mixing these feedstocks are what has garnered a lot of recent interest. It has been observed that co-gasifying mixed plastic and biomass wastes for energy or high value chemicals could be an avenue instead of direct incineration or landfilling. In addition, there is the possibility that this pathway could be a supporting chemical and fuel source, displacing the usage of some fossil fuels. Recently researchers have been investigating whether co-gasification could be applied with other waste feedstocks such as end of life tires, waste sludge and mixed plastic waste [17], [38]–[40].

1.2.2 Feedstock Characterization

Lignocellulosic biomass is comprised of two major constituents, holocellulose (cellulose and hemicellulose) and lignin [41]. Depending on the source, it will also contain inorganic metals and organic extractives (alkali and alkaline earth metals, Na, Al, silica) [42]. Table 1-2 illustrates the types of available biomass feedstocks for co-gasification of biomass wastes with plastics. there have been recent studies which have reported on the synergistic interactions between woody biomass which will be a focus in the evaluation sections of this investigation [17], [20], [43], [44]. Many of these studies used pine wood pellets with plastic feeds. Douglas fir is a sizable softwood species found in Canadian Forests [45]. It will be used as a feedstock of interest in comparison to pine wood.

Table 1-2: Biomass Waste Types adapted from [9]

Biomass Category	Variety and Biological Diversity
Woody Biomass	Pellets, Stems, Branches, Bushes, Leaves, Sawdust, Chips
Agricultural Biomass	Flowers, Straws, Fruits, Stalks, Grasses, Shells, Husks, Pits
Aquatic Biomass	Seaweed, Macroalgae, Lake Weed
Animal Waste	Chicken Litter, Animal manure, Bones
Industrial/Contaminated Waste	Demolition Wood, Refuse Derived Fuel, Sewage Sludge, MSW

Research on co-gasification as an energetic valorization route for mixed plastic waste treatment is currently being investigated at laboratory and pilot plant scale, with some analysis into commercialization [11]. The common thermoplastics found within these streams are polyethylene (PE, high density HDPE, low density LDPE), polypropylene (PP), polystyrene (PS), polyvinyl chloride (PVC) and polyethylene terephthalate (PET). These plastics are used extensively for applications such as packaging and electronics [11]. This review will discuss the conversion of polyethylene with the aforementioned biomasses. PE is of interest because of its advantageous monomer structure (only containing hydrogen and carbon) and its high energy value [9], [11]. Studies with PE were much more common because of these characteristics and its broad usage. This review will discuss the results presented during the conversion of woody biomass with polyethylene in CO₂, as many studies are investigating synergies between similar feedstocks.

1.2.3 Current Technology and Reactor Designs

The most common types of gasification processes are fixed (updraft and downdraft) and fluidized (bubbling and circulating) beds, which are summarized in Table 1-3. Other types of processes which have received less attention include plasma, supercritical water and solar assisted systems [12], [30]. This section will discuss the most common types of gasifiers that are used for mixed plastic and biomass feeds, which are fixed and fluidized beds.

Table 1-3: Breakdown of most notable gasifier configurations adapted from [9]

Gasifier Type	Temperature (°C)	Flows	
		Fuel	Oxidant
Updraft	1000	Downward	Upward
Downdraft		Downward	Downward
Bubbling	800-850	Upward	Upward
Circulating		Upward	Upward

Fixed bed reactors are slow-moving solid beds that can be categorized by the outflow of the producer gas as either updraft or downdraft [12]. The continued use of fixed bed gasifiers comes

from their simple design, easy operation, low investment/ operational costs and small-scale efficiency. However, even with these advantages, they are also challenged due to their poor heat transfer rates, limited solid gas contact times, and lower efficiencies at larger scale [11].

In updraft beds, also known as countercurrent beds, fuel enters from the top of the reactor while the co-reactant is fed from the bottom. Therefore, the flow of the two feeds counter each other, where the solid mixture descends through the uprising gas. As the solid feed falls from the top into the hotter regions at the center of the reactor, it goes through four separate stages, drying, pyrolysis, reduction and oxidation (if oxygen is present) [11]. This is where the feed is dried and then pyrolyzed into non-condensable gases, condensable gases and char [12]. Therefore, as the co-reactant enters the reactor continuously, it initially comes into contact with the hot ash and char that has reacted in the first three stages, ultimately reducing the formation of the final char output further and forming more gaseous products. The producer gas exits from the top [11].

While updraft gasifiers generate gas that exits from the top of the reactor, in downdraft gasifiers, the gas exits from the bottom, in the same direction as the fuel, (co-current) [12]. The downdraft design has the fuel fed from the top of the reactor, however the input gas is commonly fed into the sides of the gasifier. With this design, the formed chars and ash would fall down with the producer gas to the bottom of the reactor [11]. Due to the inherent design of both units, updraft gasifiers generally have an increased tar concentration, while downdraft gasifiers are typically more contaminated with chars and ash [12].

Similarly to fixed beds, there are two traditional variations for fluidized bed gasifiers, bubbling and circulating. These types of reactors are some of the most common for gasification of mixed biomass and plastic waste [9]. They have excellent mixing with good heat and solid-gas contact and therefore generally have higher gas and lower tar yields [12]. For both variations, fuel is fed from into the top of a very high temperature bed of solids which is fluidized by a gasifying agent fed from the bottom. Bubbling fluidized beds (BFB's) can be used with varying feed particle sizes and also provide very high heat transfer rates ensuring lower tar yields in the output gas [9]. CFB's are a unique design where the solids are circulated through a cyclone and back to the main reactor, increasing the char residence time and temperature and therefore char conversion

[12]. In comparison to a BFB, the primary disadvantages with the CFB are the higher investment costs, the need for pre-treatment stages for smaller particle diameters and potential operational issues such as entrainment [11]. BFB's have lower char conversion and therefore reduced gasification efficiency [9].

1.2.4 Gasification Chemistry

Gasification is a complex series of heterogenous reactions that converts a solid fuel to a producer gas [9]. The process can be summarized by four distinguishable major steps, drying, pyrolysis, reduction and oxidation. If no pre-drying is done, the moisture content of the biomass can range from 30 to 60% [46] and therefore would undergo an initial drying stage. Generally, this step takes place between 100-200°C [46]. Drying is followed by initial pyrolysis, also known as devolatilization, where the biomass thermally decomposes into three major components, non-condensable gases, condensable liquids/tars and solid residue [9]. These can also be described as volatile matter (gas/liquids) and char. If air is present in the system, these distributed products will then undergo oxidation. Depending on the ratio of air in the system to the solid feed, the constituents will follow partial or complete oxidize reactions [9]. Finally, the reduction and gasification reactions are the final and slowest steps that take place in the system. This is where the products of pyrolysis react with the co-reactant that is introduced. The major gasification reactions can be found in Table 1-4. The reaction pathways and ultimately the final yields of the products heavily depend on the solid reactant composition and gasifying agent used. In addition to these two factors, there are a variety of other parameters that must be considered.

Table 1-4: Primary Gasification Reactions adapted from [13]

Reaction Number	Reaction Name	Reaction	ΔH (MJ/kmol)
R1	Drying	$H_2O_{(l)} \leftrightarrow H_2O_{(g)}$	
R2	Partial Oxidation	$C + 1/2 O_2 \leftrightarrow CO$	-111
R3	CO Oxidation	$CO + 1/2 O_2 \leftrightarrow CO_2$	-283
R4	Carbon Oxidation	$C + O_2 \leftrightarrow CO_2$	-394
R5	Hydrogen Oxidation	$H_2 + 1/2 O_2 \leftrightarrow H_2O$	-242
R6	Water Gas	$C + H_2O \leftrightarrow CO + H_2$	131
R7	Water Gas shift	$CO + H_2O \leftrightarrow CO_2 + H_2$	-41
R8	Methane Steam Reforming	$CH_4 + H_2O \leftrightarrow CO + 3H_2$	206
R9	Steam Reforming	$C_nH_m + n H_2O \leftrightarrow nCO + (n+m/2) H_2$	Endo
R10	Hydrogasification	$C + 2H_2 \leftrightarrow CH_4$	-75
R11	Boudouard	$C + CO_2 \leftrightarrow 2CO$	172
R12	Dry Reforming	$C_nH_m + nCO_2 \leftrightarrow 2n CO + m/2 H_2$	Endo
R13	Methane Dry Reforming	$CH_4 + CO_2 \leftrightarrow 2 CO + 2 H_2$	247

Many parameters have a strong influence on the producer gas yield, gas quality, final tar formation and overall carbon conversion. It is imperative to understand the influence of these parameters to maximize the gasification efficiency. In this section, the influence of temperature, residence time, catalyst/bed materials and gasification agents will be discussed. These evaluations will be supported with studies investigating the interactions between biomasses and thermoplastics.

1. Temperature

The gasification temperature is one of the most important and influential parameters of the system. Gasification reactions have very high energy requirements and in order to thermodynamically promote them, they require a high influx of heat. Therefore, this parameter influences the final matter yields significantly. Generally, it is known that for co-gasification, higher temperatures will promote gasification reactions, ultimately increasing the producer gas yields and lowering the tar and char yields. In a steam fluidized bed experiment using pine and polyethylene [20], the yields for char were compared at different gasification temperatures from 740- 890°C. Temperature had a significant influence on conversion; at 740°C the final char yield was 10wt% while at 890°C it was 2wt% [20]. As the char is mostly composed of fixed carbon,

the increase in temperature would have promoted char gasification reactions like the water gas reactions. It was also mentioned how the increase in temperature also caused higher degrees of tar thermal cracking, lowering the final output of hydrocarbons, and increasing the hydrogen yield [20]. This helps considerably with reducing the energy and cost requirements for the downstream gas cleanup units.

2. Residence time

The residence time is the average length of time a particle of reactant spends inside of a gasifier. To ensure favorable gas yields, the residence time must be high enough to enable adequate tar cracking, reforming and char gasification reactions [12]. Higher residence times ensure a higher chance for suitable solid-gas contact, which generally promotes higher degrees of tar cracking and char gasification. One study comparing air and enriched air with rice straw and polyethylene [13] verified that higher residence times of gas improved tar cracking reactions. $pC_nH_m \rightarrow qC_xH_y + rC_zH_u + H_2$ ($x, z < n$ and $y, u < m$) illustrates a general reaction for the breakdown of tars into smaller hydrocarbons and hydrogen [13].

3. Catalyst

While tar cracking can be done thermally at elevated temperatures, another common in situ method for tar cracking and char gasification is the utilization of catalysts. Depending on the feedstock and conditions, a variety of catalysts have been used for reducing the final tar output in order to avoid larger downstream costs or the inclusion of oxygen [12]. Several examples include mineral catalysts such as dolomite or olivine, alkaline earth metal catalysts (iron, aluminum and potassium) and transition metal catalysts such as nickel [21]. Mineral catalysts are some of the most common as they are the least expensive [9]. Nickel based catalyst supported on alumina was studied in a fluidized bed gasifier using pine wood and polyethylene [47]. It was found that the catalyst was a major factor for increasing the hydrogen content within the producer gas. In support of this, dolomite, olivine, quartzite and nickel alumina-based catalysts were compared [48] and it was found that the nickel was the most efficient in reducing the tar content and increasing the hydrogen yield.

4. Gasification Agent

Gasification agents are attributed to have the most significant effect on the final composition. Depending on the application, different agents will promote or inhibit reactions as stated in Table 1-5. The most common gasification agents used are air, enriched air, steam and carbon dioxide [9]. A study [13] compared the performance of all of these co-reactants in a fluidized bed with polyethylene and rice straw.

Table 1-5: Reactions with oxygen adopted from [13]

Reaction Name	Reaction	ΔH (MJ/kmol)
Partial Oxidation	$C + 1/2 O_2 \leftrightarrow CO$	-111
CO Oxidation	$CO + 1/2 O_2 \leftrightarrow CO_2$	-283
Carbon Oxidation	$C + O_2 \leftrightarrow CO_2$	-394
Hydrogen Oxidation	$H_2 + 1/2 O_2 \leftrightarrow H_2O$	-242

The inclusion of air as a co-reactant will promote the partial oxidation reactions as seen in Table 1-5. In order to avoid complete oxidation, sub stoichiometric amounts of air must be added. This is described as the equivalency ratio [46], [49], illustrated by the following equation,

$$\text{Eq 1 } \Phi = \frac{\left(\frac{\text{Fuel}}{\text{Air}}\right)_{\text{actual}}}{\left(\frac{\text{Fuel}}{\text{Air}}\right)_{\text{stoichiometric}}} = \frac{\left(\frac{\text{Air}}{\text{Fuel}}\right)_{\text{stoichiometric}}}{\left(\frac{\text{Air}}{\text{Fuel}}\right)_{\text{actual}}}$$

Typically for co-gasification of plastics and biomass, these ER values range between 0.2-0.4 [9]. However, if a higher influx of heat is needed, some systems utilize higher ERs to promote complete oxidation of a fraction of the fuel and provide heat to a system. There is a common performance trade-off that is found with air gasification in fixed beds. They are subject to lower heat transfer rates when scaled up and therefore, it is common for more air to be fed to add temperature uniformity to the bed. Furthermore, additional available oxygen will reduce the tar production through complete combustion [12]. However, this also lowers the quality of the outgoing syngas by increasing the carbon dioxide concentration. Air as a co-reactant also introduces a large flow of nitrogen gas, which acts as a diluent. High flows of nitrogen in the syngas limit the applicability of the syngas for chemical synthesis [50].

Utilizing steam as a reagent will promote the steam reforming reactions of hydrocarbons as outlined in Table 1-6. From Table 1-6, it is evident that these reactions primarily contribute to the formation of carbon monoxide and hydrogen, both being very important products when considering the quality and applicability of the outgoing syngas (H_2/CO ratio). Generally, much higher hydrogen yields were found with steam gasification as opposed to the yields produced with air gasification [9]. Reforming of methane and hydrocarbons promotes the formation of H_2 and CO which is highly favourable for fuel and chemical synthesis. However, in comparison to air the energy requirements to produce and maintain steam are much more intensive. In addition, it is more common to produce higher amounts of tars given that there is no excess oxygen for complete combustion as seen in Table 1-6 [13].

Table 1-6: Reactions influenced by steam adopted from [13]

Reaction Name	Reaction	ΔH (MJ/kmol)
Water Gas	$C + H_2O \leftrightarrow CO + H_2$	131
Water Gas shift	$CO + H_2O \leftrightarrow CO_2 + H_2$	-41
Methane Steam Reforming	$CH_4 + H_2O \leftrightarrow CO + 3H_2$	206
Steam Reforming	$C_nH_m + n H_2O \leftrightarrow n CO + (n+m/2) H_2$	Endo

Finally, carbon dioxide utilization as a gasification agent is the least common compared to the others. Its application to co-gasification stems from the urgency induced by GHG emissions. This has generated more significant interest for its implementation considering it could be used as a carbon neutral or negative process [4]. From Table 1-7, all the reactions described are highly endothermic and form mainly carbon monoxide and hydrogen through tar and hydrocarbon reforming. They can be described as the char gasification and dry reforming reactions, requiring intensive energy inputs to take effect. The major trade-off with carbon dioxide as a co-reactant is the large energy requirements that would promote char and tar reduction. One method to counteract this barrier is to introduce a mixture of carbon dioxide and air for autothermal operation with complete combustion [13].

Table 1-7: Reactions influenced by carbon dioxide adopted from [13]

Reaction Name	Reaction	ΔH (MJ/kmol)
Boudouard	$C + CO_2 \leftrightarrow 2CO$	172
Dry Reforming	$C_nH_m + nCO_2 \leftrightarrow 2n CO + m/2 H_2$	292
Methane Dry Reforming	$CH_4 + CO_2 \leftrightarrow 2 CO + 2 H_2$	247

1.2.5 Pre/Post Treatment

Many studies referred to pre and post treatment steps included in their investigations to reduce particle size, improve feedstock mixing, and improve syngas quality. Depending on the selection of the gasifier, and the varying structure and composition of the feedstocks, pre-treatment units were commonly used for pre-drying, milling, crushing, shredding, grinding, sorting and sieving [9].

The most difficult by-product of plastic co-gasification is the tars [9], [11]. They are composed of a complex mixture of dense single or multiple ringed aromatic compounds and other longer chained hydrocarbons which can be toxic, corrosive and operationally challenging [9], [12]. They can cause damage and blockages in the main processing lines and downstream equipment. In addition, tars lower the overall conversion, efficiency and heating value of the producer gas [9], [51].

Tars can either be removed or cleaned through primary (in-situ) or secondary (syngas cleaning) methods [11]. For primary methods, either a catalyst is added directly to the reactor bed or the process parameters such as temperature, ER, or residence time are altered to promote higher gas outputs. A higher flow rate of air can be added to promote oxidation reactions to break down the tars. It is also common for synthetic or mineral catalysts to be added directly into the reactor bed to promote catalytic tar cracking, breaking the larger hydrocarbons into smaller hydrocarbons [9]. Common secondary methods added as downstream units include hot cleaning technologies such as dry, catalytic or steam reforming [12], [52]. The technology for this process is well known and is used commonly to reduce tar production. However, these additions increase the

costs of the system considerably [53]. Generally, the reactor conditions and additives such as catalysts are the preferred methods of tar reduction however most larger scale systems require additional secondary equipment [9], [54].

The solid residue is another by-product that must be addressed. This includes substances such as the ash (inorganics) and remaining char. Depending on the reactor temperature, metals that are naturally within the feedstock can agglomerate causing lower overall process efficiencies [12]. The leftover char is of low quality due to the high gas conversion therefore, it is generally recycled back to the main bed for further conversion or burned for energy [12]. If any particulate matter and ash escape the system, it is common for gas bag filters or cyclones to be added downstream for containment [12].

Finally, emissions such as nitrous oxides, sulfur oxides, dioxins, nitrogen, water vapour and particulate matter are commonly present in small and large quantities [11], [12]. The treatment of these by-products can be very well controlled with the appropriate reactor design and downstream processing units [12]. As gasification is a process which takes place in a reducing environment, the formation of nitrous and sulfur dioxides is much lower than compared to direct incineration [12]. Typical units used to remove particulates, dust, ash and tars are, downstream syngas cleaning units such as particle separators, cyclones, condensers, electrostatic precipitators and separators [12].

1.2.6 Reported Synergistic Non-linear Trends

In many of the recent studies investigating the mechanisms for the decomposition of mixed biomass and plastics, non-linear effects have been reported [55]. One study investigating the synergies of co-gasifying polyethylene and pine wood chips in a laboratory scale fixed bed reactor observed changes in the total volume of syngas and overall hydrogen yield [56].

This was reported as a synergistic effect where the yield of the hydrogen gas was considerably higher with a more favorable thermal efficiency compared to the calculated individual sum of the feeds. This was determined with a plastic to pinewood feed composition ranging between 80 to 60% [43]. Another study reported synergy while investigating wood saw dust and several different plastics including polypropylene and

high-density polyethylene in an 800°C dual gasification and pyrolysis reactor system [51]. It was found that the HDPE had the highest gas yields and the lowest tar and char outputs when mixed with a 20% ratio with the saw dust [51]. Similar results were also recorded with respect to gas yield and with various woodchips, kernel shells, polyethylene and polypropylene mixtures [31], [37], [57]–[59].

During steam co-gasification of pine pellets and high-density polyethylene (HDPE) in a dual fluidized bed reactor design, an increase in CO₂ and CO, and a decrease in tar was observed [43]. Compared to the gasification of the individual components, the co-gasification of these feedstocks reported lower tar yields due to synergies between the two feedstocks. Different trends were found in another study, where a mixture of pine wood and PE was investigated under a bubbling fluidized bed system with steam [20]. More hydrogen and hydrocarbons were produced in the producer gas than linearly expected yet less CO and CO₂ concentrations were found [20]. Another study found that when pine wood was co-fed with HDPE at 900°C in a steam environment, the tar output decreased by a factor of ten, while the gas yield increased by about two and a half [15], [60]. These effects have also been seen in various other studies done with steam co-gasification of plastics and woody biomasses [39].

One of unique benefits and motivations for carbon dioxide-based gasification is its direct conversion in this process. There are many initiatives developing globally for carbon dioxide capture, utilization, and storage (CCUS), reflecting an increased interest in this topic. CO₂ as a gasification agent has been considered as beneficial as it results in CO₂ consumption and enhances CO yields. Figure 1-3 illustrates the generally agreed influence of CO₂ on the pyrolysis/gasification mechanism of mixed plastic and biomass sources. It is agreed that the effects of CO₂ are various due to the complexity of the biomass and plastic co-gasification mechanism [4]. Biomass gasification and the effects on the final char yield have been discussed at length, with many describing the lower final char mass due to char gasification and the Boudouard reaction [13], [61].

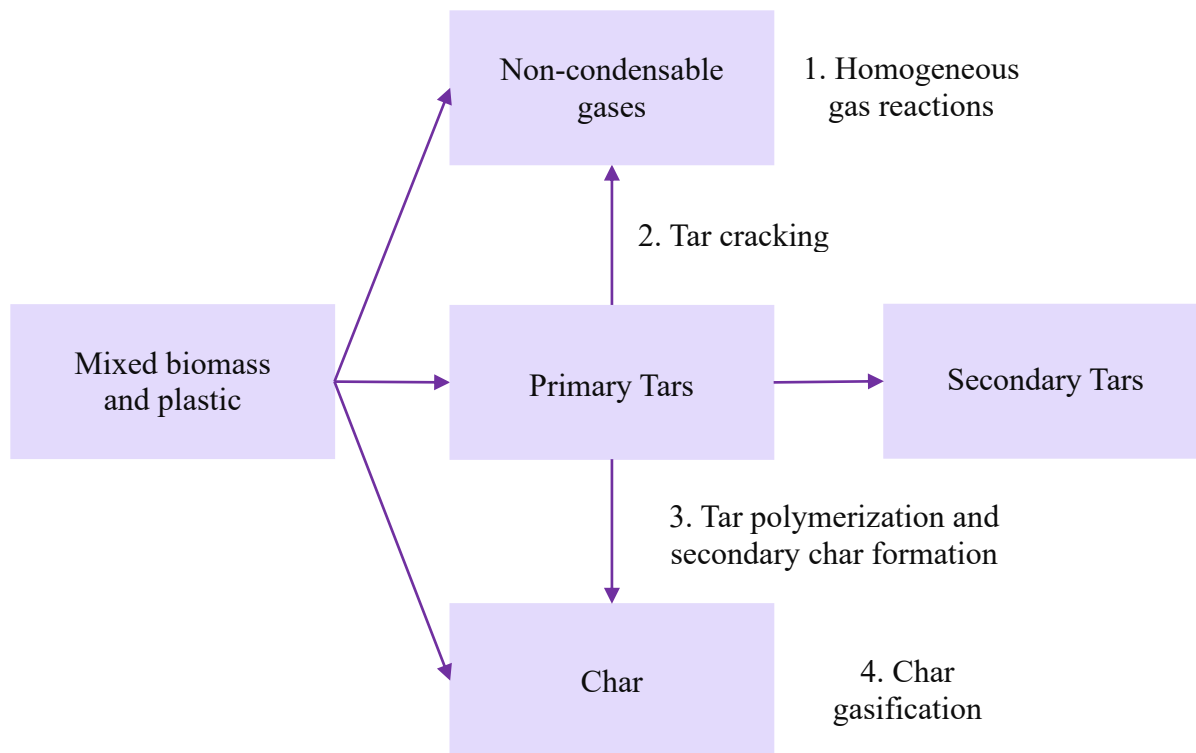


Figure 1-3: Possible mechanisms of CO₂ influence on biomass and plastic pyrolysis/gasification adapted from [32]

It has been reported that CO₂ gasification can reduce tar cracking due to dry reforming reactions of tars, small hydrocarbons, and methane [11]. It has also been discussed how adding CO₂ during the pyrolysis stage lowers the release of benzene derivatives and polycyclic aromatic hydrocarbons (PAH's) by hindering aromatization, cyclization, polymerization, and secondary char formation reactions [62]. Finally, the addition of CO₂ during pyrolysis and gasification influences the final gas yield through homogeneous gaseous reactions such as the reverse water gas shift [13]. The commonly reported higher yields of CO and lower yields of H₂ have been described as a control mechanism by which CO₂ gasification can alter the final H₂/CO ratio of the syngas [25], [63], [13]. This relationship has been described as advantageous, as CO₂ could be used as a moderator or in-situ control of the H₂/CO ratio of the syngas [63].

Waste cross linked polyethylene (XLPE), HDPE, LDPE and MDPE were individually gasified from 700-900°C in a semi batch fixed bed reactor using 75 vol% CO₂ in nitrogen as a gasifying agent [28]. Syngas yields were recorded to be 2.2 times the initial sample mass in CO₂

gasification. On a per gram basis of CO₂ consumed over each gram of feed, the point of highest consumption occurs at 900°C (2 grams of CO₂ per gram of XLPE), illustrating the endothermic nature of the CO₂ consuming reactions such as dry reforming [28]. The consumption of CO₂ was mainly attributed to the dry reforming of radical volatiles. Pinewood pellets (PWP) and HDPE were co-gasified in a semi batch fixed bed reactor with CO₂ at 800°C [17]. There was a much higher than expected production of hydrogen gas with the mixture of PWP and HDPE, an increase from the expected value by 36.7%. There was also a decrease in the expected final char mass when co-gasifying the mixed feedstocks in CO₂. Both these trends are attributed to the simultaneous degradation of the plastic melt phase on the solid residue of the biomass during co-gasification. The gasification process is ultimately accelerated as the plastic breaks the surface and enlarges the pores of the char [17]. However, lower CO₂ consumption was found when mixing the two feedstocks together.

Several studies have investigated the influence of CO₂ assisted air gasification of plastics biomass and mixed plastic biomass sources. Autothermal operation with waste wood pellets was investigated in a downdraft gasifier system with 15 vol% CO₂ and 85 vol% air [29]. This was compared with standard air gasification. Similar trends were reported with the lower H₂/CO ratio and lower yields of CH₄, yet when compared to air gasification similar producer gas energy densities were found [29]. Gasification of HDPE and rice straw was tested at 10 vol% and 50 vol% CO₂ with O₂ at an ER of 0.2 in a fluidized bed gasifier at 850°C. Addition of CO₂ led to a reduction of tars by 45% and a 70% increase in total gas yield. Tar reduction was attributed to dry reforming reactions and hindrance of the formation of tar precursors [13]. It has been observed by thermogravimetric analysis (TGA) that the utilization of CO₂ for the co-gasification of rice straw and PE has lower activation energies [40]. Japanese cedar and gulfweed were individually gasified in a downdraft gasifier at 900°C at a constant ER of 0.3 [23]. Introduction of CO₂ (79 vol%) to air gasification led to a 14% increase in carbon conversion to gas (carbon mole%). H₂/CO ratios of gulfweed lowered from 0.75 in air gasification to 0.33, also lowering the final yield of CH₄. Lower tar and char yields were seen with increasing CO₂ from 0-15-45-79 vol%, with increased gas yields due to tar reforming and char gasification reactions.

Municipal solid waste was gasified in a pilot plant fluidized bed with mixtures of air and CO₂ at ERs between 0.15 and 0.35 [64]. CO₂ flow was increased from 0-100 vol% by intervals of 20 vol% and compared. Above a vol% of 40, the high CO₂ content led to drops in gasification temperature due to the increase in endothermic reforming and char reactions. Beyond 40 vol% CO₂, the O₂ available was not sufficient to maintain the intended temperatures [64]. Increasing the ER from 0.15-0.35 decreased the carbon and CO₂ conversion, while increasing the tar conversion with a higher degree of oxidation to CO₂ and H₂O.

It has been proposed that these findings are a result of synergistic effects present only when co-gasifying these various feedstocks. This has been suggested because of reported product yields and compositions that cannot be quantified by a linear combination of the inputs [9], [65]. From the literature, the contribution of the proposed mechanisms for these synergies has not been fully agreed upon. Several theories have been proposed to elucidate these reaction mechanisms.

1.2.7 Mechanisms for feedstock synergy

There have been several interpretations for the observed synergy between the feedstocks reported in the literature. The first explanation is regarded as the most agreed upon mechanism for these observed synergies [9]. This theory claims that the catalytic effect of the alkali and alkaline earth metals from the degraded biomass catalyzes the decomposition of the plastics, resulting in a high concentration of radicals and mixed volatiles [9], [65]–[67]. It has commonly been found that the higher carbon conversion to volatiles under co-pyrolysis could be attributed to the catalytic influence of the biochar [65]. The decomposition for biomass feedstocks initiates at a lower temperature compared to plastics. The products from the initial pyrolysis are then present during the degradation of the plastic portion. The degradation mechanism has been considered to be in sequence and thus the resulting chars influence the decomposition mechanism of the plastics present in the mixture [65]. This has been argued to be more prevalent in studies investigating higher heating rates that induce overlap between the degradation phases.

Another theory attributes these effects to a possible synergy with the plastics intermediate melt phase, which forms alongside the thermal deterioration of the biomass components [38]. It has

been proposed that this phase acts as a hydrogen donor platform for the biomass radicals, reacting and stabilizing the biomass components [38]. These species are then trapped until they are released during the breakdown of the main polymer chains rather than as they directly volatilize [38]. The final proposed theory describes that the pyrolytic products mix causing further interactions between the radical and volatiles. These intermediate products from the separate feedstocks have been speculated to interact and enhance the overall syngas production due to the increased availability of hydrogen content originating from plastic component of the mixture[9]. This theory has been mainly supported by co-pyrolysis studies, as this would have isolated the pyrolytic breakdown of the feeds from the ensuing gasification reactions [9].

1.2.8 Value of Current Research and Objectives

This study aims to address gaps found in the literature on carbon dioxide assisted co-gasification of mixed plastic and biomass. The literature on individual biomass and plastic air gasification is extensive. There was an abundance of studies with different reactor types, reactor conditions and co-reactants. There were also many studies that investigated the kinetics of mixed plastic and biomass through thermogravimetric analysis [42], [44]. These either primarily focused on individual co-reactants and the distribution of plastic versus biomass feed. There were also several studies investigating CO₂ biomass gasification with interest in the mechanism [17], [22], [24], [68], [69]. However, the literature on co-gasification of mixed plastic and biomass in CO₂ assisted air gasification was limited. The utility of CO₂ as a moderator to produce CO in air gasification, and therefore any investigation of a ratio of CO₂ with air for plastic gasification was not discussed in the literature. Therefore, the main objectives of this study were to investigate the influence of added CO₂ on the mechanism and product distribution of air gasification. TGA tests were done in parallel at scale with an updraft micro-gasifier (MG). The mechanisms discussed in previous literature was used to identify the co-gasification mechanism of HDPE and Douglas fir at TGA scale. This was done in common air to fuel ratios of 0.2 and 0.3, with added percentages of 0, 10, 20 and 40% CO₂ based on the input air flow. Therefore, the effects of added CO₂ on air gasification was investigated. These tests were also run at scale in a micro-gasifier (MG) to evaluate the changes in gas, tar and char production. The utility of added CO₂ in air gasification will be evaluated by an analysis of the product distribution with discussion of the co-gasification

mechanisms observed in the TGA. Ultimately, this study aims to improve on existing knowledge of the co-gasification mechanisms of mixed co-reactants and feed, with the possibility of recognizing mechanistic synergies. This study will therefore help in exploring the possibility of consuming CO₂, plastics and biomass waste feeds in one system for chemical and fuel synthesis.

2 Experimental Methods and Materials

2.1 Feedstock Preparation and Characterization

2.1.1 Feedstock Selection and Preparation

The purpose of this study was to address gaps in the literature discussing mixed plastic and biomass feedstock synergies. Pure materials of high-density polyethylene (HDPE) and Douglas fir were mixed in different ratios in order to understand interactions between these materials during gasification. The HDPE pellets were sourced from NOVA Chemicals Ltd (Sarnia, Ontario), and the Douglas fir sawdust was obtained from the Institute of Chemicals and Fuels from Alternative Resources (ICFAR), (London, Ontario) supply. To ensure uniform mixing of these feeds, each was sieved to a particle size range of 250-350 μm for all experiments. The HDPE pellets were first ground in a blender (Vitamix) and sieved to the specified particle size, while the Douglas fir only required sieving. The required mass for these feedstocks were then separately measured and then mixed meticulously by hand with a spatula. Figure 2-1 shows the unprepared individual feedstocks of HDPE Douglas fir used for all experiments done. Figure 2-2 shows the prepared pre-mixed feeds.

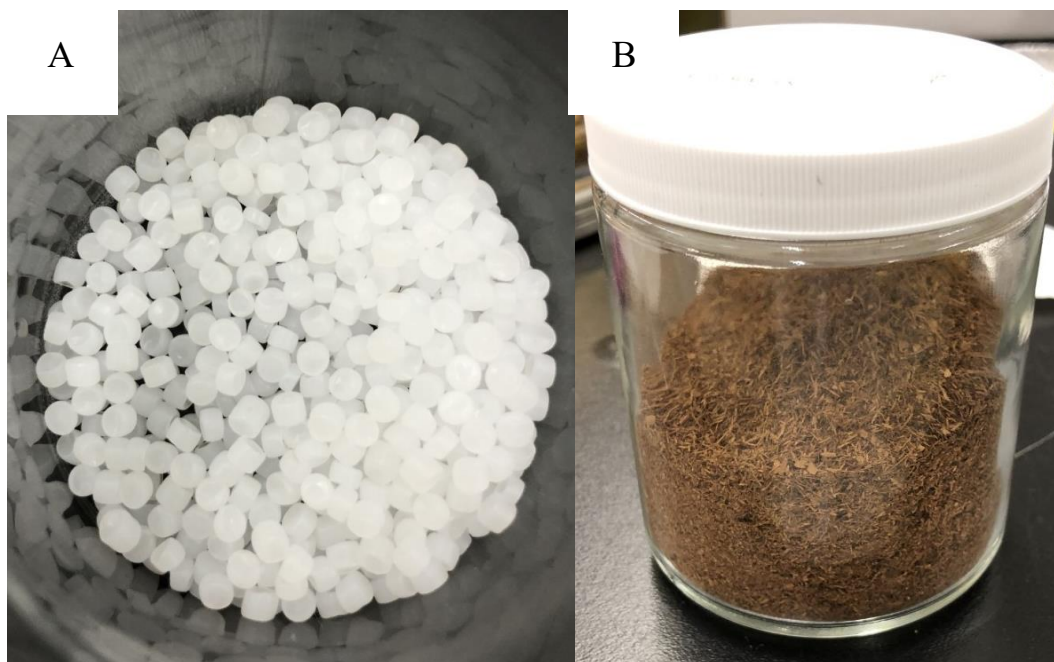


Figure 2-1: Collected feedstocks of HDPE (A) and Douglas fir (B)

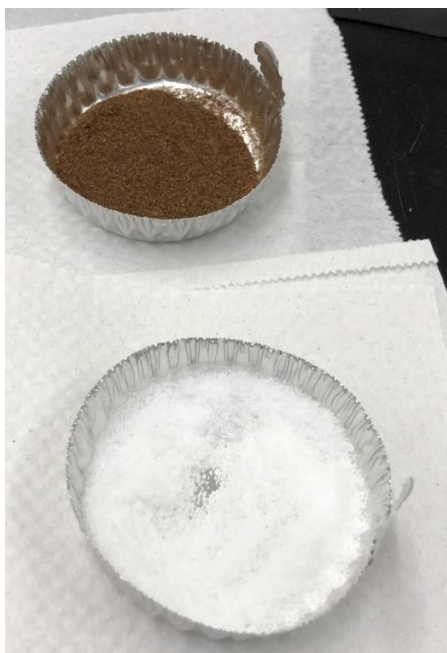


Figure 2-2: Ground and sieved Douglas fir and HDPE

2.1.2 Ultimate Analysis

To determine the elemental composition of the feeds, ultimate analysis was done using a Thermo Flash EA 1112 series elemental analyzer. The carbon, hydrogen, nitrogen, sulphur and oxygen composition (CHNSO) for both feedstocks are illustrated in Table 2-1.

Table 2-1: Ultimate Analysis (wt%, dry basis) of HDPE and Douglas fir

Feedstock	C	H	O*	N	S
Douglas Fir	50.45	5.77	43.66	0.09	0.02
HDPE	85.31	14.41	0.23	0.05	0.00

*by difference

To calibrate the elemental analyzer, a by-pass, a blank and five samples of BBOT (2,5- Bis (5-tert-butyl-benzoxazol-2-yl) thiophene) were run before analyzing the feedstocks. Each BBOT sample was prepared with 8-10mg of vanadium oxide and the following masses of BBOT respectively (0.5, 1, 1.5, 2, 1-2mg). These samples were prepared in small tin capsules and

loaded into the automatic tray sampling system of the analyzer. Each a sample was combusted at 900°C in a controlled stream of oxygen and helium. The combusted gases of SO₂, CO₂, H₂O and N₂ were identified using a Propack thermal conductivity detector (TCD) and quantified using gas chromatography. The remaining weight percent of the sample would be determined as the oxygen content.

2.1.3 Proximate Analysis

The moisture (M), volatile matter (VM), fixed carbon (FC) and ash (A) contents of the feeds were determined through proximate analysis adapted from the ASTM D1762 standard procedure [70], in a thermogravimetric analyzer (TGA 5500, TA Instruments). Figure 2-3 shows the results for the proximate analysis of Douglas Fir, where each color-coded step represents the loss of moisture, volatile matter, fixed carbon and ash. 30 mg samples were loaded onto individual pans and heated to 105°C in a 35 ml/min (10 ml/min balance flow of nitrogen included) stream of nitrogen. This was held for 80 minutes to dry the samples and account for moisture loss. The sample was then heated at 20°C/min up to 900°C in the same environment. After reaching 900°C, 25 ml/min of air was introduced (with 10 ml/min of nitrogen balance flow) and held for 20 minutes. The mass loss of each recorded stage is the total composition of the moisture, volatile matter, fixed carbon and ash [70]. Table 2-2 illustrates the proximate analysis for the Douglas fir and HDPE. Both the proximate and ultimate analysis for these feedstocks was similar to that of previous literature values [71].

Table 2-2: Proximate analysis (wt%) of HDPE and Douglas fir

Materials	Weight %			
	M	VM	FC	A
Douglas Fir	8.38	64.54	19.71	1.85
HDPE	0.04	99.96	0.00	0.00

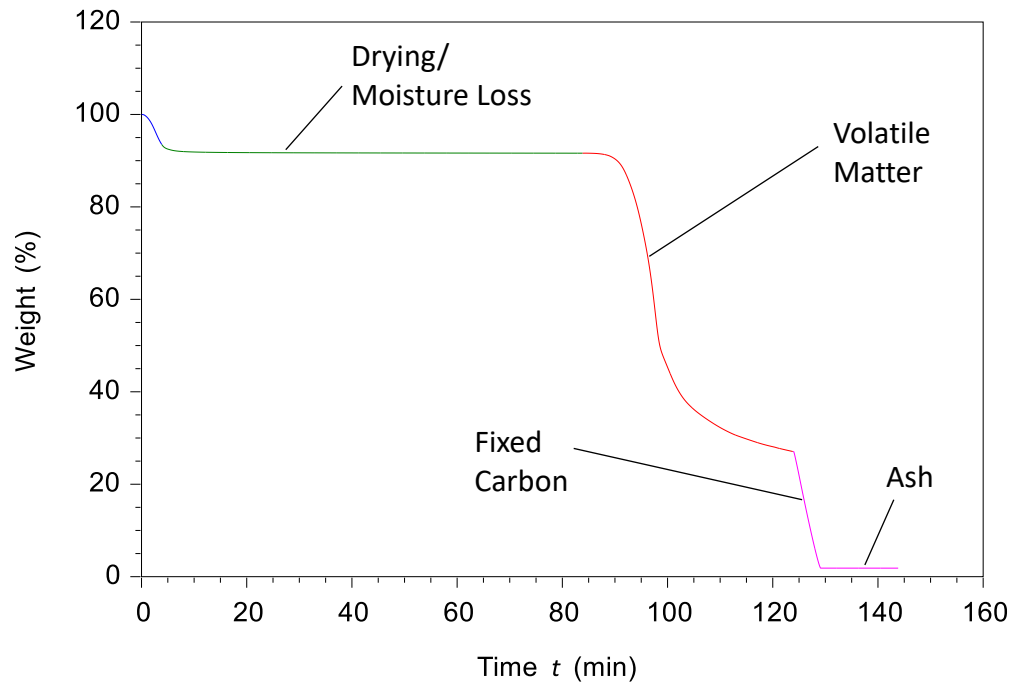


Figure 2-3: Mass loss graph of Douglas fir (Proximate analysis)

2.2 Experimental Setup

The co-gasification experiments were carried out in the TGA unit described in Section 2.1.3 and in a bench scale updraft micro gasifier, which was built for this experimental work.

2.2.1 Thermogravimetric Analysis

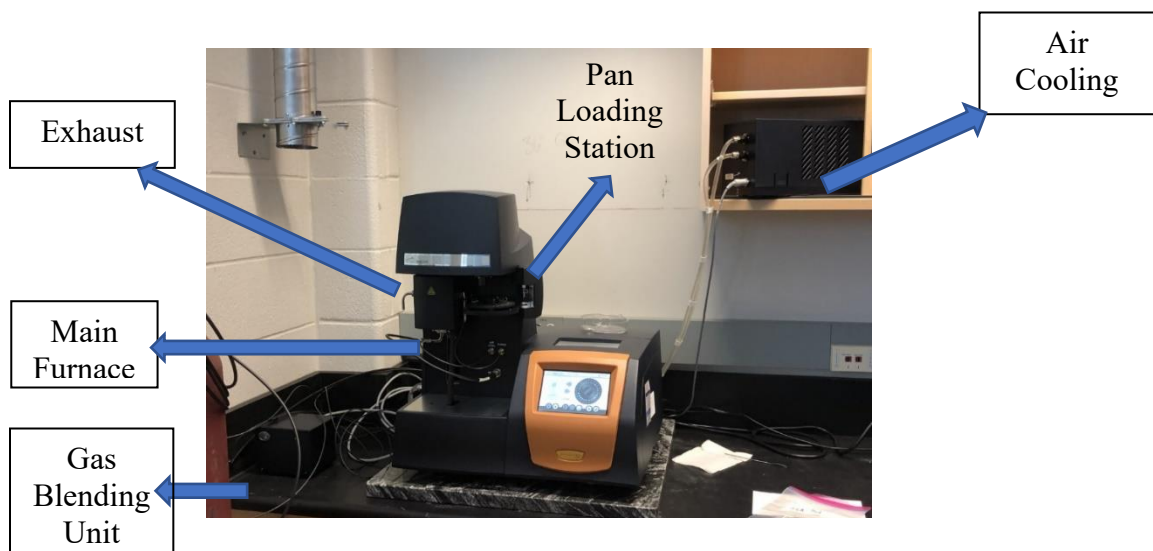


Figure 2-4: Picture of thermogravimetric analyzer setup used, a nearly fully automated system with air cooling, touch screen and blending gas delivery module (GDM).

2.2.2 Micro Fixed Bed Gasifier

Experiments done in the bench size micro-gasifier are shown in Figure 2-6. This system was a flow through reactor where product compositions could be analyzed. The results were performed at similar conditions to TGA experiments and information from the two reactor systems was used to develop an understanding of reaction mechanisms. Figure 2-5 illustrates the setup for the bench scale updraft micro-gasifier with a legend (Table 2-3). Where possible, all connections were compression fittings.

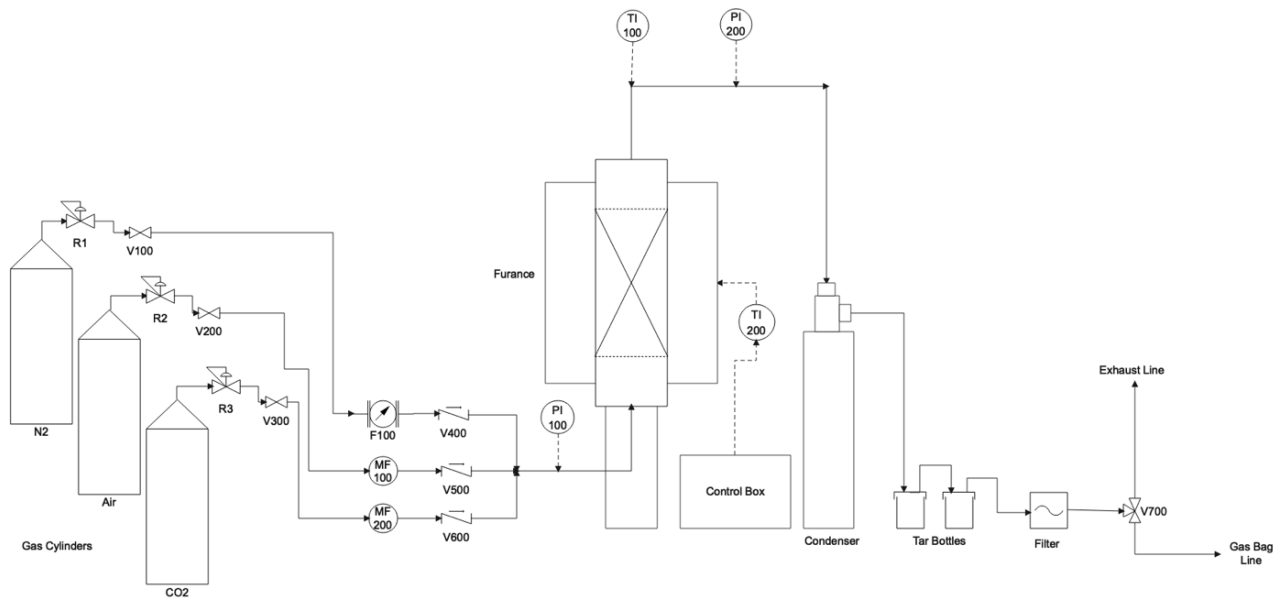


Figure 2-5: Updraft (fixed bed) micro-gasifier diagram

Table 2-3: Legend for micro gasifier parts

Title	Description	Title	Description
R1	N ₂ Pressure Regulator	V400	Check Valve
R2	Air Pressure Regulator	V500	Check Valve
R3	CO ₂ Pressure Regulator	V600	Check Valve
V100	Ball Valve	PI100	Pressure Gauge
V200	Ball Valve	PI200	Pressure Gauge
V300	Ball Valve	TI100	K-Type Thermocouple
F100	N ₂ Rotameter	TI200	K-Type Thermocouple
MF100	Air Mass Flow Controller	V700	Three-way Ball Valve
MF200	CO ₂ Mass Flow Controller		

Three gas cylinders (N₂, Air and CO₂) were attached in parallel with their respective pressure regulators and ball valves. The nitrogen stream which was used for system purging and start up was controlled by a rotameter. The carbon dioxide and air streams which were used for gasification had individual mass flow controllers (MFC, Aalborg) for more precise flow control. After each MFC and rotameter was a check valve to prevent backflow. A four-way union connected each of the flow regulated gas inputs before connecting to the bottom of the main reactor. Pressure gauges were placed at the entrance and exit of the reactor to detect potential blockages in the reactor due to the melting plastic. The main reactor was a 316 stainless steel tube with total height of 86 cm, a 2.54 cm outer diameter (OD) and 2.2 cm inner diameter (ID). The main bed is supported by a 43 cm ceramic inner tube with an OD of 1.9 cm and an ID of 1.43 cm.

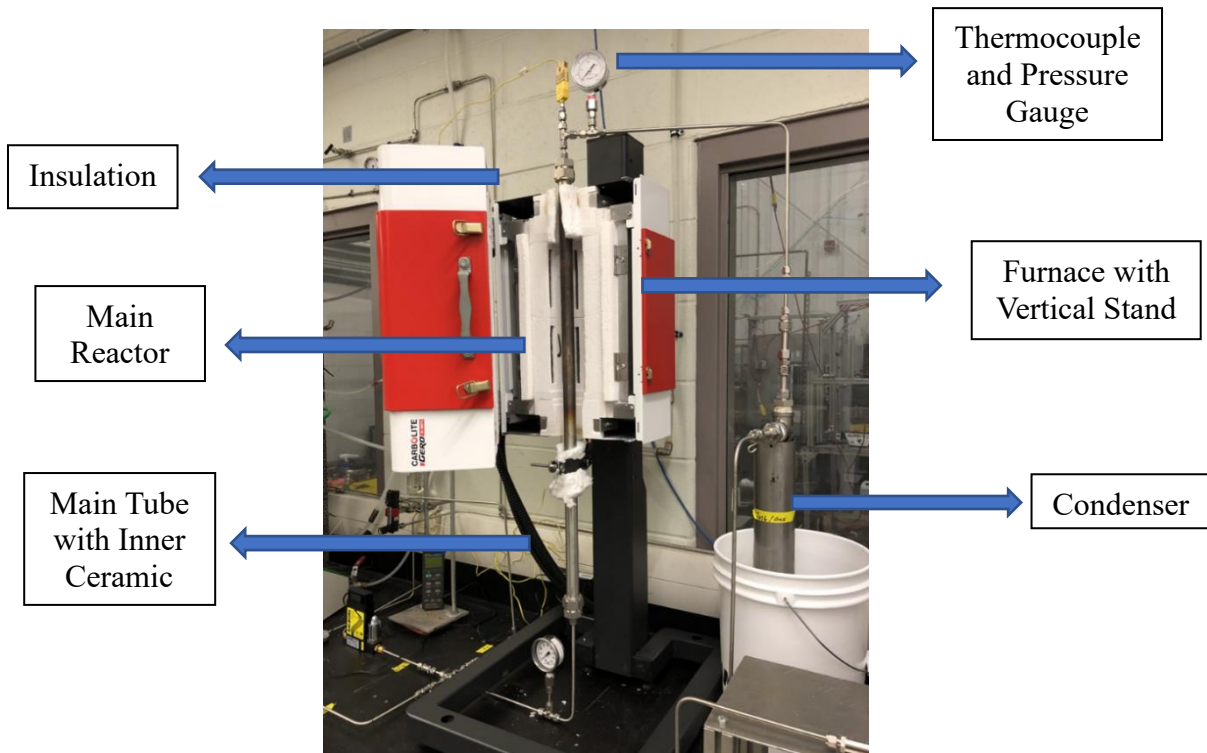


Figure 2-6: Main reactor setup of updraft micro-gasifier

A small layer of quartz wool rested on top of the ceramic tube to hold the mixed feed and better distribute the input gas flow throughout the bed. All testing in the MG used a 10-gram binary mixture of HDPE and Douglas fir which had a bed height of approximately 11.4 cm. A 30.5 cm k-type thermocouple was connected to the top which sat directly above the bed of the reactor.

The furnace for the main reactor was a split tube furnace (Carbolite Gero, Model #: TF1 12/60/300), that could operate continuously up to 1100°C and intermittently (1-2 hours) at 1200°C. The furnace was connected to a vertical stand with a programmable control box. A thermocouple relayed the temperature of the system back to the control box for regulated heating. The thermocouple from the top of the reactor was connected to a separate temperature reader. The hot gas would then exit from the top of the reactor into an ice bath condenser, followed by collection bottles containing isopropanol solvent and a particulate filter. Any evolving tars, moisture or particulate matter would be captured in the condenser, bottle units and filter. Gas samples were taken with 1-liter Tedlar gas bags using a three-way valve splitting between the sampling line and the exhaust line.

2.3 Experimental Method

The objectives of these experiments were to elucidate the mechanisms proposed in the literature using the TGA while also characterizing the products formed in the MG. All char, tar and gas samples collected from the MG were considered for analysis. This section explains the experimental procedure for the TGA, CHNSO, MG and Micro-GC.

2.3.1 *Thermogravimetric Analysis*

The TGA was used in two phases for this project. The first phase was investigating the synergies between the feedstocks solely with the TGA. The second phase compared TGA mass loss profiles of the feedstocks to the product distribution in the MG. TGA samples ranged from 10-50 mg depending on the testing phase. Each pan was tared in the TGA before measuring out the needed mass on a balance. The pan was then loading onto the TGA docking station. The method for the runs TGA were programmed into the TRIOS software which controlled all the flows and temperature changes while recording the mass loss. After the method was formatted, the gas cylinders used for the TGA were opened accordingly (typically CO₂, N₂ and air). The gases were introduced and blended in the GDM before the TGA. The TGA always required a balance flow of 10 ml/min of nitrogen, therefore this flow must always be considered when creating the experimental method. After testing, pans were cleaned with acetone washing or by running a combustion method in the TGA, where the furnace temperature would be raised to 900°C in an air environment. The mass loss vs time plots would be generated by the software as shown in

Figure 2-3. Small sections at the beginning of every subchapter in chapter 3 contain tables with all experiments and conditions completed respectively.

2.3.2 Updraft Micro-Gasifier

When operating the MG, as it is a semi batch system, the main reactor was disconnected after every run and cleaned thoroughly. For experimentation, the temperature program was preprogrammed into the furnace control box before manual setup. 10 grams of mixed sample was prepared before every run. The main reactor was disconnected from the quarter inch inlet at the bottom reducing union, while the top union was disconnected at the 1-inch connection to allow for mass loading. The alumina ceramic tube was first loaded as the main support for the bed, with a small 0.5-gram piece of quartz wool on top which prevented any feedstock from falling further than the center of the bed. An updraft model was chosen for its simplistic operation and lower char production. The 10 grams of mixed sample was then loaded using a funnel. The difference of the beaker and funnel mass were considered in order to accurately measure the total mass in the reactor bed. After connecting the reducing unions and the reactor thermocouple to the main tube, all piping to the condenser was connected. This included the output as well to the tar bottles and particulate filter. Tar bottles were filled with 100 ml of isopropanol solvent, and the condenser bucket was filled with a bag of ice water. After all piping is connected, 50ml/min of nitrogen from the first cylinder is used to purge the unit and allow for leak checking with leak detector. Nitrogen was also used for system cooling and purging before cleanup.

Table 2-4: Example of input flows for tests in ER of 0.3

Tests	Vol% CO ₂	Input Flows (ml/min)		
		O ₂	N ₂	CO ₂
1	0	88.2	331.8	0.0
2	10			46.7
3	20			105.0
4	40			280.0

When the system is purged and leak tested, the program is started on the control box for the initiation of the run. The system had a constant heating rate of 20 °C/min, which was first heated to 120°C for 30 minutes of drying. After drying, the nitrogen flow was stopped and the mass

flow controllers for air and carbon dioxide were opened. Table 2-4 illustrates the flow parameters chosen for specific runs in chapter 3.2. Input air flow was constant and the flowrate of CO₂ was varied for different tests. All input gas flow rates remained constant throughout the test. All tests included a temperature ramp to 850°C which held for ten minutes. At every 100°C intervals starting at 300°C, gas bag samples were taken. This included a gas sample when reaching 850°C and after the ten-minute dwell (ten total gas bag samples per test run). After sampling the final bag, the mass flow controllers were shut off and the nitrogen flow was reopened for cooling and cleanup. After cooling, the mass of the char samples leftover in the reactor were collected, weighed and stored for elemental analysis. The tar samples extracted in the condenser bottles were preserved in the lab fridge. All gas bags were stored for Micro-GC analysis.

2.3.3 CHNSO Analysis

Elemental analysis was also investigated with the final chars produced from the MG. The methodology for this experimentation was identical to that of the ultimate analysis of the feeds. Each sample was tested three times and the average weight percentages were calculated and reported. Carbon, hydrogen, sulfur and nitrogen were measured and oxygen was calculated by difference.

2.3.4 Micro-Gas Chromatography

The micro gas chromatograph (Micro-GC) was used to analyze the concentrations of the gases collected with the 1-liter Tedlar gas bags from the updraft gasifier. Quick connect fittings were attached to the sample line, Micro-GC and the end of each bag which allowed for effective gas sampling. A Varian CP-4900 mobile Micro-GC was equipped with three individual columns for identifying specific gases. The M5 (Molecular Sieve., 10 m) column was used to quantify H₂, CH₄, CO, O₂ and N₂. The PPU (Polar Plot U, 10m) and 5 CB (CP-Sil, 5 CM, 8 meter) column modules were used to analyze the concentrations of CO₂, C₂H₄, C₂H₆, C₃H₆, C₃H₈, C₄H₁₀ and C₅H₁₂. High purity Helium and Argon were used as carrier gases. The Micro-GC had the option of programming specific methods for analysis with the Galaxie software. After attaching a Tedlar bag full of gas to the inlet, the Micro-GC would pump the gas into the columns for a

three-minute sample time while the bag was squeezed to release the sample, after which the carrier gas was injected as a sweep gas.

After this allotted time, the software would construct a chromatograph with each of the analyzed gases integrated over their respective peaks. To ensure the system was properly purged, multiple samples were taken from each gas bag until there were three repeatable chromatograms.

Cylinders with appropriate concentrations of all calibration gases were used for calibrating the Micro-GC. After running all calibration gases, calibration curves were made for each gas. The areas of the peaks for the three samples were averaged for each gas. These were then normalized and then multiplied by the slope of the calibration curves in order to calculate the accurate concentrations of the gases.

3 Experimental Results and Discussion

3.1 Synergies between blended feedstocks in N₂ and CO₂ environments

3.1.1 Experimental Plan

This section uses TGA studies to understand the synergies between biomass and plastics during decomposition. Specifically, this phase of testing aimed to build on previous literature identifying the influences of carbon dioxide at key stages of decomposition. The HDPE and Douglas fir feeds were tested individually and then combined (1:1) in N₂ and CO₂. The individual mass loss tests of HDPE and Douglas fir were used to calculate the expected mass loss. This would simulate the decomposition of the mixed feed assuming there are no interactions between HDPE and DG fir. This was then compared to the experimental results. Table 3-1 summarizes the parameters for all tests done with the TGA for this section. This includes an analysis of mass loss with various conditions specifically focusing on CO₂.

Table 3-1: Conditions for all TGA tests done in this section

TGA									
Test Number	Gas Conc (%)			Flowrate (mL/min)	Ramp Rate (°C/min)	Mix %		Temp (°C)	Groups
	CO ₂	N ₂	Air			HDPE	DGFIR		
1	-	100	-	35	20	100	0	700	1
2	-	100	-	35	20	0	100	700	
3	-	100	-	35	20	50	50	700	
4 (Calc)	-	100	-	35	20	50	50	700	
5	20	80	-	35	20	100	0	700	2
6	20	80	-	35	20	0	100	700	
7	20	80	-	35	20	50	50	700	
8 (Calc)	20	80	-	35	20	50	50	700	
9	20	80	-	35	10	50	50	700	
10	20	80	-	35	50	50	50	700	

3.1.2 Temperature Phases and Mass Loss

The first tests of the individual and mixed feedstocks were done in N₂ to establish a base for comparison with added CO₂. Figure 3-1 shows the decomposition of Douglas fir, HDPE and

their 50:50 mix in N₂ up to 700°C. DG fir starts its decomposition at 280°C, while the much more stable plastic melt phase starts to decompose at 425°C. Almost all the plastic is volatile matter so when it does begin to lose mass, it quickly decomposes into volatiles. The grey line shows the mass loss of the mixture of the two feeds, staying in between the individual feedstock mass loss profiles. Figure 3-1 compares the experimental mixture and calculated mixture, where the calculated is the combination of the individual experimental runs. The experimental mass loss of the mixed feedstocks nearly identical to that of the calculated. This indicates that by simply mixing the feedstocks there were no significant synergies present with the rate of mass loss. Table 3-2 shows that the final mass of the calculated and experimental mixtures were nearly identical.

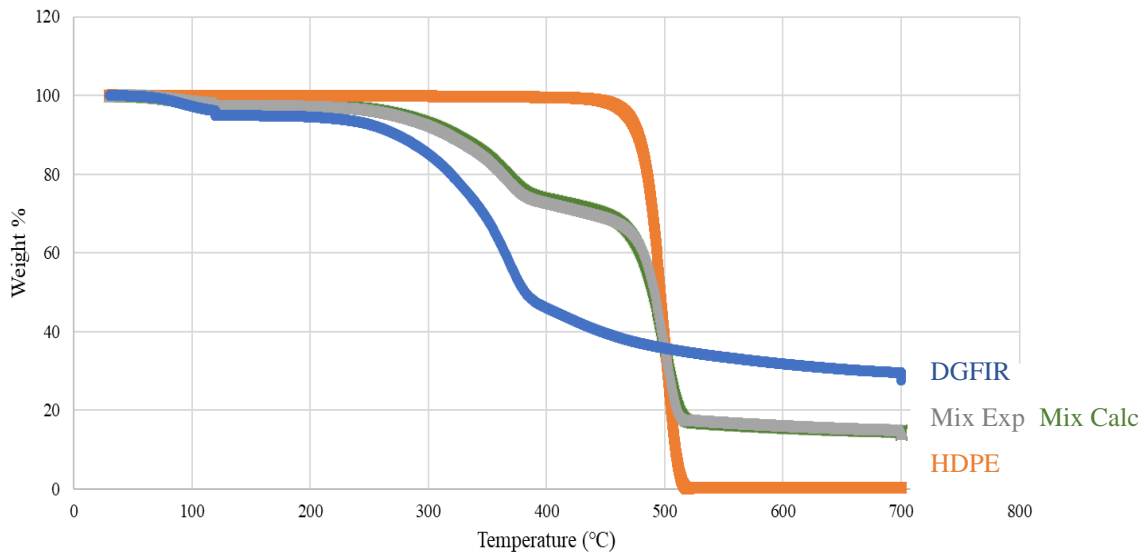


Figure 3-1 Comparison of individual and mixed feedstock decomposition up to 700°C in N₂ environment

Table 3-2: Final Mass in TGA of mixed HDPE and DGFIR (50:50) in N₂

Mass	Blend Experimental	Blend Calculated
Final % of mass	13.8	13.9
Final mass (mg)	1.56	1.57

Figure 3-2 illustrates the same decomposition profile as the previous runs but with 20% CO₂ (7 ml/min) integrated into the total input mass flow (18 ml/min N₂, 25 ml/min total). There were two notable temperature ranges that signify changes in mass loss with added CO₂, from 280-380°C and following the breakdown of the plastic melt phase at 425-520°C. From 280-380°C, the mass loss for the blended feedstock is lower than the calculated mass loss based on individual feedstocks.

This contrasts with what was observed with a pure N₂ environment, where there were no synergies for the blended feedstock. This shows that CO₂ influences reactions in this temperature range for blended feedstocks. In the 280-380°C temperature range, the decomposition of the holocellulose of the biomass accounts for the expected mass loss, by depolymerization and condensation reactions [25]. It has been observed that the presence of CO₂ may hinder the polymerisation and secondary char formation reactions during this decomposition [32]. At 425°C, the melted plastic starts to decompose by random scission [28]. The long carbon chains of the plastic break, depolymerize into larger oligomers and smaller radicals, and rapid mass loss is observed until 520°C. In this temperature range, the experimental mass loss exceeds the calculated mass loss, indicating that there are positive synergies which enhance decomposition of mixed feedstocks in the presence of CO₂. One of the suggested mechanisms for this synergy is the influence of CO₂ on the products of the initial decomposition of the Douglas fir [4], [9], specifically the char and tars. The final mass for the experimental was 8.2 wt% with the calculated being 11.3 wt%. The difference in mass loss after the synergy seen at 520°C was 7 wt%.

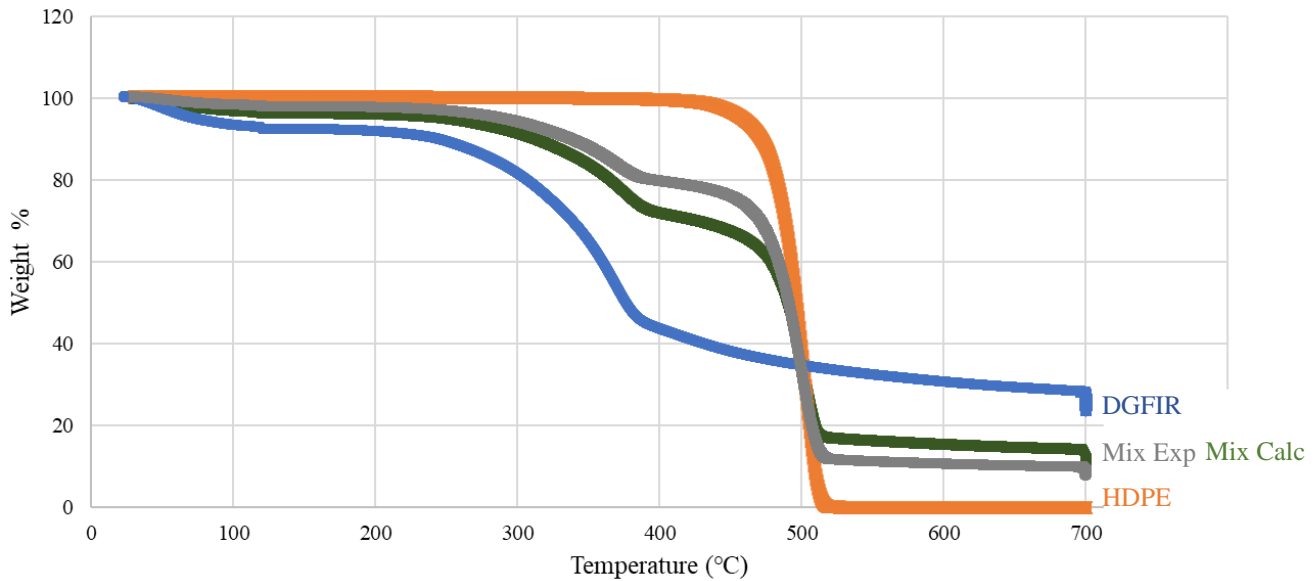


Figure 3-2: Comparison of individual, mixed and calculated feeds up to 700°C with 20% CO₂ injected

It was observed that higher heating rates may promote a higher degree of overlap between the decomposition of the biomass and plastic [72]. Therefore, different heating rates were tested to see if there were any changes with higher heating rates. The same procedure and injection of CO₂ was used, and the heating rates were altered from 20 to 10 and 50°C/min. Figure 3-3, shows the mass loss profile of the different heating rates. From Figure 3-3, there are no distinct synergies seen as the mass loss profiles are very similar. Table 3-3 shows the final mass residue from each heating rate run. 50°C/min had the highest final char mass and lowest change in mass between 425-520°C.

Table 3-3: Final Mass percentages of heating rate TGA runs

Heating Rate (°C/min)	Final wt%
10	10.2
20	8.2
50	10.8

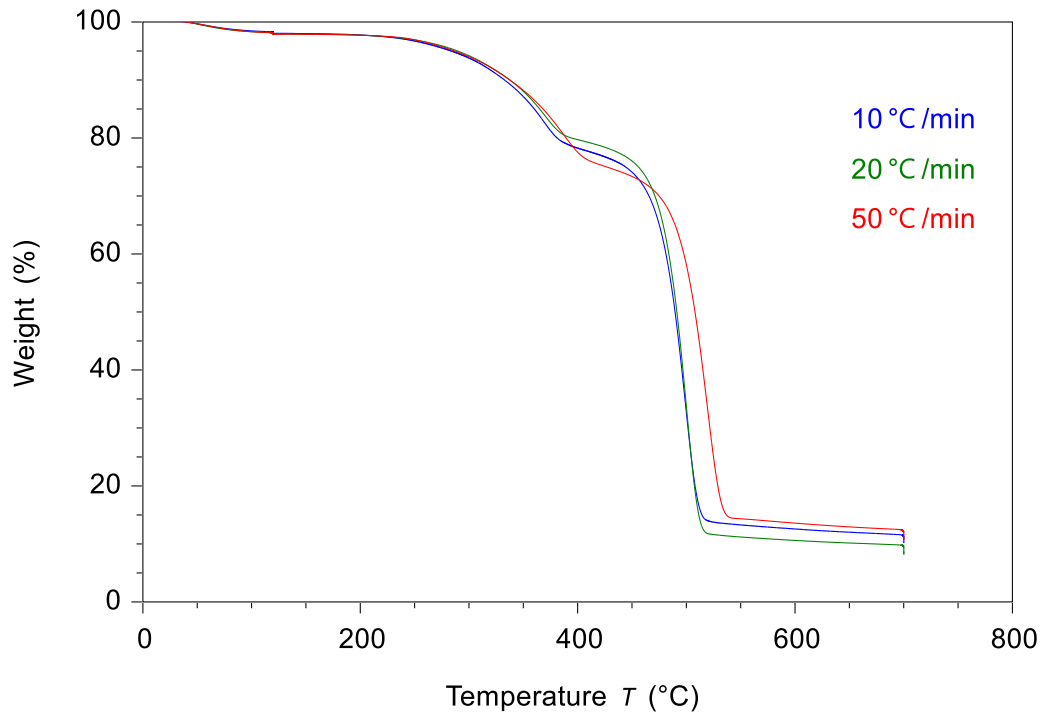


Figure 3-3: Comparison of heating rates (°C/min) TGA curves in 20 vol% CO₂ environments

3.2 Influence of CO₂ injections at Equivalence Ratio of 0.3

3.2.1 Experimental Plan

Tables 3-4 and 3-5 summarize the parameters for all tests done with the TGA and MG for this section. The main objective was to understand the influence of CO₂ on the gasification reactions and products formed (gas, tar, and char) during the various stages of decomposition, using both a TGA and a flow-through micro gasifier. Each test had a constant air flow rate, corresponding to an initial air to fuel ratio of 0.3. CO₂ was added in concentrations of 10%, 20%, and 40%, with the CO₂ flow rate being constant throughout each experiment.

Table 3-4: TGA tests with 0.3 ER

TGA Runs					
Test	Sample Mass (mg)	% CO ₂ Added	Total Gas Flowrate (mL/min)	Ramp Rate (°C/min)	Max Temperature (°C)
1	30	0	1.428	20	850
2		10	1.587		
3		20	1.785		
4		40	2.380		

Table 3-5: Micro-gasifier tests with 0.3 ER

Micro-Gasifier Runs					
Test	Sample Mass (g)	% CO ₂ Added	MG Total Gas Flowrate (SLPM)	Ramp Rate (°C/min)	Max Temperature (°C)
1	10	0	0.420	20	850
2		10	0.467		
3		20	0.525		
4		40	0.700		

3.2.2 Adding CO₂ to Air Gasification (ER=0.3), TGA and Micro-Gasifier Analysis

Figure's 3-4 and 3-5 illustrate the mass loss curves of binary mixtures of HDPE and Douglas fir in air gasification (ER = 0.3) with added flows of CO₂. These tests were done to observe any changes in mass loss with the addition of CO₂ to air gasification (ER = 0.3) with high accuracy. After the moisture had evaporated, there were three notable temperature ranges that showed changes in mass loss with added CO. Between 280-380°C, devolatilization is observed. This corresponds to the release of gases such as H₂, CO, and CO₂. The breakdown of the plastic melt phase takes place at 425-520°C, shown as a steep drop in mass in this temperature range. The release of volatile matter from the plastic overlaps with the decomposition of the biomass. Finally, gasification of lignin takes place from 550-850°C.

Firstly, increases of added CO₂ to air gasification slowed the rate of mass loss until the plastic melt phase. The addition of CO₂ showed a lower rate of mass loss from 280-425°C indicating that the presence of CO₂ influenced the initial decomposition of the biomass as seen in section 3.1.2. This is apparent until the breakdown of the plastic melt phase beginning at 425°C. The plastic carbon chains rapidly deteriorate into volatiles leading to a surge in mass loss up to 520°C. The air run (blue) had the fastest rate of mass loss, with a lower mass percentage at all temperatures except between 520-540°C. The presence of 10% and 40% CO₂ showed lower mass loss compared to only air, however after the plastic melt phase, 20% CO₂ showed increased mass loss surpassing that of air gasification. Following these trends, higher mass loss was seen with air gasification of the lignin constituent. Addition of CO₂ resulted in a slower rate of mass loss after 520°C as seen with 20 and 40%.

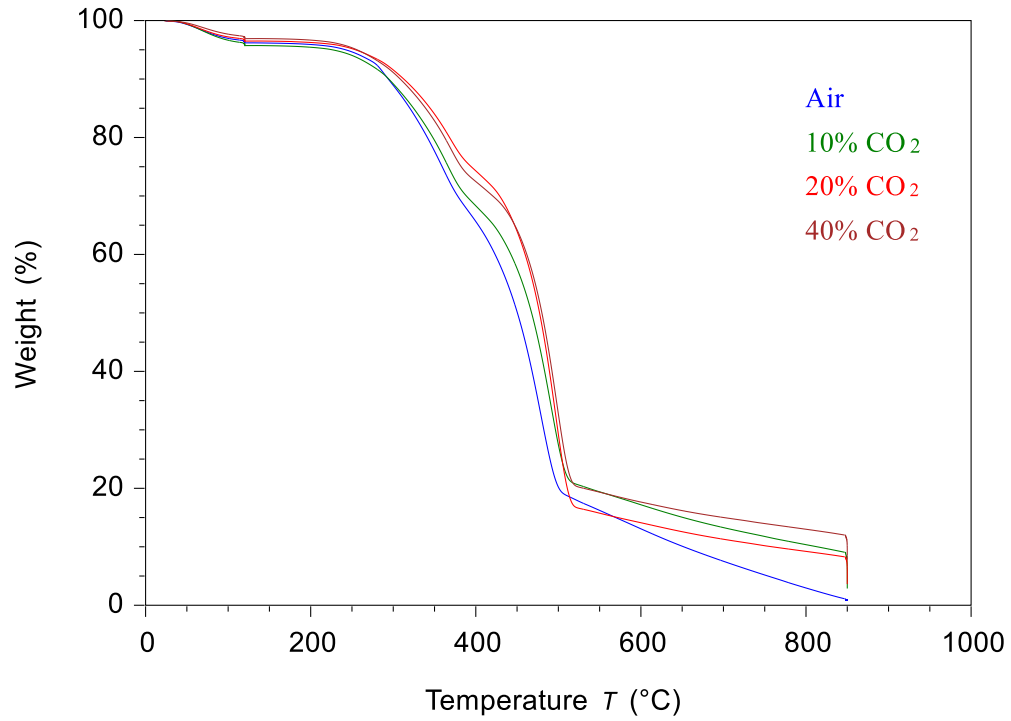


Figure 3-4: Mass loss curves of HDPE and Douglas fir (1:1) over temperature in air and CO₂

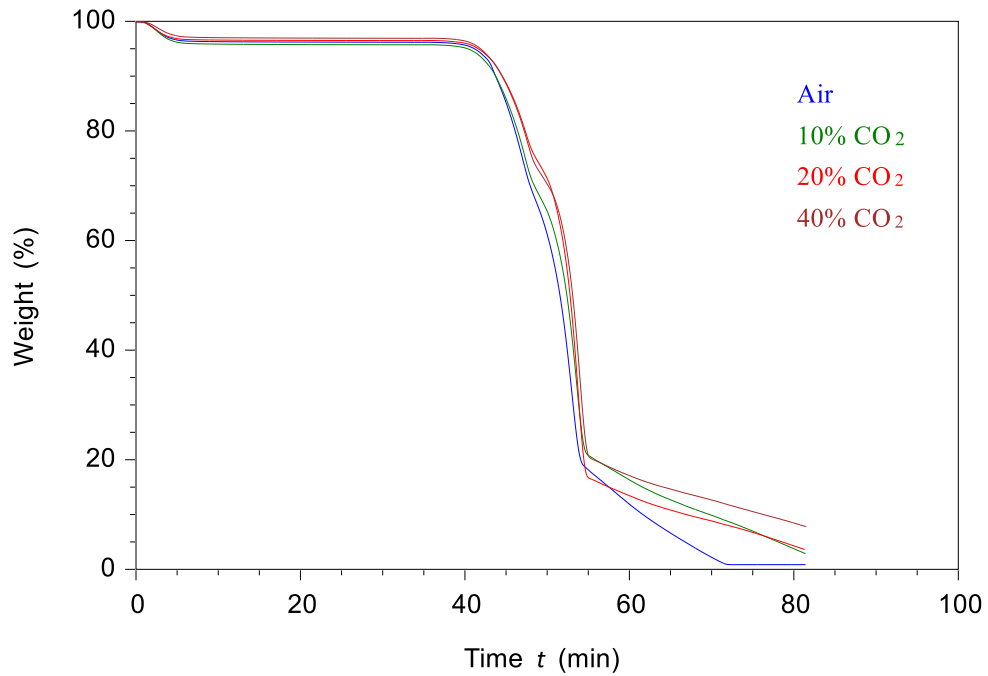


Figure 3-5: Mass loss curves of HDPE and Douglas fir (1:1) over time in air and CO₂

Figure 3-6 shows the derivative thermogravimetric curves of the TGA runs in Figures 3-4 and 3-5. For each curve, three distinct peaks can be seen. The first is the loss of moisture during the drying stage at 100°C. The second is the devolatilization stage of the Douglas Fir, where air had a slightly higher rate of mass loss compared to the CO₂ runs. The greatest change is seen with the melt phase of the plastic, where the air run has the fastest initial rate of mass loss at 0.23 wt%/°C at 400°C, peaking at a rate of 0.76 wt%/°C at 462°C. However, the 20 and 40% injected CO₂ runs surpass the air and 10% runs at 480°C, peaking 1.12 and 1.04 wt%/°C. Figure 3-6 illustrates an increased rate of mass loss with the addition of CO₂ to air gasification of HDPE and Douglas fir.

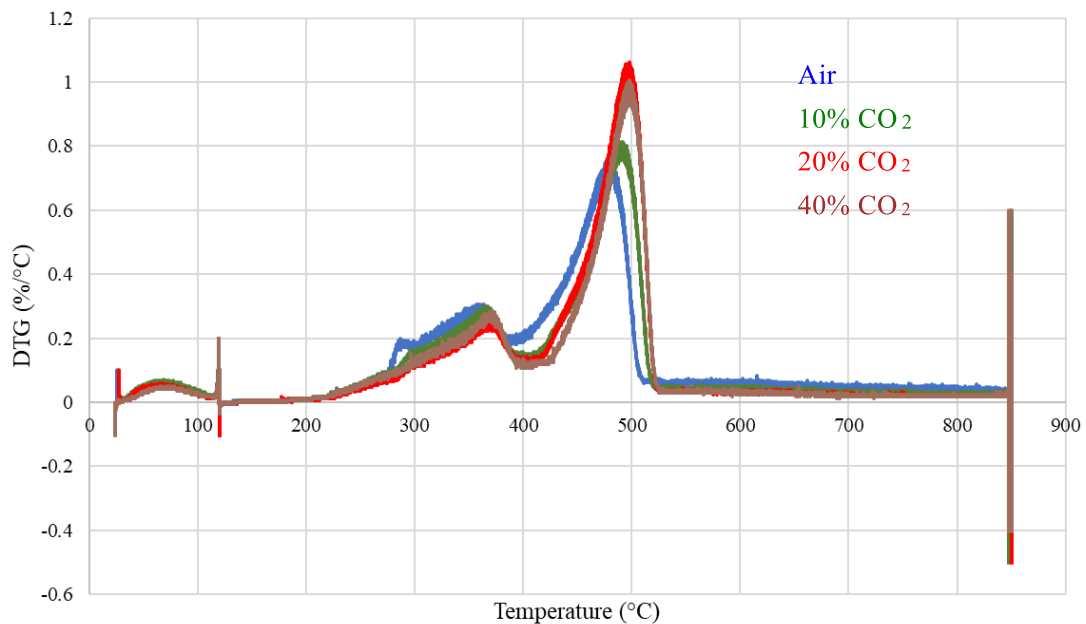


Figure 3-6: DTG curves of all TGA runs with air (ER=0.3) and injections of CO₂

3.2.3 TGA Final Char/ Residue Analysis

Figures 3-7 and 3-8 show the final weight % of the char residues produced with increasing amounts of CO₂ added to the air gasification medium. These are the chars that came from the TGA runs described in section 3.2.2. The maximum temperature was 850°C with a ten-minute dwell at the maximum temperature. Figure 3-7 shows that char mass increases with increasing CO₂ flow. When 40% CO₂ is added, there is 7.8% char residue compared to only 0.9% with only air. Figure 3-8 compares the amount of residue before and after the ten-minute dwell at the maximum temperature of 850°C. In this case we see that the addition of CO₂ results in a higher

amount of residue both before and after the dwell. However, under air, most of the reaction takes place before the temperature reaches 850°C, therefore the dwell does not have a significant impact on the amount of residue. Under CO₂, there is more solid residue remaining when the temperature reaches 850°C, and then there is a more significant mass loss during the dwell. This suggests that if the dwell time was increased, higher conversion could be achieved with CO₂, increasing the amount of syngas produced. Even though more CO₂ was added, Figure 3-8 highlights the slowness of the Boudouard reaction [63] and the faster oxidation of char with air.

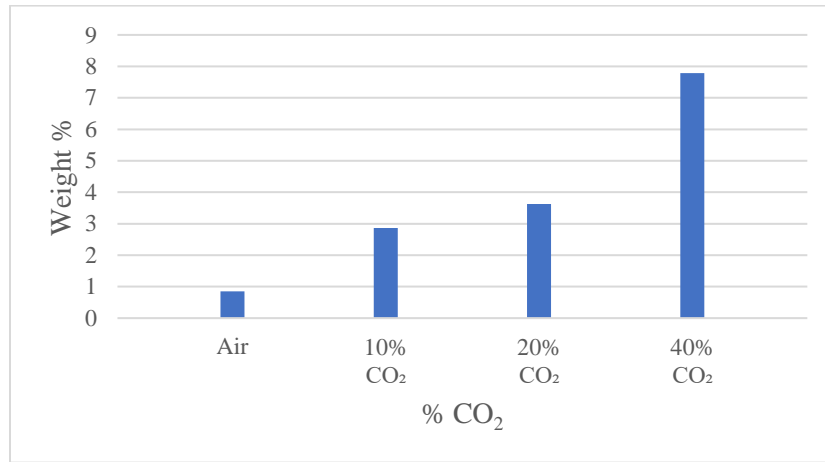


Figure 3-7: The final char residues recorded after dwell in air gasification with increasing percentages of CO₂ (HDPE and DGFIR mix at 850°C)

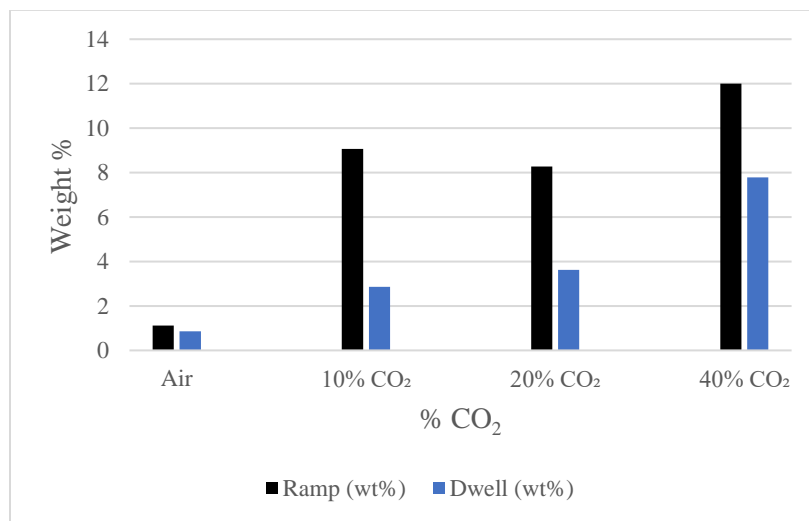


Figure 3-8: Comparison of final char after ramp to 850°C and after 10-minute dwell at 850°C

3.2.4 Fixed Bed Micro Gasifier Gas Composition and Yields

Gasification experiments with HDPE and DG fir 1:1 mixtures were done in a flow through micro gasifier to better understand the role of CO₂ injection on the air gasification process. Table 3-6 shows the tests done with constant input air flow and increasing CO₂ flow (added percent) for this section. Gas bag samples were taken at various times throughout the gasification test (during the ramp to 850°C) and the evolution of the primary gas species is reported here. The evolutions of all the gases for runs with ER 0.3 and 0.2 are shown in Appendix A. The following section will analyze trends of specific gases in detail however overall comparison's between the gases for the same run are illustrated in the appendix.

Figures 3-9, 3-10 and 3-11 illustrate the evolution of H₂, CO and CH₄ gases with increasing amounts of CO₂ in the input flow. Figure 3-9 shows that the addition of CO₂ to air gasification produces less H₂ at every temperature. This trend was most evident at 40% CO₂, where a minimum of 10 ml/min difference in hydrogen was seen at every recorded temperature below 850°C between the air and 40% runs. The highest hydrogen production in all runs was seen at 600°C, with air gasification recording 23 ml/min compared to 40% CO₂ recording 10 ml/min. 10 and 20% CO₂ followed very similar trends in hydrogen production until 700°C, where 20% produced a very similar hydrogen flow as the 40% CO₂ stream. Figure 3-10 illustrates the evolution of CH₄, where air, 10% and 20% CO₂ showed little change in CH₄ flow until reaching 600°C. For 40% CO₂, the overall output of CH₄ and H₂ gas was lower than that of the air, 10% and 20% runs. Looking at the TGA data in Figure 3-4, there was greater mass loss with just air compared to the 40% CO₂ injection run, which could explain the lower CH₄ and H₂ production with CO₂ injection. Another mechanism that has been proposed at this temperature range, is the melt phase of the plastic acting as a hydrogen donator, therefore transferring hydrogen due to the cracking of polymer chains, which stabilize biomass formed radicals, resulting in higher condensable fraction's [9].

Table 3-6: Input flowrates of air (O₂ and N₂) and CO₂ for each MG run

Tests	Initial Mass of solid feed (g)	Vol% CO ₂	Input Flows (ml/min)		
			O ₂	N ₂	CO ₂
1	10	0	88.2	331.8	0.0
2		10			46.7
3		20			105
4		40			280

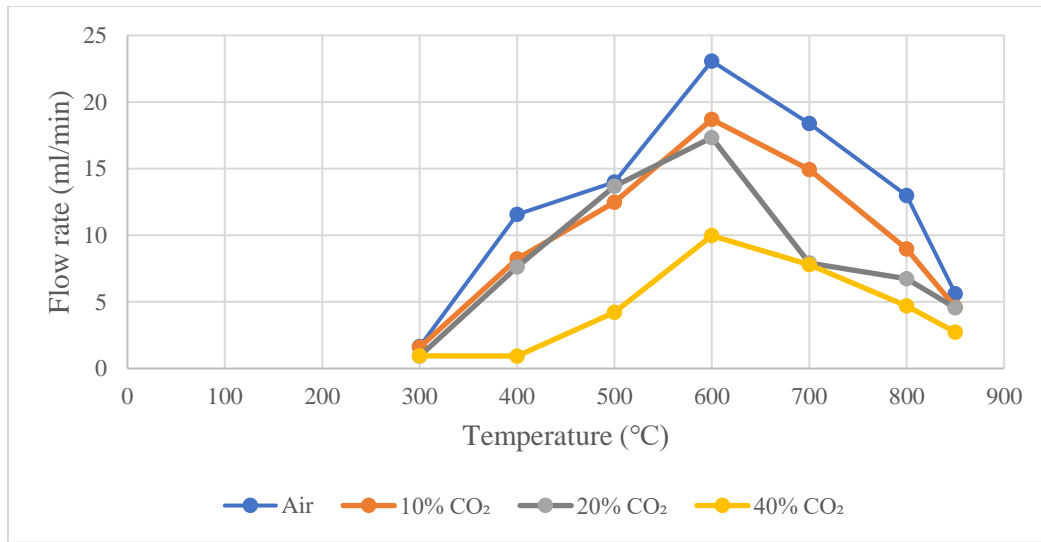


Figure 3-9: Evolution of hydrogen gas with increasing input flow of CO₂

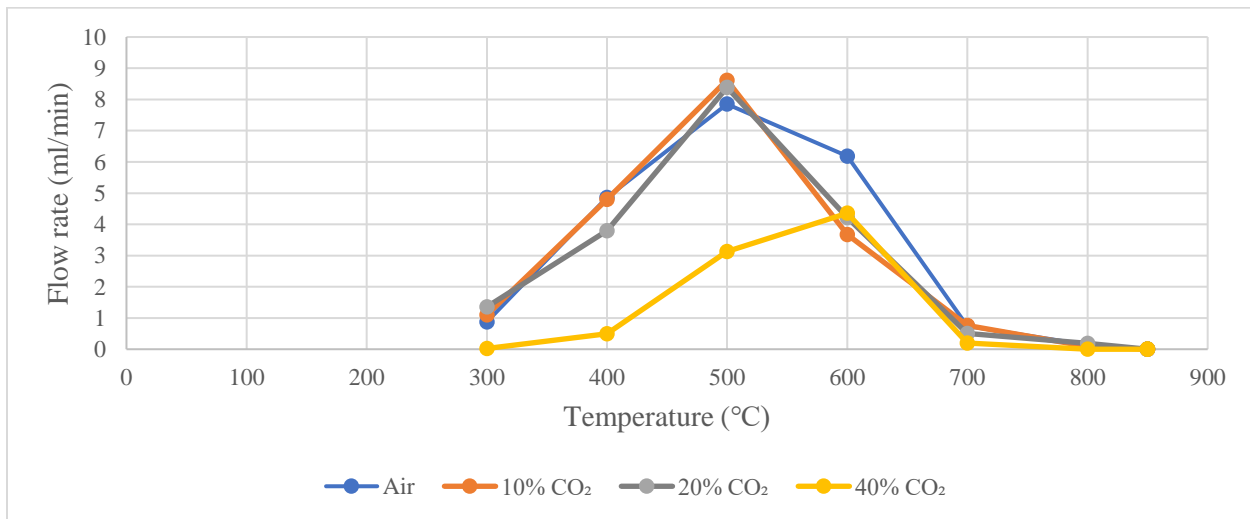


Figure 3-10: Evolution of methane gas with increasing CO₂ input flow

The evolution of CO in Figure 3-11 highlights two key temperature ranges with observable change. While standard air and 10% CO₂ followed very similar trends, at 300°C, the CO flows for 20 and 40% CO₂ were lower. 400°C the CO flow was higher with 40% CO₂ and lower with 20% CO₂. This trend consistent with the lower H₂ and CH₄ flow rates and lower mass loss at this temperature in the TGA. This could be due to the water gas shift reaction, corresponding to the increase and CO and decrease in H₂. After increasing the temperature past 600°C, there was an increase in the production of CO with added CO₂. The CO production increased significantly in 40% CO₂, peaking at 850°C with a flow rate of 87 ml/min, while air gasification was the lowest at 24 ml/min. This is most likely due to the Boudouard reaction, becoming more prevalent between 700-750°C. Figure 3-12 depicts the emergence of C₅H₁₂ with the addition of CO₂ to air gasification. Pentane was not present in the gas phase with only air gasification (ER 0.3), and only emerged with the introduction of CO₂.

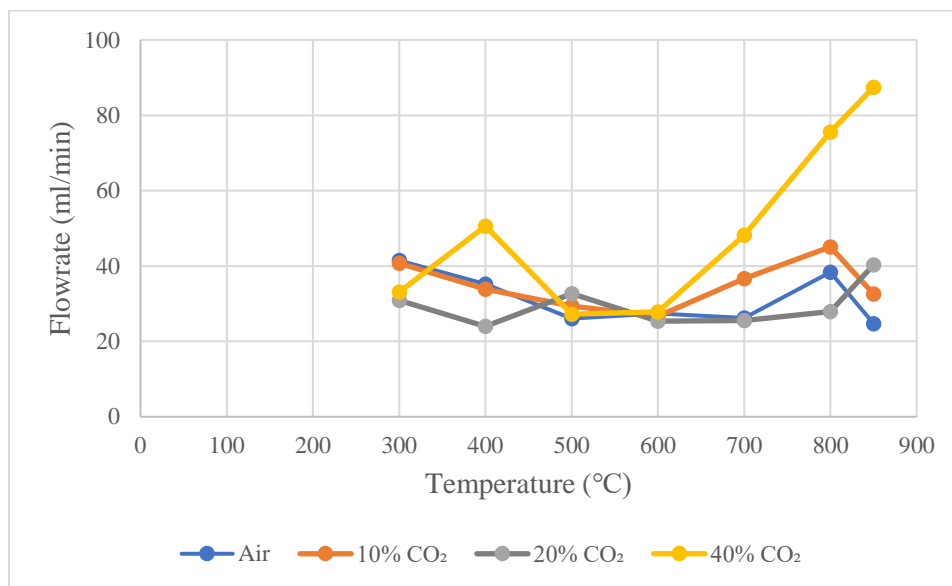


Figure 3-11: Evolution of carbon monoxide gas with increasing CO₂ input flow

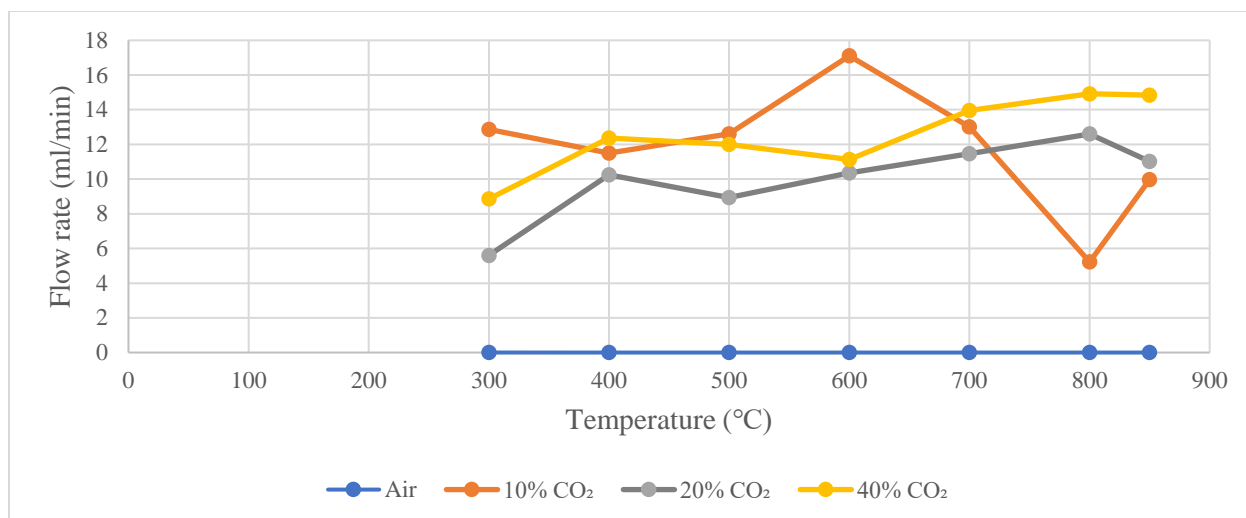


Figure 3-12: Evolution of pentane gas with increasing CO₂ input flow

Previous figures in this chapter portrayed the evolution of gases that were formed by gasification reactions with CO₂ and O₂ (from air). Because CO₂ is a co-reactant that is injected into the reactor and is also a product that can be formed from the feedstock, it is important to look at the CO₂ balance for the process to understand if the process results in a net conversion of CO₂ to CO. Figures 3-13 and 3-14 portray the changes in flow of this co-reactant. Figure 3-13 shows the changes in output flow of CO₂ relative to the CO₂ flow into the system and Table 3-6 shows the input flows of CO₂ for comparison. Air gasification (blue), where no CO₂ was mixed into the input flow of the MG reactor, consistently produced over 50 ml/min of CO₂ at every temperature. The addition of 10, 20 and 40% CO₂ co-reactant (46.7, 105 and 280 ml/min respectively) to the input flow, resulted in a higher output flow of CO₂ throughout each of the runs. Figure 3-14 and Table 3-7 illustrate the overall change in the output flow of CO₂ subtracting the added input flow, to quantify the overall change in CO₂. By increasing the CO₂ fraction in the feed gas to 40%, we see a change in the gasification mechanisms, resulting in a net consumption of CO₂ at a rate of close to 50 ml/min. In comparison, under just air, there is a net production of CO₂ of 50 ml/min. The addition of CO₂ to the input flow reduced its production at every stage of the gasification except with 10% CO₂ at 600°C, which can be assumed to be within reasonable error. As more CO₂ is added to the system, a greater extent of CO₂ conversion is observed, as the equilibrium of the process changes. This trend was most significant at 300°C for 20 and 40% CO₂. This temperature range further demonstrates the

presence of CO₂ is related to the reduced mass loss shown in the TGA. Various changes in the overall output flow were seen with each of the added percentages of CO₂ at 600°C. This would be influenced by the reverse water gas shift reaction and the dry reforming reactions.

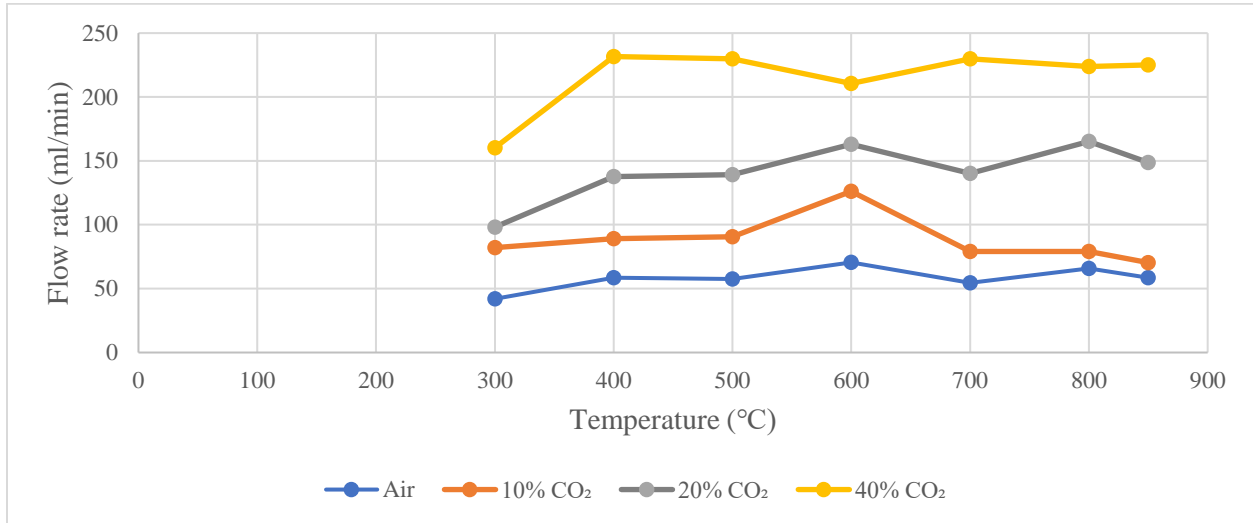


Figure 3-13: Evolution of CO₂ gas with increasing CO₂ input flow

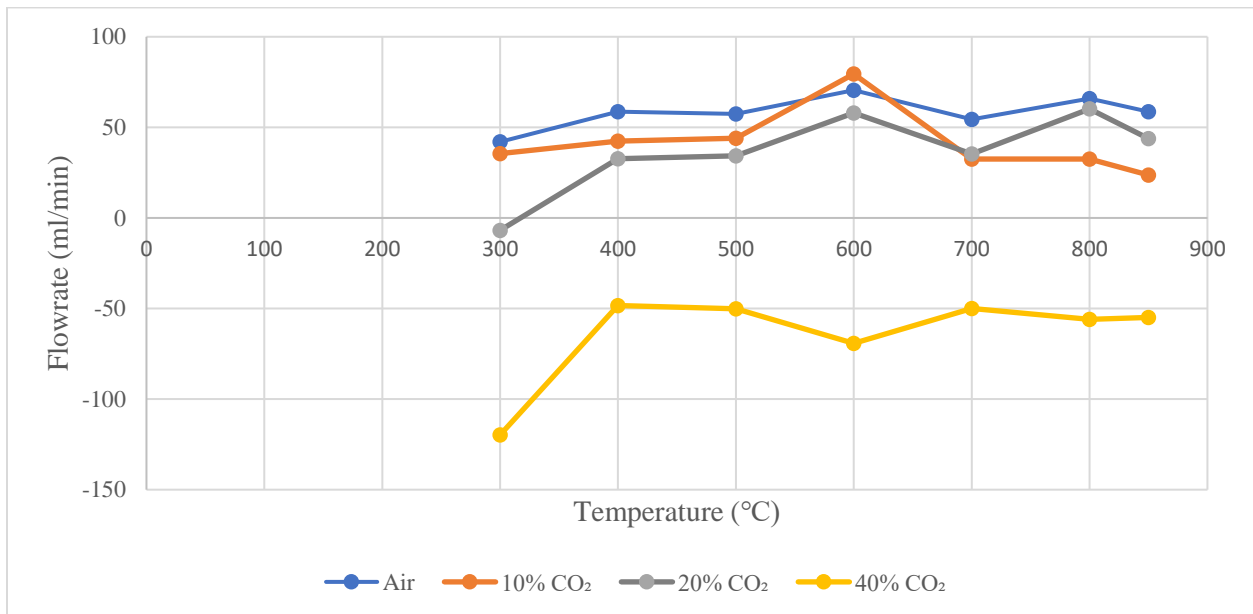


Figure 3-14: Flowrates output of CO₂ gas with increasing input flow of CO₂

Table 3-7: Overall change in CO₂ flow based on input flow

Temperature (°C)	Air	10% CO ₂	20% CO ₂	40% CO ₂
	ΔCO ₂ Flow rate (ml/min)			
300	42.0	35.4	-6.8	-119.8
400	58.6	42.3	32.7	-48.3
500	57.5	44.0	34.2	-50.2
600	70.5	79.5	58.0	-69.3
700	54.4	32.5	35.3	-50.0
800	65.9	32.5	60.2	-56.1
850	58.7	23.7	43.8	-55.0

3.2.5 Fixed Bed Micro Gasifier Char Composition and Yields

Figures 3-15, 16 and 17 show the final char residues recorded after each run in the MG and these are discussed with the TGA data in section 3.1.3. Figure 3-15 illustrates the final mass residues of the MG char. All final char masses were less than 2.5% relative to the loaded feed (10 grams). From the proximate analyses of HDPE and Douglas fir, the expected ash content would be 1%. Figure 3-16 compares these MG chars to those recorded in the TGA. Each of the MG chars with added CO₂ were lower than those in the TGA. The TGA had exceptional temperature control and was able to provide mass measurements throughout the test run. After completing the programmed method, the TGA furnace would lower, and air would cool the sample automatically. The MG was a larger scale fixed bed, and it required 40 minutes of nitrogen cooldown time, during which it is possible that some additional reactions could have taken place. In addition, the MG was a flow through system where there was high contact between all of the feedstock and the reactive gases. In contrast, the TGA provided a small sample on a pan with gas flowing around the sample. This could explain the higher degrees of mass loss with the MG experiments compared to the TGA experiments.

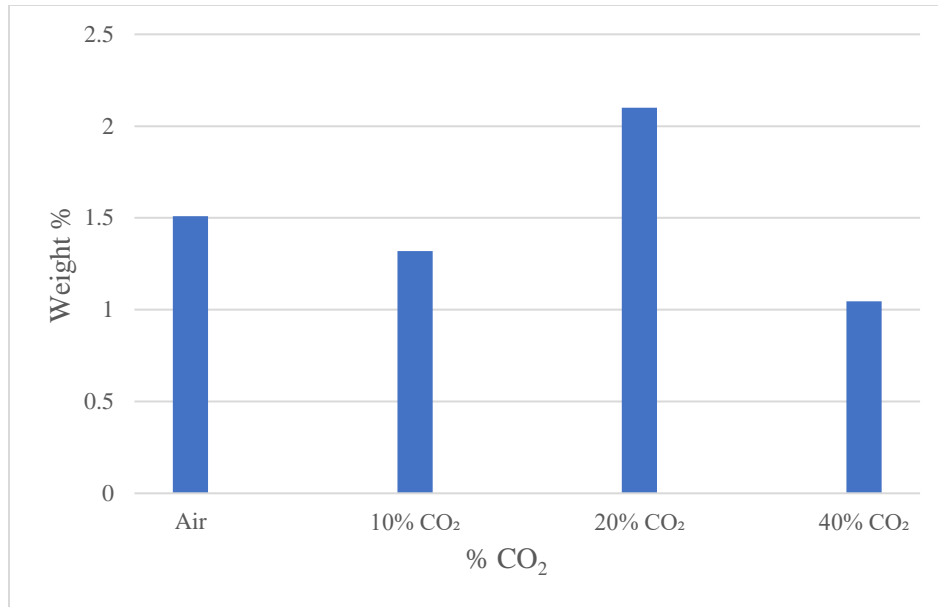


Figure 3-15: Final char mass in MG with increasing input flow of CO₂

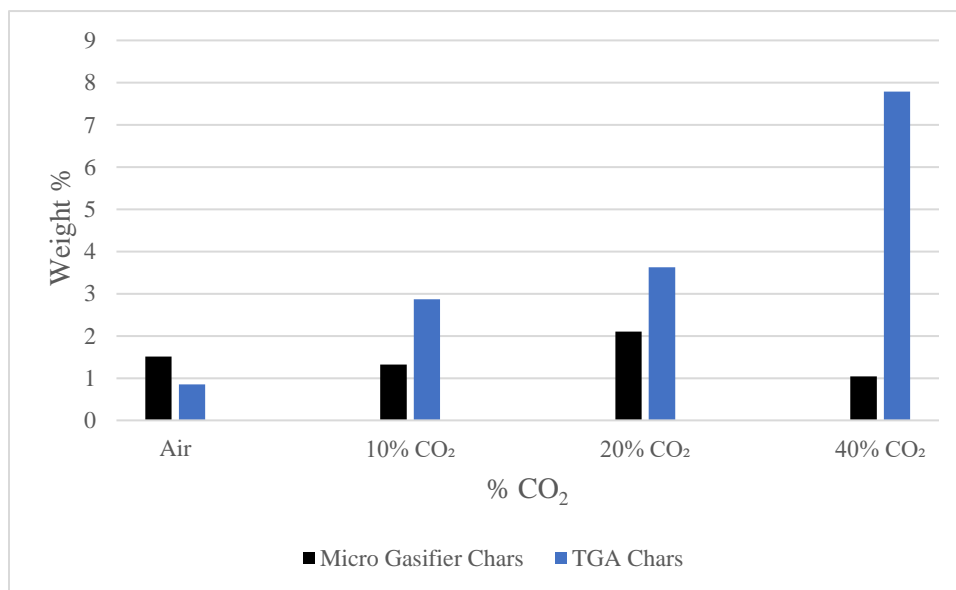


Figure 3-16: Comparison of final char masses in TGA and MG

Figure 3-17 portrays the elemental analysis of the chars collected from the MG reactor. With air only, the residue was primarily ash with 0.3% carbon. The most significant differences in the composition of the other samples are observed with the carbon. The increase of CO₂ from 10-40% lowered the final carbon weight percent of the char, which is likely due to the Boudouard reaction.

Eq 3 Boudouard Reaction $C + CO_2 \rightarrow 2CO$

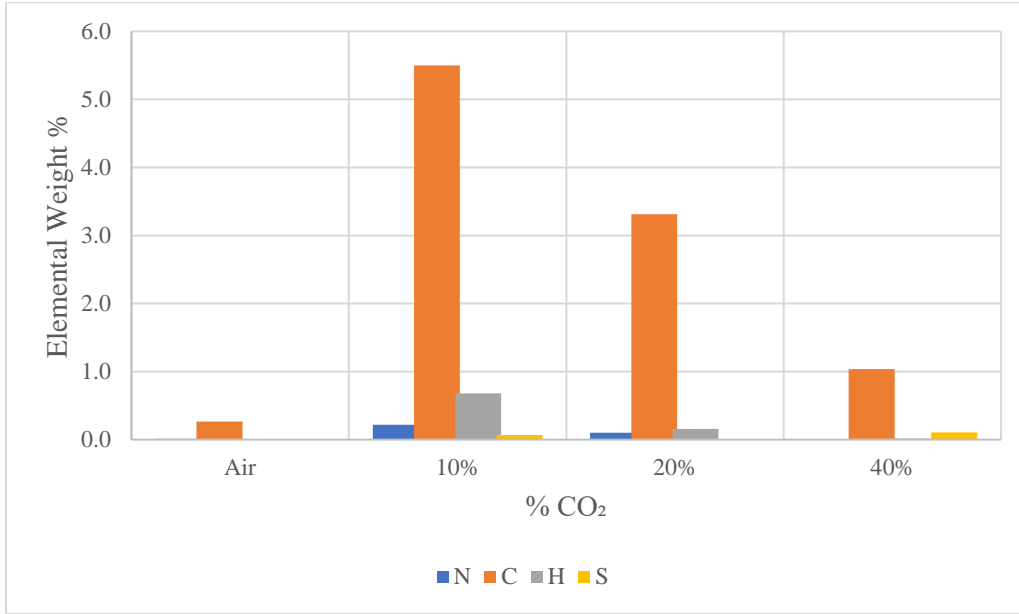


Figure 3-17: Elemental compositions of chars from MG with increasing input flow of CO₂

3.2.6 Influence of CO₂ in Fixed Bed Micro Gasifier

A carbon balance was done for the MG in order to evaluate the overall carbon conversion, and understand the breakdown of the gas, tar and char products. For a 10-gram run, 6.788 grams of carbon would theoretically be placed in the fixed bed reactor. The CO₂ that was injected into the system for certain runs was accounted for when calculating the output of CO₂. The gas flowrates were extrapolated over 5 minutes of assumed production and summed. Then the flows were converted into moles and mass of carbon. Elemental analysis was done with all of the chars, therefore the difference would be the remaining carbon found in the tars/liquid portion. Table 3-8 outlines the carbon distribution among the products. Due to the high volatile matter content of plastics, the tar/liquid constituent was very high for all runs. This could explain the very high output of pentane as seen in Figure 3-12. However, the introduction of CO₂ lowered the wt% of tars and in turn increased the output of the gas, improving the systems carbon conversion by 20 carbon wt%.

Table 3-8: Carbon balance of MG runs with ER 0.3

Runs	Carbon Weight (g)			Carbon Weight %		
	Gas	Char	Tar*	Gas	Char	Tar
Air	1.86	0.0004	4.93	27.4	0.006	72.6
10% CO ₂	3.62	0.007	4.12	46.7	0.09	53.2
20% CO ₂	4.84	0.007	4.06	54.3	0.08	45.6
40% CO ₂	6.76	0.001	5.65	54.5	0.008	45.5

*By difference

Figure 3-18 shows the energy of the produced syngas (CO and H₂) at all temperatures recorded. This was calculated by multiplying the flow rate of H₂ and CO individually by their LHV (10.78 and 12.63 MJ/Nm³ for hydrogen and carbon monoxide gas). These were then plotting along the recorded temperatures. The injection of CO₂ as a co-reactant increased the overall energy densities of the output syngas in most cases. This increased greatly with the production of CO as seen with 40% CO₂ after 600°C. This indicates that by adding CO₂ to the gasification system, a gaseous stream with a higher heating value is produced. Therefore, this could provide a pathway for converting CO₂ into fuel without the use of expensive catalysts or high-pressure reactors. From Figure 3-18, there is crossover between the runs at different temperatures therefore, the total energy of the combined CO and H₂ streams was calculated and shown in Table 3-9. Each individual curve was integrated over the elapsed time (the first point, 300C° for 2.5 minutes and the others for 5 minutes) to calculate the total energy density of the syngas. The highest energy densities were found to be with CO₂ injections, with the 40 vol% being the highest at 23.1 kJ.

Table 3-9: Total energy of syngas (CO and H₂) ER 0.3

Air	10% CO ₂	20% CO ₂	40% CO ₂
Energy (kJ)			
13.1	18.1	15.9	23.1

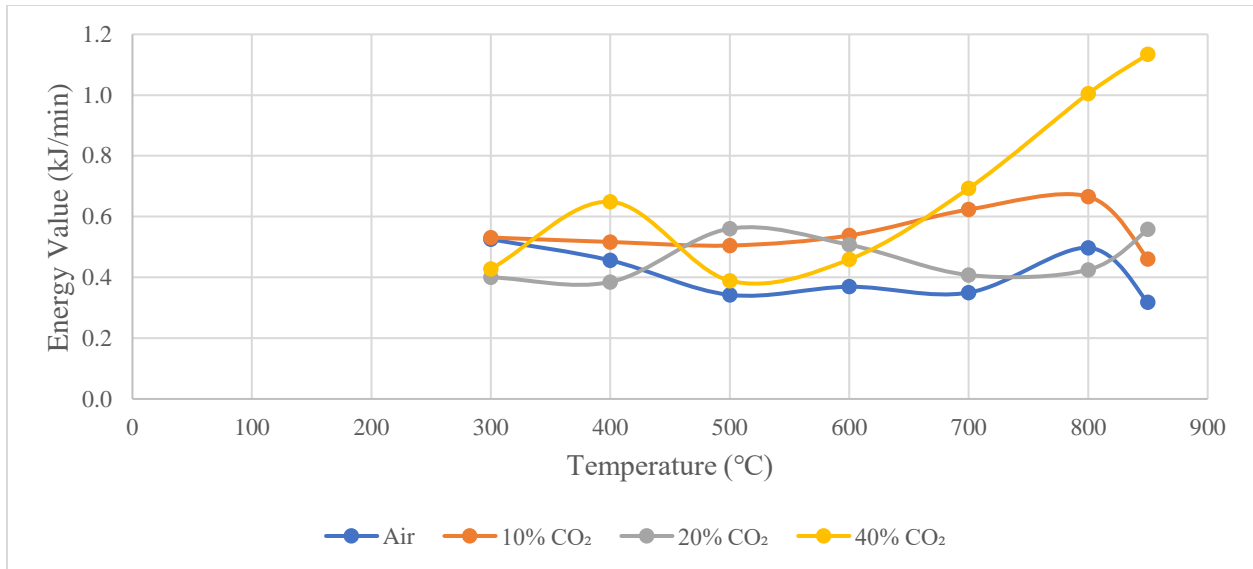


Figure 3-18: Combined energy of syngas at different temperature with increasing input flow of CO₂

Figure 3-19 compares the molar ratio of hydrogen and carbon monoxide (H_2/CO) in the syngas which is an indicator for how the syngas can be used. At all recorded temperatures, the addition of CO₂ reduced the overall hydrogen/carbon monoxide ratio. This would not be ideal for chemical synthesis given the lower H_2/CO ratios. This is a definite drawback with CO₂ gasification, the reduction in hydrogen gas. However, after considering all three figures, the injection of 10% CO₂ improved carbon conversion by 20 carbon wt% and increased the overall energy density of the syngas.

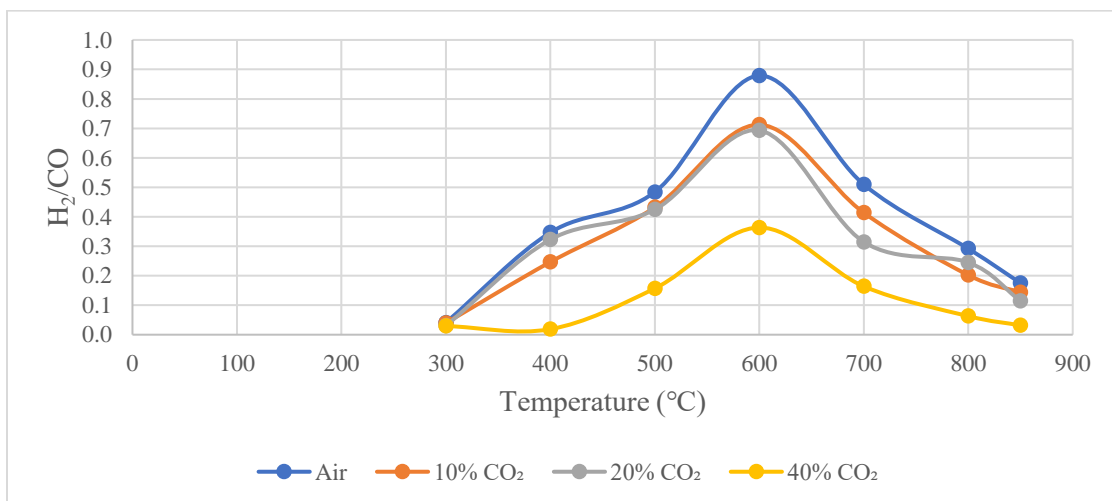


Figure 3-19: Changes in molar hydrogen and carbon monoxide ratio of syngas (H_2/CO)

3.3 Influence of CO₂ injection at Equivalence Ratio of 0.2

3.3.1 Experimental Test Plan

The objective of this section was to understand the influence of CO₂ injection at an equivalence ratio of 0.2. This ratio was chosen because typically gasification shows the best performance at equivalence ratios between 0.2-0.4. This lower equivalence ratio means less oxygen is injected into the system, which reduces the extent of complete combustion (which produces CO₂ and H₂O) and increases the extent of partial oxidation, producing desired products of H₂ and CO. However, lower equivalence ratios can also result in higher production of tar and char. The following tables summarize the parameters for the tests done with the TGA and MG for this section. The results from the two test systems were compared in order to better understand the reactions taking place. Each test had a constant air flow rate, corresponding to an initial air to fuel ratio of 0.2 and tests were done with different amounts of CO₂ injected. Tables 3-10 and 3-11 show the corresponding test plans for the TGA and MG runs discussed in this section.

Table 3-10: Conditions for TGA runs for equivalence ratio 0.2

Test	Sample Mass (mg)	% CO ₂	Total Gas Flowrate (mL/min)	Ramp Rate (°C/min)	Dwell Time (min)	Max Temperature (°C)
1	50	0	1.65	20	10	850
2		10	1.83			
3		20	2.06			
4		40	2.75			

Table 3-11: Completed runs in gasifier for equivalence ratio 0.2

Micro-Gasifier						
Test	Sample Mass (g)	% CO ₂	Total Gas Flowrate (SLPM)	Ramp Rate (°C/min)	Dwell Time (min)	Max Temperature (°C)
1	10	0	0.280	20	10	850
2		10	0.311			
3		20	0.350			
4		40	0.467			

3.3.2 Adding CO₂ to Air Gasification (ER=0.2), TGA and Micro-Gasifier Analysis

Figures 3-20 and 3-21 illustrate similar mass loss curves as seen in section 3.2.2, binary mixtures of HDPE and Douglas fir in air gasification with increasing amounts of injected CO₂. Each of these curves are an average of three runs and therefore was repeatable. Similar to what was observed at an equivalence ratio of 0.3 (Section 3.2), for 10% and 20% CO₂ with an ER of 0.2, there was an initial slower mass loss before the plastic melt phase, in the temperature range of 280-380°C. With a lower equivalency ratio, increasing the volume of injected CO₂ increased the rate of mass loss in this devolatilization stage. Increasing the volume of injected CO₂ in air gasification with an ER of 0.3, slowed the mass loss rate at this stage. However, at this stage for ER 0.2, 10% injected CO₂ had the slowest mass loss rate. Furthermore, 40% CO₂ had the fastest rate of mass loss, surpassing the air gasification curve.

As the plastic melt phase began to decompose, the rate of mass loss for 10% injected CO₂ increased until 520°C. This followed the same trends seen with the ER 0.3 runs, where there is a slower mass loss rate until the plastic melt phase undergoes random scission. After the plastic melt phase began to degrade, slower mass loss rates were seen with 20 and 40% CO₂ in comparison to air and 10% CO₂. At temperatures above 520°C, 40% CO₂ had that highest rate of mass loss throughout the ramp to 850°C.

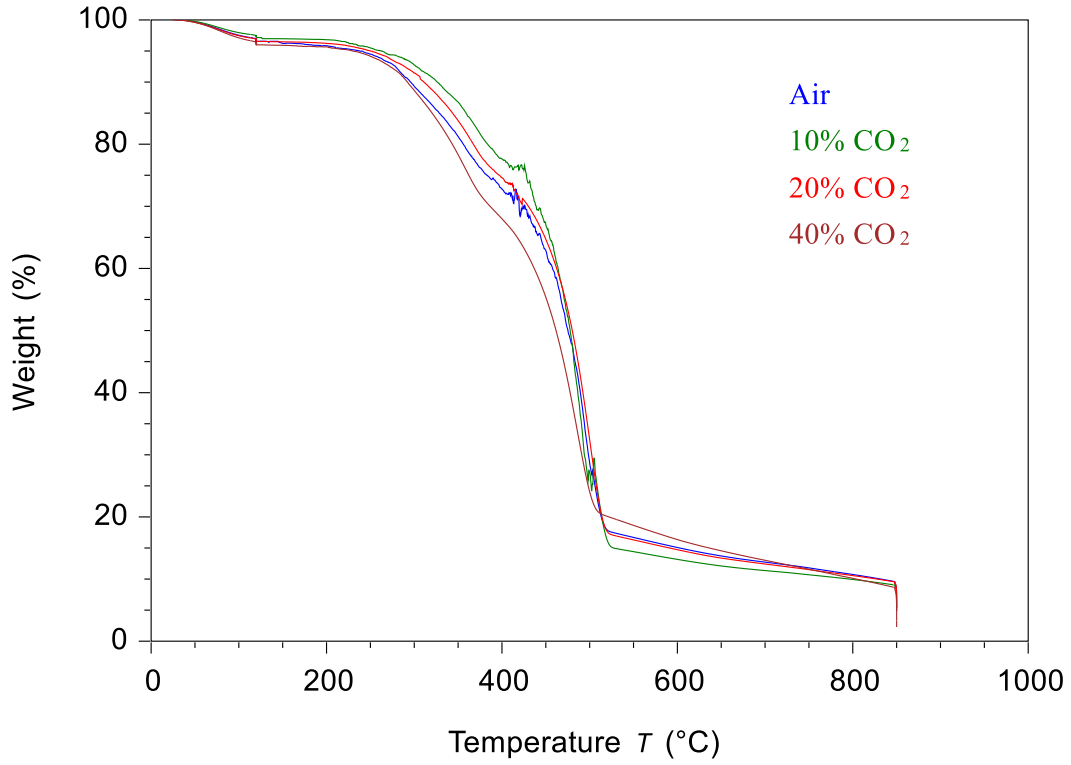


Figure 3-20: Mass loss curves of HDPE and Douglas fir (1:1) over temperature

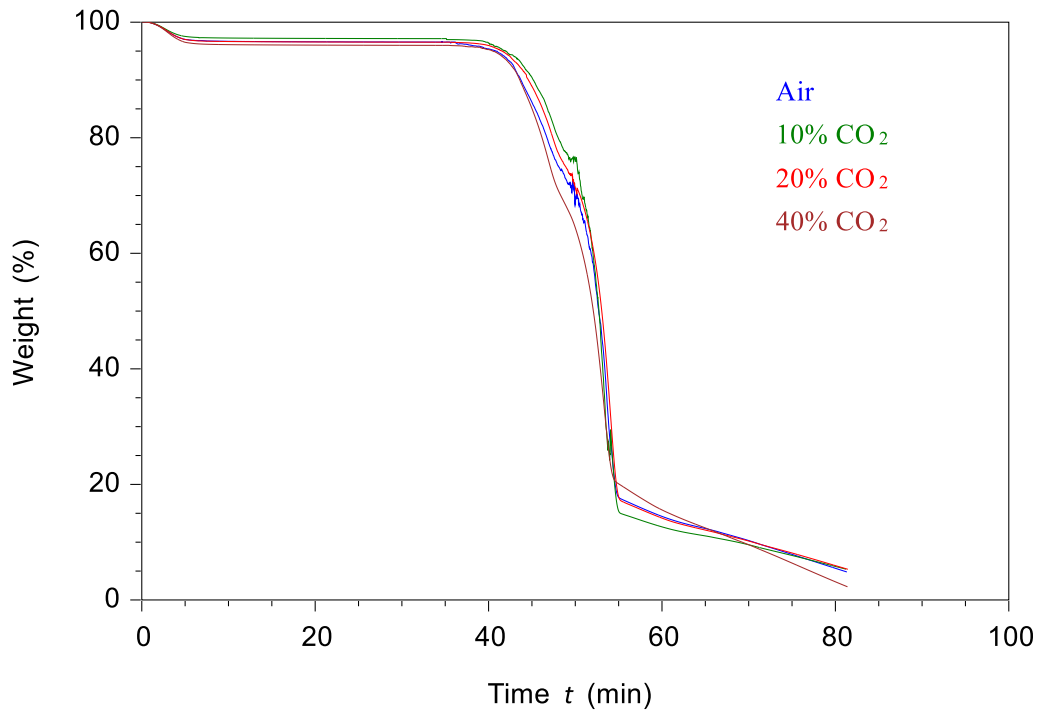


Figure 3-21: Mass loss curves of HDPE and Douglas fir (1:1) over time

3.3.3 TGA Final Char/ Residue Analysis

Figures 3-22 and 3-23 show the final char residue after the initial ramp to 850°C and following a ten-minute dwell in the TGA. Figure 3-22 shows that the lowest final char weight % was found with added 40% CO₂ while 0, 10 and 20% CO₂ showed little change. Figure 3-20 illustrates that at the end of the ramp, the mass was very similar in all runs. After the dwell, a mass loss is observed at all conditions, with the greatest change in mass observed with 40% CO₂ over the 850°C dwell. Therefore, the addition of CO₂ resulted in a lower mass of the char in comparison to just air gasification at an ER of 0.2. The opposite trend was seen with more air in the 0.3 ER air gasification TGA runs. This is likely because at a lower equivalence ratio there is less oxygen available for partial oxidation, resulting in a lower conversion and slower rate of mass loss.

Figure 3-23 shows that the lowest final char weight % was found with 40% injected CO₂ while 0, 10 and 20% CO₂ showed little change. The final ramp mass was very similar in all runs, with the greatest change in mass loss found with 40% CO₂ over the 850°C dwell. Therefore, the addition of CO₂ reduced the overall mass of the char in comparison to just air gasification at an ER of 0.2. The opposite trend was seen with more air in the 0.3 ER air gasification TGA runs. The Boudouard reaction would be the most logical explanation for the increased mass loss over the dwell, because of the favourable temperature.

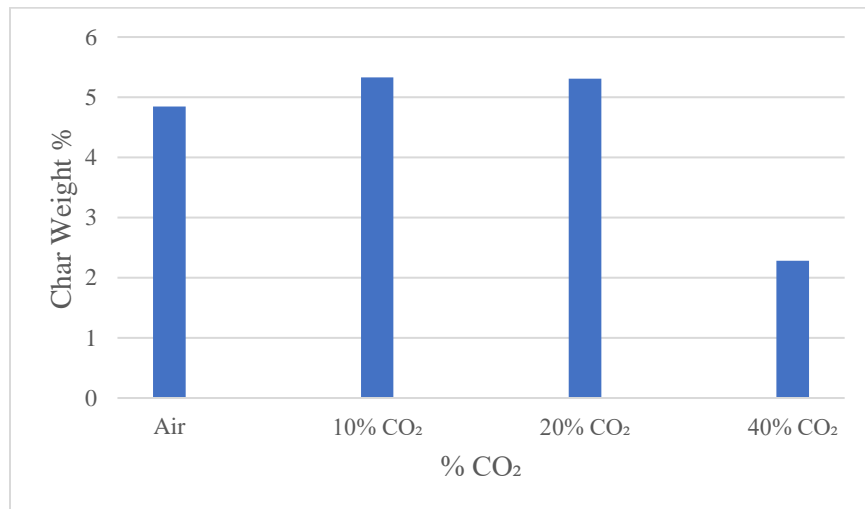


Figure 3-22: The final char residues recorded in air gasification with increasing percentages of CO₂

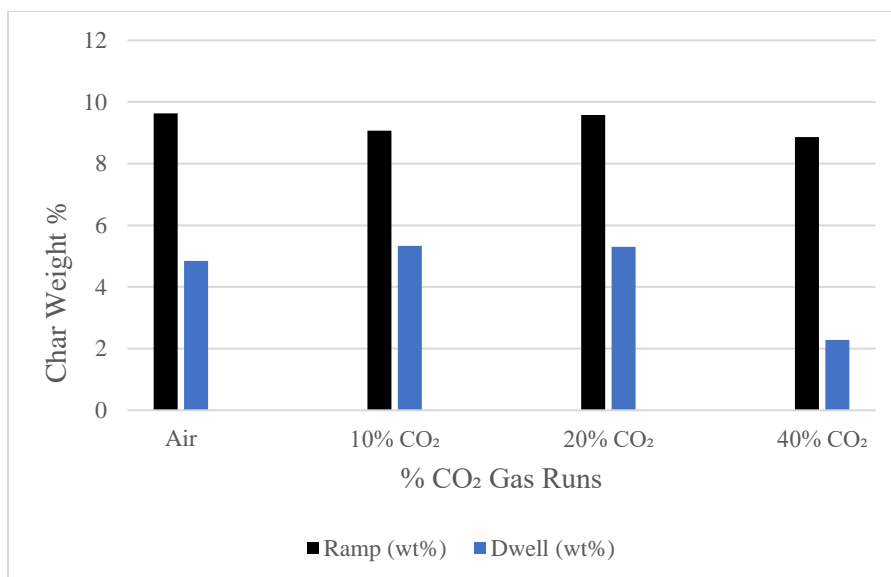


Figure 3-23: Comparison of final char after ramp to 850°C versus after 10-minute dwell

3.3.4 Fixed Bed Micro Gasifier Gas Composition and Yields

The following figures illustrate the gas evolution of the primary products that were identified at specific temperatures with the Micro-GC. The evolution of these gases will be analyzed alongside the mass loss profiles recorded with the TGA. Table 3-12 shows the tests done with constant input air flow with various CO₂ flow rates (0%, 10%, 20% or 40%) for this section.

Figures 3-24, 25 and 26 illustrate the evolution of H₂, CH₄ and CO gases throughout the tests, each with different amounts of CO₂ in the input flow. Figure 3-24 shows that the addition of CO₂ to air gasification above 20% produces less H₂ gas. With an equivalence ratio of 0.2, the reduction in H₂ gas production because of CO₂ injection was less than at an equivalence ratio of 0.3. While H₂ gas production was lower for air gasification with an ER 0.2 compared to 0.3, on a percentage basis, 40% CO₂ in 0.2 ER air gasification consumed 5 times less H₂ than 0.3 air gasification. For example, at 600°C, the H₂ flow was 1.8 ml/min lower in 40% CO₂ than in air at ER 0.2 whereas at ER 0.3 this difference was 13 ml/min. With an ER of 0.3, inherently there is a higher air flow rate. This also means even on a percentage basis there will be more injected CO₂ than in ER 0.2 runs. Therefore, the higher flow rates of CO₂ in ER 0.3, could be a factor for the lower production of H₂ gas. The hydrogen production peaked in air gasification at 800°C with 13 ml/min. 20 and 40% peaked at 700°C for 12 and 10.1 ml/min respectively. The overall lower

flow rates of H₂ were much less in 0.2 air gasification, even with similar trends seen with the TGA mass loss profiles in this temperature range.

Table 3-12: Input flowrates of air (O₂ and N₂) and CO₂ for each MG run

Tests	Initial Mass of solid feed (g)	Vol% CO ₂	Initial Flows (ml/min)		
			O ₂	N ₂	CO ₂
1	10	0	58.8	221.2	0.0
2		10			31.1
3		20			70.0
4		40			186.7

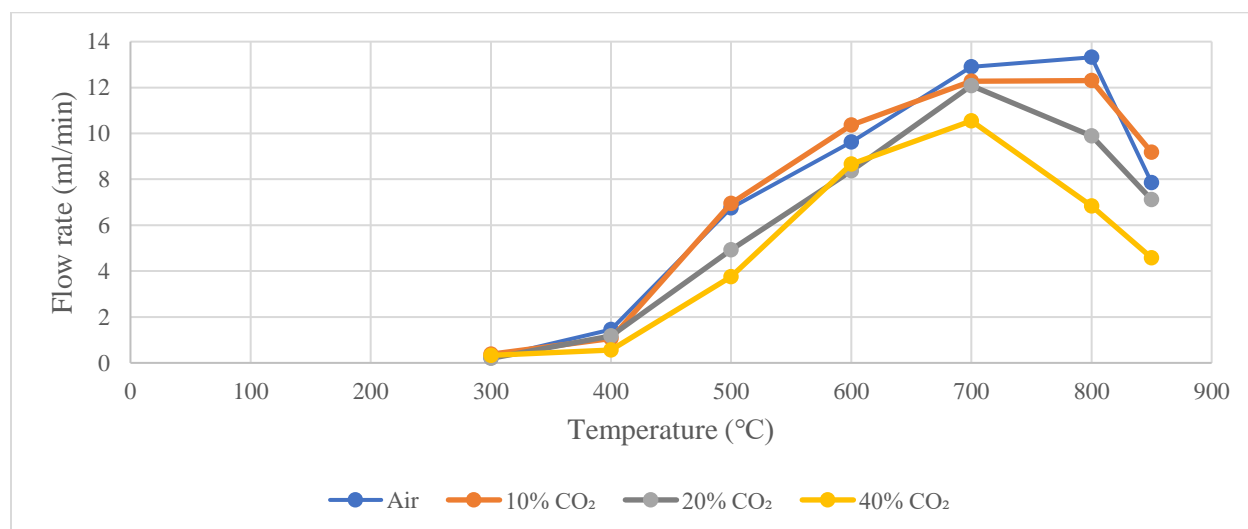


Figure 3-24: Evolution of hydrogen gas with increasing input flow CO₂

Figure 3-25 portrays the evolution of methane throughout all the ER 0.2 runs. There was not the significant reduction in CH₄ output at the lower temperature ranges as seen with ER 0.3 gasification, yet the output flows were still slightly lower. CH₄ during the devolatilization stage may be tied as closely with H₂ gas, as neither followed trends seen with ER 0.3 The delay in mass loss is still seen for both in the TGA profiles. At 600°C, the 20% and 40% CO₂ runs peaked with 10.1 and 8.2 ml/min of CH₄ gas respectively. The decrease seen after 600°C can be attributed to methane dry reforming.

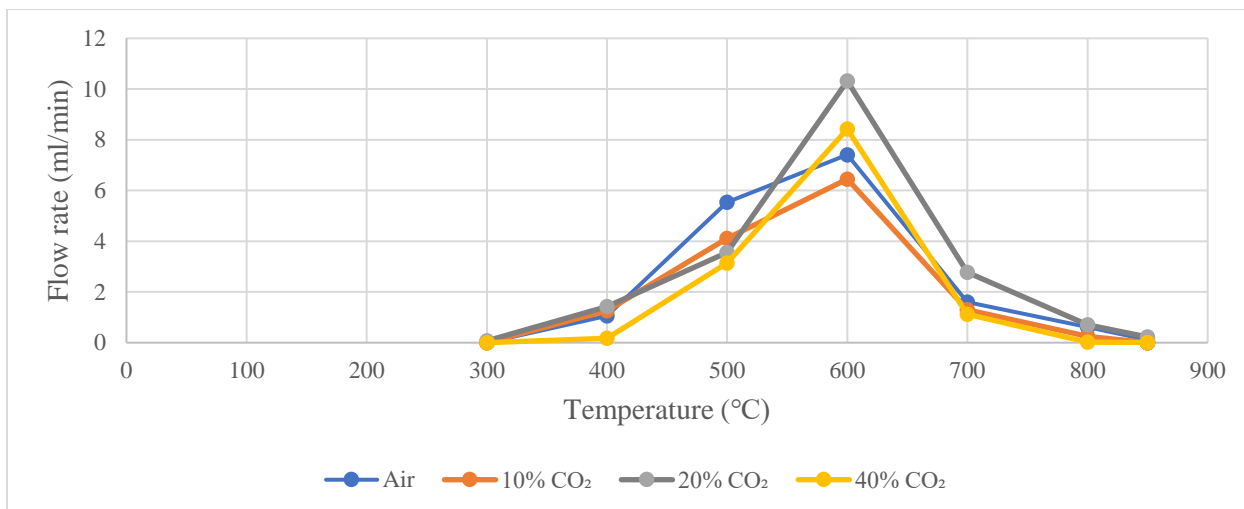


Figure 3-25: Evolution of methane gas with increasing CO₂ input flow

The evolution of CO gas is shown in Figure 3-26. There were very consistent changes in CO output flow with the addition of CO₂. Over 400°C, the CO flow increased for every run with added CO₂ compared to air gasification. CO flow increased with temperature after 600°C and peaked for all gases at 850°C with 40% CO₂ at 78 ml/min of CO gas. The flow rates of H₂, CH₄ and C₅H₁₂ begin to decrease as the CO is rapidly increasing. This could be due to the reverse water gas shift, dry reforming reactions which are more favourable over 700°C. Figure 3-27 shows the evolution of pentane gas, which was present in every run. 40% CO₂ had the highest overall output flow of pentane (12 ml/min) peaking at 700°C. Pentane gas was lower in ER 0.2 than 0.3 runs however it was also present in pure air gasification run. This would mean that the tars evolving from the plastic decomposition are not being cracked and oxidized at an ER of 0.2.

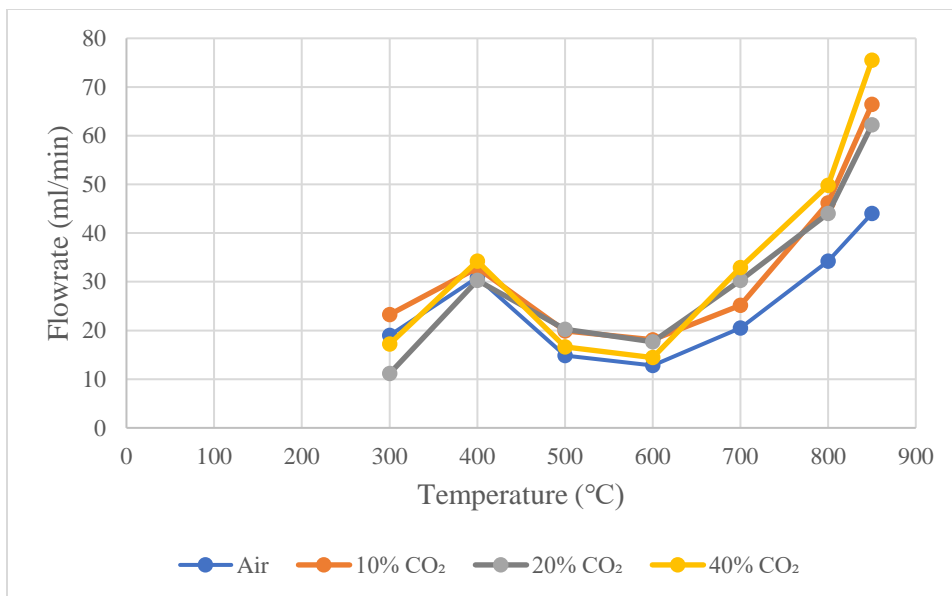


Figure 3-26: Evolution of carbon monoxide gas with increasing CO₂ input flow

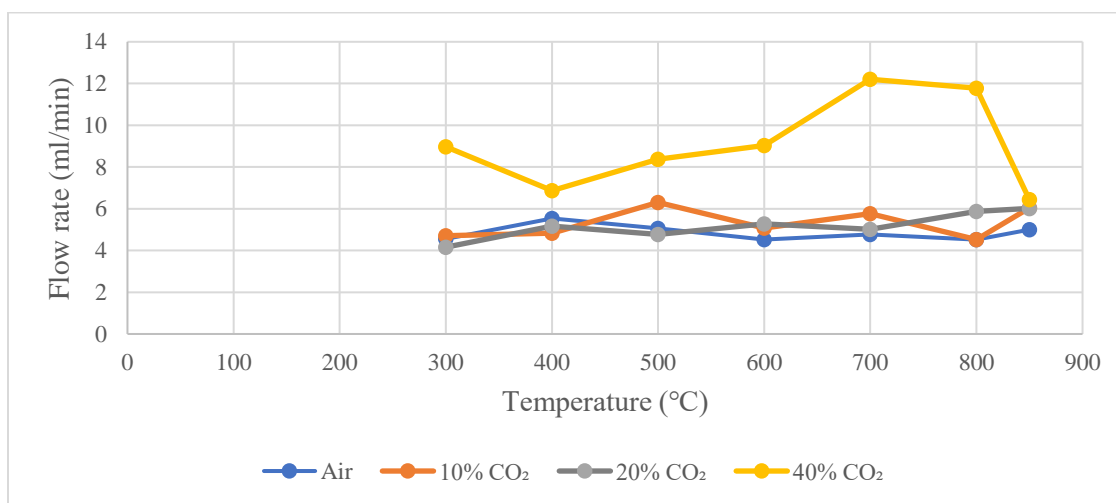


Figure 3-27: Evolution of pentane gas with increasing CO₂ input flow

Previous figures in this chapter portrayed the evolution of gases that were formed by gasifying with CO₂ and air. Figures 3-28 and 3-29 portray the changes in flow of CO₂. Because CO₂ is being added to the system and can also be a product of gasification, it is important to understand the net CO₂ generation or consumption. Figure 3-28 illustrates the changes in output flow of CO₂ and Table 3-12 shows the input flows of CO₂ for comparison. The addition of 10, 20 and 40% CO₂ as a co-reactant (31.1, 70 and 186.7 ml/min respectively) to the input flow increased the

output flow of CO₂ throughout each of the runs. For air gasification, over 20 ml/min of CO₂ was produced at every temperature throughout the run. Negative values in Figure 3-28 indicate a net consumption of CO₂ whereas positive values indicate a net generation of CO₂. The injection of CO₂ lowered the generation of CO₂. With just 10% CO₂ addition, there is a net generation of CO₂, indicating that the CO₂ introduced is not consumed, and additional CO₂ is generated from the gasification reactions. At higher CO₂ concentrations of 20% and 40%, there is a net consumption of CO₂, indicating that this process provides a low-cost pathway for converting CO₂ into CO. Under air, the net CO₂ production at 850°C is 22 ml/min whereas under 40% CO₂, there is a net consumption of 80 ml/min of CO₂. This changes the process from a CO₂ generating to a CO₂ consuming process. Even when the CO₂ consumption was reduced to 20%, there was an overall consumption throughout every stage of the decomposition. At lower temperatures the consumption of CO₂ at 20 and 40% was most prevalent and similar to the trends seen with ER 0.3 gasification. However, the production of H₂ and CH₄ in ER 0.2, 40% CO₂ did not change to the same extent as in ER 0.3.

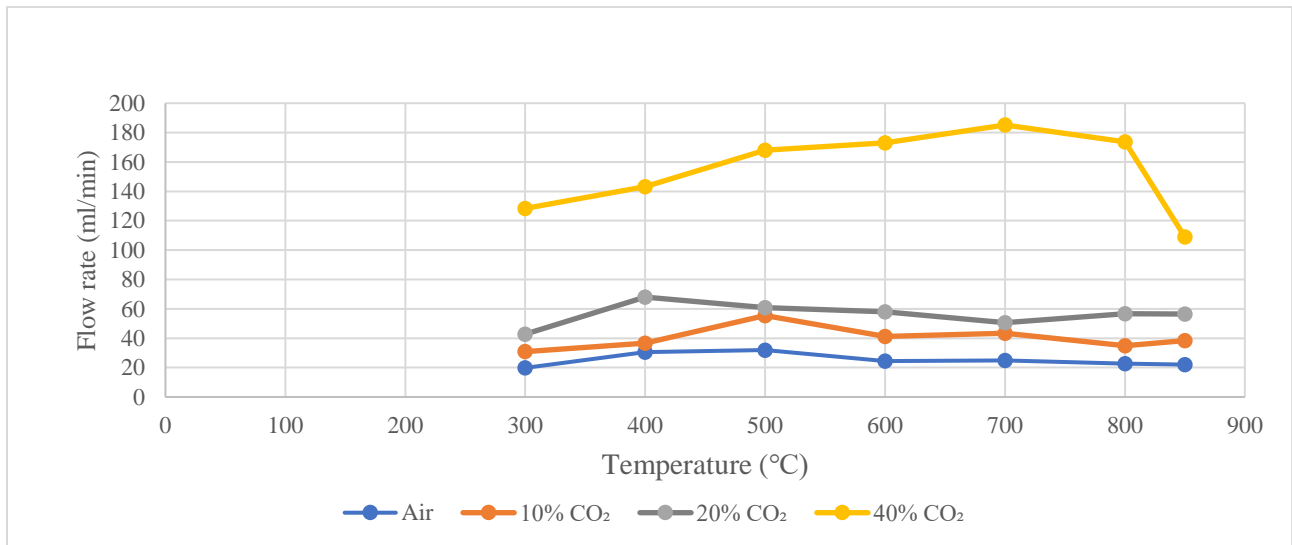


Figure 3-28: Evolution of CO₂ gas with increasing CO₂ input flow

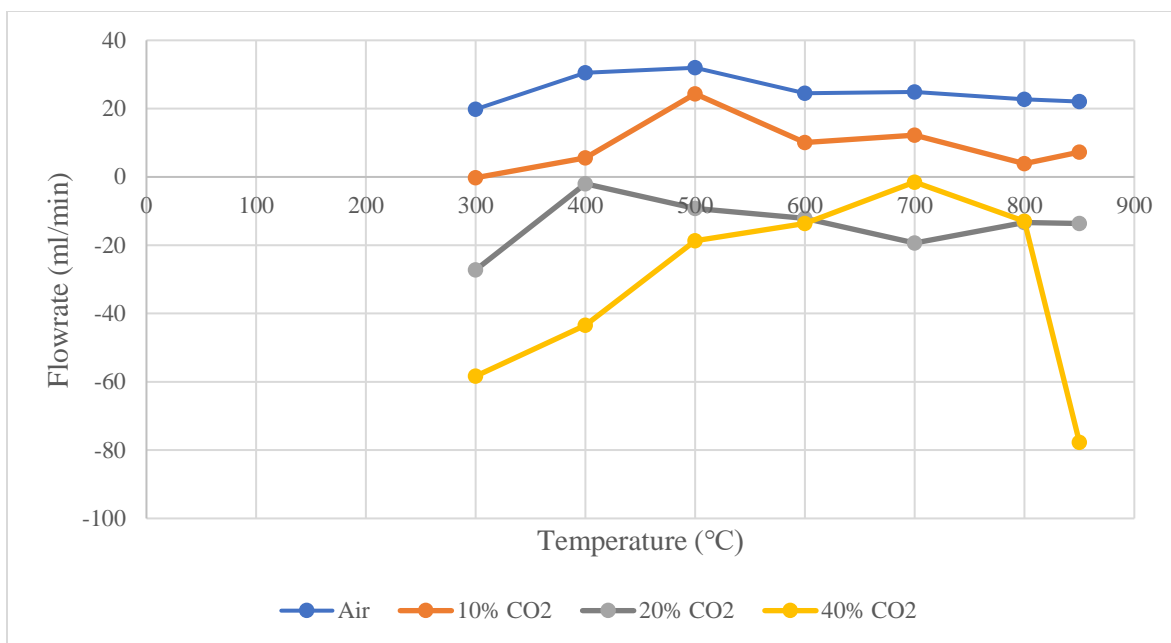


Figure 3-29: Output flow rates of CO₂ gas with increasing injection volume of CO₂

Table 3-13: Overall change in CO₂ flow based on input flow (ER= 0.2)

Temperature (°C)	Air	10% CO ₂	20% CO ₂	40% CO ₂
	Δ CO ₂ flow (ml/min)			
300	19.8	-0.2	-27.2	-58.4
400	30.5	5.6	-2.0	-43.4
500	32.0	24.3	-9.2	-18.7
600	24.5	10.1	-12.1	-13.6
700	24.8	12.3	-19.4	-1.5
800	22.7	3.9	-13.0	-13.0
850	22.0	7.3	-13.6	-77.7

3.3.5 Fixed Bed Micro Gasifier Char Composition and Yields

Figures 3-30, 31 and 32 show the final char residues after each run in the MG and these are discussed in connection with the TGA data in section 3.2.3. Figure 3-30 shows the final mass residues of the MG char, which were below 5 wt%. The mass of the final char was lower in the MG with the increase in CO₂, with 20% having the lowest final char weight. However, this is most likely an error given the cooldown apparatus for the MG. Figure 3-31 compares the final

TGA chars with the final MG chars. Air and 40% CO₂ were very similar however 10 and 20% CO₂ showed higher final chars in the TGA than the MG. Figure 3-32 shows the elemental distribution of the MG chars. The primary component in the char was carbon. The test that was done with pure air resulted in char with the highest carbon content, indicating that CO₂ injection supported char gasification. Increasing the amount of CO₂ added resulted in a lower carbon content in the char. 40% CO₂ had a higher final char mass and therefore higher carbon weight % than 20% CO₂. However, given that a higher flow of CO₂ was injected at 40%, there may be some error especially given the behaviours shown in Figure 3-31 with the TGA char.

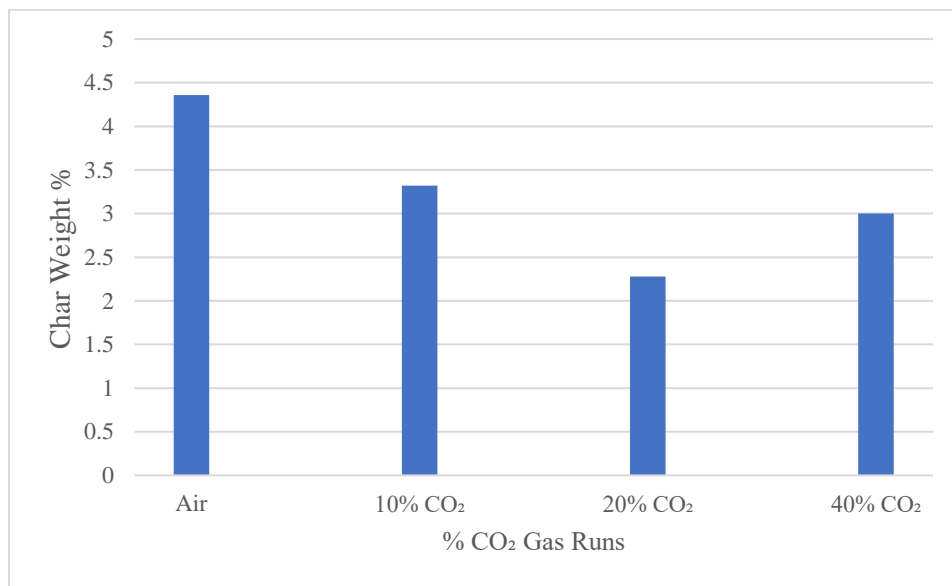


Figure 3-30: Final char mass in MG with increasing input flow of CO₂

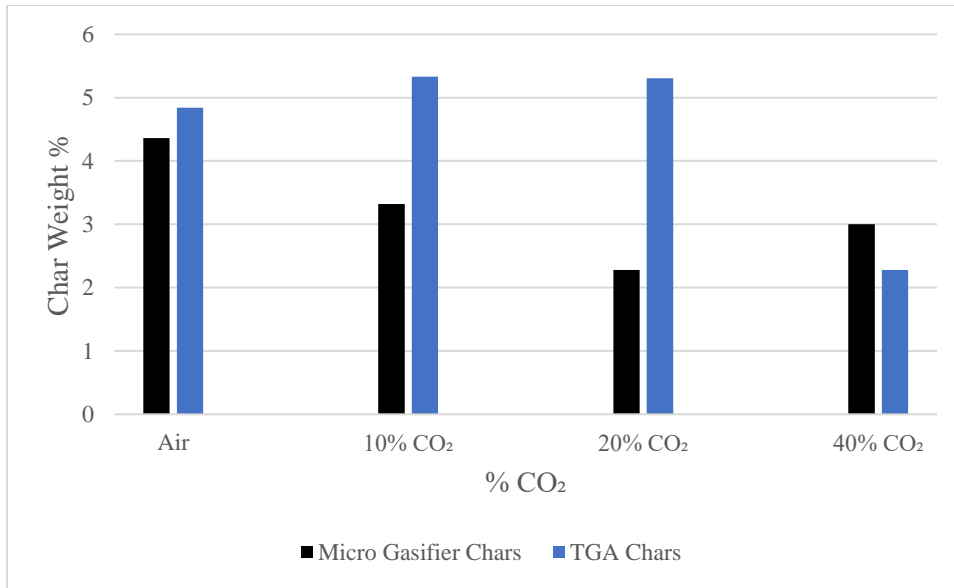


Figure 3-31: Comparison of final char masses in TGA and MG

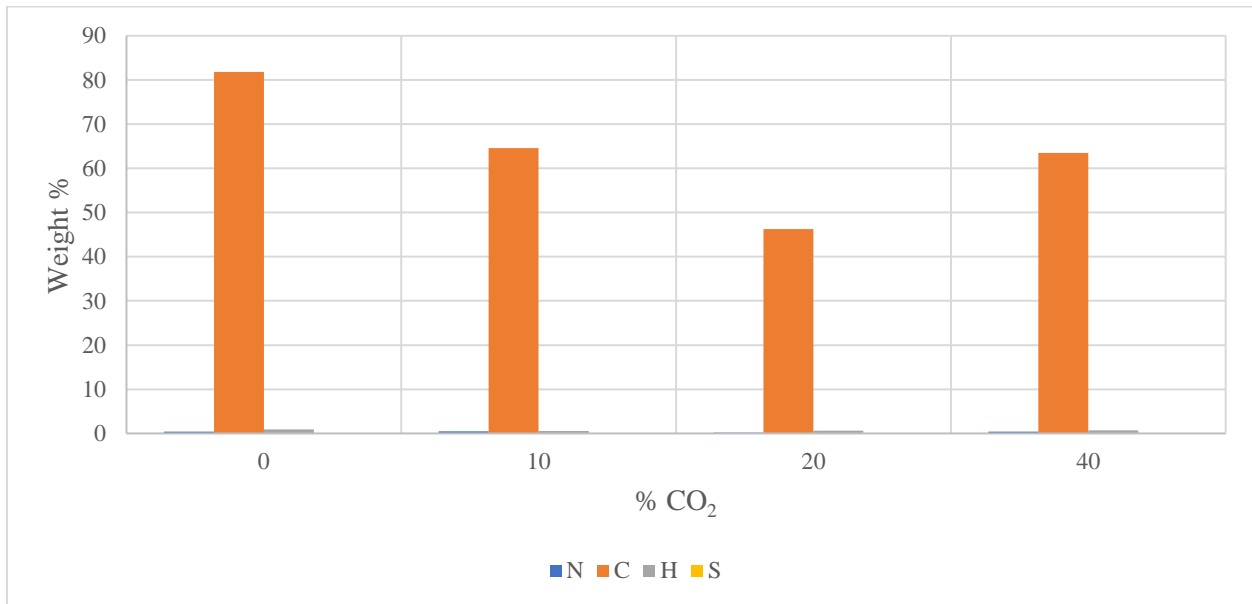


Figure 3-32: Elemental compositions of chars with increasing input flow of CO₂

3.3.6 Influence of CO₂ in Fixed Bed Micro Gasifier

Another carbon balance was done for the MG to evaluate the overall carbon conversion, and understand the breakdown of the gas, tar and char products. For a 10-gram run, 6.788 grams of carbon would theoretically be placed in the fixed bed reactor. The CO₂ that was injected into the

system for certain runs was accounted for when calculating the output of CO₂. The gas flowrates were extrapolated over 5 minutes of assumed production and summed. Then the flows were converted into moles and mass of carbon. Elemental analysis was done all with of the chars, therefore the difference would be the remaining carbon found in the tars/liquid portion. Table 3-14 outlines the respective carbon weight preents for each product. While increases in CO₂ lowered the carbon conversion of char, the gas conversion increased by 4 carbon wt% and the tar decreased by 2 carbon wt%. The injection of CO₂ was not beneficial in the updraft bed design with an equivalence ratio of 0.2. However, lower air flow (ER 0.2) had a very similar gas, tar and char carbon conversions to the higher ER.

Table 3-14: Carbon balance of MG runs with ER 0.2

Runs	Carbon Weight (g)			Weight %		
	Gas	Char	Tar*	Gas	Char	Tar
Air	1.70	0.357	4.73	25.1	5.3	69.7
10% CO ₂	2.18	0.215	5.02	29.4	2.9	67.7
20% CO ₂	2.50	0.106	5.59	30.5	1.3	68.2
40% CO ₂	4.87	0.191	5.47	46.2	1.8	52.0

*By difference

Figure 3-33 shows the energy of the produced syngas (CO and H₂) at all temperatures recorded. The addition of CO₂ as a co-reactant increased the overall energy densities of the output syngas at nearly every temperature. This is attributed to a higher production of CO as seen with 10, 20 and 40% CO₂ after 400°C. The increasing trend seen in Figure 3-33 can almost be directly compared to Figure 3-26, with the evolution of CO gas increasing over temperature with a very similar curve. Therefore, the energy density of the syngas for CO₂ assisted air gasification at equivalence ratios of 0.2 and 0.3 is closely tied with the production of CO. However, there was less production of H₂ gas seen with an air to fuel ratio of 0.3, due to the higher flows of injected CO₂, and therefore the higher degree of the reverse water gas shift reaction. The total energy of the combined CO and H₂ streams was calculated and presented in Table 3-15. The highest energy densities were found to be with CO₂ injections, with 10 and 40 vol% being the highest at 16.7 and 16.6 kJ respectively.

Table 3-15: Total energy of syngas (CO and H₂) ER 0.2

Air	10% CO ₂	20% CO ₂	40% CO ₂
Energy (kJ)			
10.8	16.7	15.6	16.6

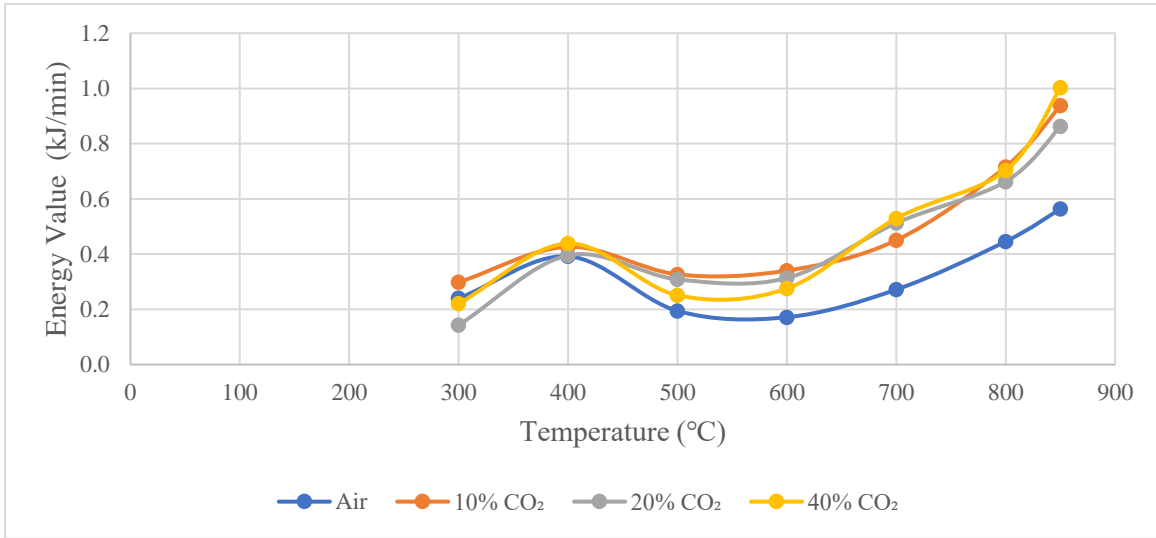


Figure 3-33: Combined energy of syngas at different temperature with increasing input flow of CO₂

Figure 3-34 shows the molar ratio of hydrogen and carbon monoxide (H₂/CO) in the syngas. The CO₂ injected streams again had lower hydrogen carbon monoxide ratio's, especially at the higher temperatures due to the higher production of CO. All the H₂/CO ratios are lower with the ER 0.2 runs than the ER 0.3. However, at 600°C there is a spike in the ratio for 40% CO₂, this is believed to be an error with low CO production compared to the other CO₂ injection runs.

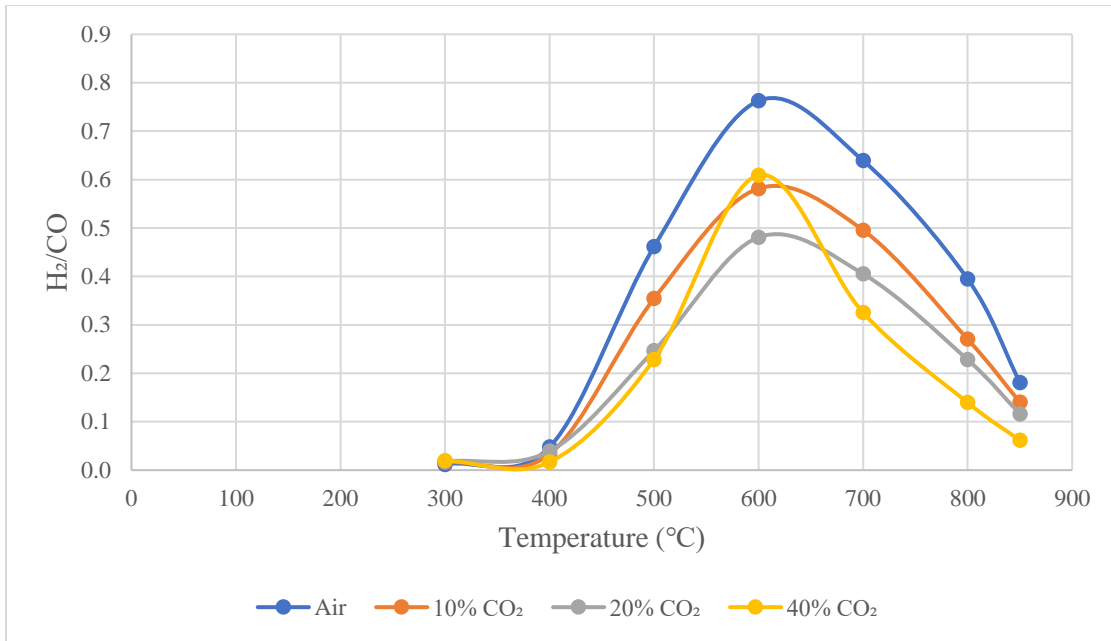


Figure 3-34: Changes in molar hydrogen and carbon monoxide ratio of syngas

4 Conclusions and Recommendations

4.1 Conclusions

The shift to a circular economy is slow but developing alongside the growing alarm of GHG emissions and inefficient waste disposal. Landfilling and direct incineration of mixed plastics for energy recovery are not renewable nor viable long-term solutions for managing these waste materials. This has translated to a need for new sustainable technologies to displace fossil fuel feedstocks for mainstream chemical synthesis and energy production. Gasification is an attractive technology that could be employed locally to convert non-recycled plastic wastes into valuable products. This could be done in stride with carbon dioxide utilization and therefore CO₂ emission displacement. Ultimately, the research and development of this technology could justify the implementation of carbon capture and storage technologies at larger scales. For example, it could be used in conjunction with onsite flue gas carbon capture systems or even Direct Air Capture (DAC) systems which capture CO₂ directly from the atmosphere.

The main objective of this thesis was to investigate CO₂ assisted co-gasification of HDPE and Douglas fir in a bench scale updraft micro-gasifier and a TGA. The influence of CO₂ on the decomposition of mixed HDPE and Douglas fir was highlighted with the TGA, and possible behaviours were considered. An updraft micro-gasifier was built for co-gasifying the mixed feed at a maximum temperature 850°C. Tests were repeated with a TGA to compare the behaviours identified with the mass loss curves with the tar, char, and gas products from the gasifier. Decomposition temperature phases illustrated in the TGA were linked to gas evolution to further explain the influences of CO₂ on the well-known air gasification mechanism.

The injection of 10 and 20% CO₂ in air gasification with an air to fuel ratio of 0.3 was found to improve carbon conversion from the tar to the gas phase by 20 and 28 carbon wt% respectively, with a peak H₂/CO ratio of 0.7 at 600°C. By increasing the CO₂ fraction in the feed gas to 40 vol% injected CO₂ with an ER of 0.3, there were clear changes in the gasification behaviour, resulting in a net consumption rate of CO₂ at a rate of close to 50 ml/min. In comparison, under just air, there is a net production rate of CO₂ of 50 ml/min. The net consumption of CO₂ was demonstrated in the gasifier at temperatures ranging from 280-400°C, and 245-520°C where the

synergistic effects have been observed. This was also discussed with respect to changes in the evolution of H₂, CH₄, CO and other hydrocarbons.

CO₂ assisted air gasification could be designed to possibly operate auto thermally or with some energy input to support the endothermic dry reforming and char gasification reactions promoted by the presence of injected CO₂. The inclusion of CO₂ in the air gasification process illustrated its utility in controlling the H₂/CO ratio of the syngas. This can be advantageous as it provides flexibility with an in-situ method for controlling the main syngas constituents, which strongly influence the applicability of the syngas. In addition, increased energy densities were observed with higher volume injections of CO₂, especially at higher temperature where CO production was enhanced. The highest achieved total energy flows were found with the highest injections of CO₂ for both equivalence ratios and at 10% CO₂ for ER 0.2.

Due to the limitations of fixed beds with gasifying plastics, ER 0.2 injected runs showed lower gas carbon conversion with injected CO₂. ER's of 0.3 or higher are generally recommended for mixed plastic gasification however there have been some reported investigations where lower ER's were more effective for syngas production [64]. Investigations with fluidized beds would be ideal for future work with mixed plastics.

4.2 Recommendations

To improve upon this work, CO₂ assisted co-gasification of plastics in a fluidized bed design would be very beneficial to address the limitations of fixed beds with the tendency of plastics forming tars. Also, further testing of air and CO₂ gasification in the TGA, exploring other mixtures of HDPE and types of feedstock/plastics would be beneficial. With the evidence that CO₂ can reduce the formation of tars and improve biochar properties, it would be relevant to investigate other avenues where carbon dioxide utilization can be promoted. Also, some repetitions of data to enable a more in depth analysis of the error, given the variability of biomass properties would also be beneficial for this work.

The current literature on CO₂ assisted gasification is growing because of the technology's flexibility in addressing multiple prominent environmental issues. It could be very beneficial to explore the possibilities of carbon dioxide utilization with gasification. However, current explanations of the mechanisms of these mixed wastes with different mixed co-reactants are not fully understood. The literature has several different theories for the synergies seen with co-gasified mixed feedstocks. In addition, the combinations of co-reactants are an avenue that could offer a lot of promise. Studies investigating autothermal gasification with injected or possibly recycled carbon dioxide is needed. The optimal combinations of different gasifying agents with mixed waste feedstocks need to be explored. Specifically, that of CO₂, air and O₂ with different mixed nonrecycled plastic and biomass wastes.

References

- [1] US EPA, “Plastics: Material-Specific Data,” 2020.
- [2] ECCC, “Greenhouse Gas Emissions- CANADIAN ENVIRONMENTAL SUSTAINABILITY INDICATORS,” *Encyclopedia of Soils in the Environment*, vol. 4, 2020.
- [3] F. A. Rahman *et al.*, “Pollution to solution: Capture and sequestration of carbon dioxide (CO₂) and its utilization as a renewable energy source for a sustainable future,” *Renewable and Sustainable Energy Reviews*, vol. 71. 2017. doi: 10.1016/j.rser.2017.01.011.
- [4] A. M. Parvez, M. T. Afzal, T. G. Victor Hebb, and M. Schmid, “Utilization of CO₂ in thermochemical conversion of biomass for enhanced product properties: A review,” *Journal of CO₂ Utilization*, vol. 40, p. 101217, Sep. 2020, doi: 10.1016/j.jcou.2020.101217.
- [5] Environment and Climate Change Canada, *Economic study of the Canadian plastic industry, markets and waste: summary report to Environment and Climate Change Canada*. 2019.
- [6] Canadian Council of Ministers of the Environment (CCME), “CANADA-WIDE ACTION PLAN ON ZERO PLASTIC WASTE Phase 2,” 2018. Accessed: Jul. 19, 2022. [Online]. Available: https://ccme.ca/en/res/ccmephase2actionplan_en-external-secured.pdf
- [7] F. T. Zangeneh, S. Sahebdehfar, and M. T. Ravanchi, “Conversion of carbon dioxide to valuable petrochemicals: An approach to clean development mechanism,” *Journal of Natural Gas Chemistry*, vol. 20, no. 3, pp. 219–231, May 2011, doi: 10.1016/S1003-9953(10)60191-0.
- [8] J. J. Klemeš, Y. Van Fan, R. R. Tan, and P. Jiang, “Minimising the present and future plastic waste, energy and environmental footprints related to COVID-19,” *Renewable and Sustainable Energy Reviews*, vol. 127, 2020, doi: 10.1016/j.rser.2020.109883.
- [9] A. Ramos, E. Monteiro, V. Silva, and A. Rouboa, “Co-gasification and recent developments on waste-to-energy conversion: A review,” *Renewable and Sustainable Energy Reviews*, vol. 81, pp. 380–398, Jan. 2018, doi: 10.1016/j.rser.2017.07.025.
- [10] K. G. Burra, P. Chandna, and A. K. Gupta, “Thermochemical Solutions for CO₂ Utilization to Fuels and Value-Added Products,” in *Green Energy and Technology*, 2021, pp. 59–89. doi: 10.1007/978-981-15-5667-8_4.
- [11] G. Lopez, M. Artetxe, M. Amutio, J. Alvarez, J. Bilbao, and M. Olazar, “Recent advances in the gasification of waste plastics. A critical overview,” *Renewable and Sustainable Energy Reviews*, vol. 82, pp. 576–596, Feb. 2018, doi: 10.1016/j.rser.2017.09.032.
- [12] J. A. Ruiz, M. C. Juárez, M. P. Morales, P. Muñoz, and M. A. Mendivil, “Biomass gasification for electricity generation: Review of current technology barriers,” *Renewable and Sustainable Energy Reviews*, vol. 18, pp. 174–183, Feb. 2013, doi: 10.1016/j.rser.2012.10.021.
- [13] F. Pinto, R. André, M. Miranda, D. Neves, F. Varela, and J. Santos, “Effect of gasification agent on co-gasification of rice production wastes mixtures,” *Fuel*, vol. 180, pp. 407–416, Sep. 2016, doi: 10.1016/j.fuel.2016.04.048.

- [14] P. García-Bacaicoa, J. F. Mastral, J. Ceamanos, C. Berrueco, and S. Serrano, "Gasification of biomass/high density polyethylene mixtures in a downdraft gasifier," *Bioresour Technol*, vol. 99, no. 13, 2008, doi: 10.1016/j.biortech.2007.11.003.
- [15] C. Block, A. Ephraim, E. Weiss-Hortala, D. P. Minh, A. Nzihou, and C. Vandecasteele, "Co-pyrogasification of Plastics and Biomass, a Review," *Waste Biomass Valorization*, vol. 10, no. 3, pp. 483–509, Mar. 2019, doi: 10.1007/s12649-018-0219-8.
- [16] E. E. Kwon, S. Kim, and J. Lee, "Pyrolysis of waste feedstocks in CO₂ for effective energy recovery and waste treatment," *Journal of CO₂ Utilization*, vol. 31. 2019. doi: 10.1016/j.jcou.2019.03.015.
- [17] Z. Wang *et al.*, "Synergetic Effect on CO₂-Assisted Co-Gasification of Biomass and Plastics," *J Energy Resour Technol*, vol. 143, no. 3, Mar. 2021, doi: 10.1115/1.4048062.
- [18] S. K. Thengane, A. Gupta, and S. M. Mahajani, "Co-gasification of high ash biomass and high ash coal in downdraft gasifier," *Bioresour Technol*, vol. 273, pp. 159–168, Feb. 2019, doi: 10.1016/j.biortech.2018.11.007.
- [19] J. Li, K. R. G. Burra, Z. Wang, X. Liu, and A. K. Gupta, "Co-gasification of high-density polyethylene and pretreated pine wood," *Appl Energy*, vol. 285, 2021, doi: 10.1016/j.apenergy.2021.116472.
- [20] F. Pinto, C. Franco, R. N. André, M. Miranda, I. Gulyurtlu, and I. Cabrita, "Co-gasification study of biomass mixed with plastic wastes," *Fuel*, vol. 81, no. 3, pp. 291–297, Feb. 2002, doi: 10.1016/S0016-2361(01)00164-8.
- [21] M. Shahbaz, T. Al-Ansari, M. Inayat, S. A. Sulaiman, P. Parthasarathy, and G. McKay, "A critical review on the influence of process parameters in catalytic co-gasification: Current performance and challenges for a future prospectus," *Renewable and Sustainable Energy Reviews*, vol. 134. 2020. doi: 10.1016/j.rser.2020.110382.
- [22] M. Policella, Z. Wang, K. G. Burra, and A. K. Gupta, "Characteristics of syngas from pyrolysis and CO₂-assisted gasification of waste tires," *Appl Energy*, vol. 254, 2019, doi: 10.1016/j.apenergy.2019.113678.
- [23] T. Hanaoka, S. Hiasa, and Y. Edashige, "Syngas production by CO₂/O₂ gasification of aquatic biomass," *Fuel Processing Technology*, vol. 116, 2013, doi: 10.1016/j.fuproc.2013.03.049.
- [24] N. Sadhwani, S. Adhikari, and M. R. Eden, "Biomass Gasification Using Carbon Dioxide: Effect of Temperature, CO₂/C Ratio, and the Study of Reactions Influencing the Process," *Ind Eng Chem Res*, vol. 55, no. 10, 2016, doi: 10.1021/acs.iecr.5b04000.
- [25] H. C. Butterman and M. J. Castaldi, "Influence of CO₂ injection on biomass gasification," in *Industrial and Engineering Chemistry Research*, 2007, vol. 46, no. 26. doi: 10.1021/ie071160n.
- [26] K. Burra and A. K. Gupta, "Kinetics of Co-gasification of biomass and plastic wastes in CO₂," in *IT3/HWC 2018 - 36th International Conference on Thermal Treatment Technologies and Hazardous Waste Combustors*, 2018, vol. 2018-March.
- [27] X. Zheng, Z. Ying, B. Wang, and C. Chen, "Hydrogen and syngas production from municipal solid waste (MSW) gasification via reusing CO₂," *Appl Therm Eng*, vol. 144, pp. 242–247, Nov. 2018, doi: 10.1016/j.applthermaleng.2018.08.058.
- [28] P. Singh, N. Déparrois, K. G. Burra, S. Bhattacharya, and A. K. Gupta, "Energy recovery from cross-linked polyethylene wastes using pyrolysis and CO₂ assisted gasification," *Appl Energy*, vol. 254, 2019, doi: 10.1016/j.apenergy.2019.113722.

- [29] Y. Shen, X. Li, Z. Yao, X. Cui, and C. H. Wang, "CO₂ gasification of woody biomass: Experimental study from a lab-scale reactor to a small-scale autothermal gasifier," *Energy*, vol. 170, 2019, doi: 10.1016/j.energy.2018.12.176.
- [30] S. Farzad, M. A. Mandegari, and J. F. Görgens, "A critical review on biomass gasification, co-gasification, and their environmental assessments," *Biofuel Research Journal*, vol. 3, no. 4, pp. 483–495, Dec. 2016, doi: 10.18331/BRJ2016.3.4.3.
- [31] S. Zhang, S. Zhu, H. Zhang, X. Liu, and Y. Xiong, "High quality H₂-rich syngas production from pyrolysis-gasification of biomass and plastic wastes by Ni–Fe@Nanofibers/Porous carbon catalyst," *Int J Hydrogen Energy*, vol. 44, no. 48, pp. 26193–26203, Oct. 2019, doi: 10.1016/j.ijhydene.2019.08.105.
- [32] C. Guizani, F. J. Escudero Sanz, and S. Salvador, "Effects of CO₂ on biomass fast pyrolysis: Reaction rate, gas yields and char reactive properties," *Fuel*, vol. 116, 2014, doi: 10.1016/j.fuel.2013.07.101.
- [33] S. Portofino *et al.*, "Optimizing H₂ production from waste tires via combined steam gasification and catalytic reforming," *Energy and Fuels*, vol. 25, no. 5, 2011, doi: 10.1021/ef200072c.
- [34] S. Portofino *et al.*, "Optimizing H₂ production from waste tires via combined steam gasification and catalytic reforming," *Energy and Fuels*, vol. 25, no. 5, 2011, doi: 10.1021/ef200072c.
- [35] A. K. Panda, R. K. Singh, and D. K. Mishra, "Thermolysis of waste plastics to liquid fuel. A suitable method for plastic waste management and manufacture of value added products-A world prospective," *Renewable and Sustainable Energy Reviews*, vol. 14, no. 1. 2010. doi: 10.1016/j.rser.2009.07.005.
- [36] J. S. Tumuluru, S. Sokhansanj, C. T. Wright, R. D. Boardman, and N. A. Yancey, "A review on biomass classification and composition, co-firing issues and pretreatment methods," in *American Society of Agricultural and Biological Engineers Annual International Meeting 2011, ASABE 2011*, 2011, vol. 3. doi: 10.13031/2013.37191.
- [37] I. G. Harouna *et al.*, "Experimental study of the co-gasification of wood and polyethylene in a two-stage gasifier," *Energy Sci Eng*, vol. 8, no. 7, pp. 2322–2334, Jul. 2020, doi: 10.1002/ese3.667.
- [38] D. v. Suriapparao, D. K. Ojha, T. Ray, and R. Vinu, "Kinetic analysis of co-pyrolysis of cellulose and polypropylene," *J Therm Anal Calorim*, vol. 117, no. 3, 2014, doi: 10.1007/s10973-014-3866-4.
- [39] K. G. Burra and A. K. Gupta, "Synergistic effects in steam gasification of combined biomass and plastic waste mixtures," *Appl Energy*, vol. 211, 2018, doi: 10.1016/j.apenergy.2017.10.130.
- [40] T. Yang, K. Hu, R. Li, Y. Sun, and X. Kai, "Cogasification of typical plastics and rice straw with carbon dioxide," *Environ Prog Sustain Energy*, vol. 34, no. 3, 2015, doi: 10.1002/ep.12041.
- [41] S. Wang, G. Dai, H. Yang, and Z. Luo, "Lignocellulosic biomass pyrolysis mechanism: A state-of-the-art review," *Progress in Energy and Combustion Science*, vol. 62. 2017. doi: 10.1016/j.peccs.2017.05.004.
- [42] L. Burhenne, J. Messmer, T. Aicher, and M.-P. Laborie, "The effect of the biomass components lignin, cellulose and hemicellulose on TGA and fixed bed pyrolysis," *J Anal Appl Pyrolysis*, vol. 101, pp. 177–184, May 2013, doi: 10.1016/j.jaap.2013.01.012.

- [43] V. Wilk and H. Hofbauer, "Co-gasification of plastics and biomass in a dual fluidized-bed steam gasifier: Possible interactions of fuels," *Energy and Fuels*, vol. 27, no. 6, 2013, doi: 10.1021/ef400349k.
- [44] A. Meng, S. Chen, Y. Long, H. Zhou, Y. Zhang, and Q. Li, "Pyrolysis and gasification of typical components in wastes with macro-TGA," *Waste Management*, vol. 46, 2015, doi: 10.1016/j.wasman.2015.08.025.
- [45] Canada's Natural Forest Inventory, "National Forest Inventory. Standard reports," 2021. Accessed: Jul. 19, 2022. [Online]. Available: https://nfi.nfis.org/resources/general/summaries/t1/en/CA/html/CA_T16_LSAGE20_VOL_en.html
- [46] P. Basu, *Biomass Gasification, Pyrolysis and Torrefaction: Practical Design and Theory*. 2013. doi: 10.1016/C2011-0-07564-6.
- [47] G. Ruoppolo, P. Ammendola, R. Chirone, and F. Miccio, "H₂-rich syngas production by fluidized bed gasification of biomass and plastic fuel," *Waste Management*, vol. 32, no. 4, 2012, doi: 10.1016/j.wasman.2011.12.004.
- [48] F. Miccio, B. Piriou, G. Ruoppolo, and R. Chirone, "Biomass gasification in a catalytic fluidized reactor with beds of different materials," *Chemical Engineering Journal*, vol. 154, no. 1–3, 2009, doi: 10.1016/j.cej.2009.04.002.
- [49] S. A. Salaudeen, P. Arku, and A. Dutta, "Gasification of plastic solid waste and competitive technologies," in *Plastics to Energy: Fuel, Chemicals, and Sustainability Implications*, 2018. doi: 10.1016/B978-0-12-813140-4.00010-8.
- [50] J. G. Speight, *Gasification of Unconventional Feedstocks*. 2014. doi: 10.1016/C2013-0-14152-9.
- [51] J. Alvarez *et al.*, "Hydrogen production from biomass and plastic mixtures by pyrolysis-gasification," *Int J Hydrogen Energy*, vol. 39, no. 21, 2014, doi: 10.1016/j.ijhydene.2014.04.189.
- [52] N. Abdoulmoumine, S. Adhikari, A. Kulkarni, and S. Chattanathan, "A review on biomass gasification syngas cleanup," *Applied Energy*, vol. 155, 2015. doi: 10.1016/j.apenergy.2015.05.095.
- [53] U. Arena, "Process and technological aspects of municipal solid waste gasification. A review," *Waste Management*, vol. 32, no. 4, 2012, doi: 10.1016/j.wasman.2011.09.025.
- [54] S. K. Sansaniwal, K. Pal, M. A. Rosen, and S. K. Tyagi, "Recent advances in the development of biomass gasification technology: A comprehensive review," *Renewable and Sustainable Energy Reviews*, vol. 72, pp. 363–384, May 2017, doi: 10.1016/j.rser.2017.01.038.
- [55] V. I. Sharypov *et al.*, "Co-pyrolysis of wood biomass and synthetic polymer mixtures. Part I: Influence of experimental conditions on the evolution of solids, liquids and gases," *J Anal Appl Pyrolysis*, vol. 64, no. 1, 2002, doi: 10.1016/S0165-2370(01)00167-X.
- [56] I. I. Ahmed, N. Nipattummakul, and A. K. Gupta, "Characteristics of syngas from co-gasification of polyethylene and woodchips," *Appl Energy*, vol. 88, no. 1, 2011, doi: 10.1016/j.apenergy.2010.07.007.
- [57] R. A. Moghadam, S. Yusup, Y. Uemura, B. L. F. Chin, H. L. Lam, and A. Al Shoabi, "Syngas production from palm kernel shell and polyethylene waste blend in fluidized bed catalytic steam co-gasification process," *Energy*, vol. 75, 2014, doi: 10.1016/j.energy.2014.04.062.

- [58] L. Zaccariello and M. L. Mastellone, "Fluidized-bed gasification of plastic waste, wood, and their blends with coal," *Energies (Basel)*, vol. 8, no. 8, 2015, doi: 10.3390/en8088052.
- [59] F. Pinto *et al.*, "Effect of experimental conditions on co-gasification of coal, biomass and plastics wastes with air/steam mixtures in a fluidized bed system," in *Fuel*, 2003, vol. 82, no. 15–17. doi: 10.1016/S0016-2361(03)00160-1.
- [60] G. Lopez, A. Erkiaga, M. Amutio, J. Bilbao, and M. Olazar, "Effect of polyethylene co-feeding in the steam gasification of biomass in a conical spouted bed reactor," *Fuel*, vol. 153, 2015, doi: 10.1016/j.fuel.2015.03.006.
- [61] R. Roncancio and J. P. Gore, "CO₂ char gasification: A systematic review from 2014 to 2020," *Energy Conversion and Management: X*, vol. 10, p. 100060, Jun. 2021, doi: 10.1016/j.ecmx.2020.100060.
- [62] J. Lee, D. Choi, Y. F. Tsang, J.-I. Oh, and E. E. Kwon, "Employing CO₂ as reaction medium for in-situ suppression of the formation of benzene derivatives and polycyclic aromatic hydrocarbons during pyrolysis of simulated municipal solid waste," *Environmental Pollution*, vol. 224, pp. 476–483, May 2017, doi: 10.1016/j.envpol.2017.02.028.
- [63] M. Pohořelý, M. Jeremiáš, K. Svoboda, P. Kameníková, S. Skoblia, and Z. Beňo, "CO₂ as moderator for biomass gasification," *Fuel*, vol. 117, no. PART A, 2014, doi: 10.1016/j.fuel.2013.09.068.
- [64] N. Couto, V. Silva, and A. Rouboa, "Municipal solid waste gasification in semi-industrial conditions using air-CO₂ mixtures," *Energy*, vol. 104, 2016, doi: 10.1016/j.energy.2016.03.088.
- [65] K. G. Burra and A. K. Gupta, "Kinetics of synergistic effects in co-pyrolysis of biomass with plastic wastes," *Appl Energy*, vol. 220, 2018, doi: 10.1016/j.apenergy.2018.03.117.
- [66] Y. Lin, X. Ma, Z. Yu, and Y. Cao, "Investigation on thermochemical behavior of co-pyrolysis between oil-palm solid wastes and paper sludge," *Bioresour Technol*, vol. 166, 2014, doi: 10.1016/j.biortech.2014.05.101.
- [67] P. Lahijani, Z. A. Zainal, A. R. Mohamed, and M. Mohammadi, "Co-gasification of tire and biomass for enhancement of tire-char reactivity in CO₂ gasification process," *Bioresour Technol*, vol. 138, 2013, doi: 10.1016/j.biortech.2013.03.179.
- [68] E. Alper and O. Yuksel Orhan, "CO₂ utilization: Developments in conversion processes," *Petroleum*, vol. 3, no. 1, pp. 109–126, Mar. 2017, doi: 10.1016/j.petlm.2016.11.003.
- [69] J. Luo *et al.*, "Leveraging CO₂ to directionally control the H₂/CO ratio in continuous microwave pyrolysis/gasification of waste plastics: Quantitative analysis of CO₂ and density functional theory calculations of regulation mechanism," *Chemical Engineering Journal*, vol. 435, 2022, doi: 10.1016/j.cej.2022.134794.
- [70] J. F. Saldarriaga, R. Aguado, A. Pablos, M. Amutio, M. Olazar, and J. Bilbao, "Fast characterization of biomass fuels by thermogravimetric analysis (TGA)," *Fuel*, vol. 140, 2015, doi: 10.1016/j.fuel.2014.10.024.
- [71] S. Link, S. Arvelakis, M. Hupa, P. Yrjas, I. Külaots, and A. Paist, "Reactivity of the biomass chars originating from reed, douglas fir, and pine," *Energy and Fuels*, vol. 24, no. 12, 2010, doi: 10.1021/ef100926v.
- [72] I. G. Donskoy, A. N. Kozlov, M. A. Kozlova, M. v. Penzik, and V. A. Shamanskiy, "Thermochemical interaction of wood and polyethylene during co-oxidation in the conditions of thermogravimetric analysis," *Reaction Kinetics, Mechanisms and Catalysis*, vol. 131, no. 2, 2020, doi: 10.1007/s11144-020-01880-y.

5. Appendices

Appendix A: Supplementary Data Tables and Figures

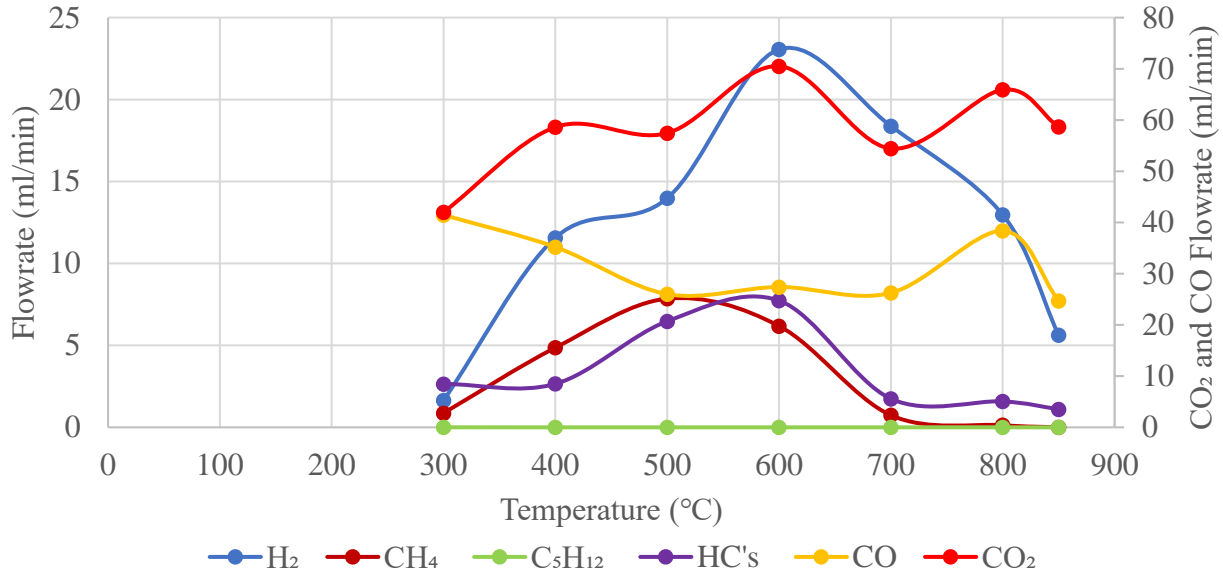


Figure 5-1: Evolution of gases with air (ER 0.3)

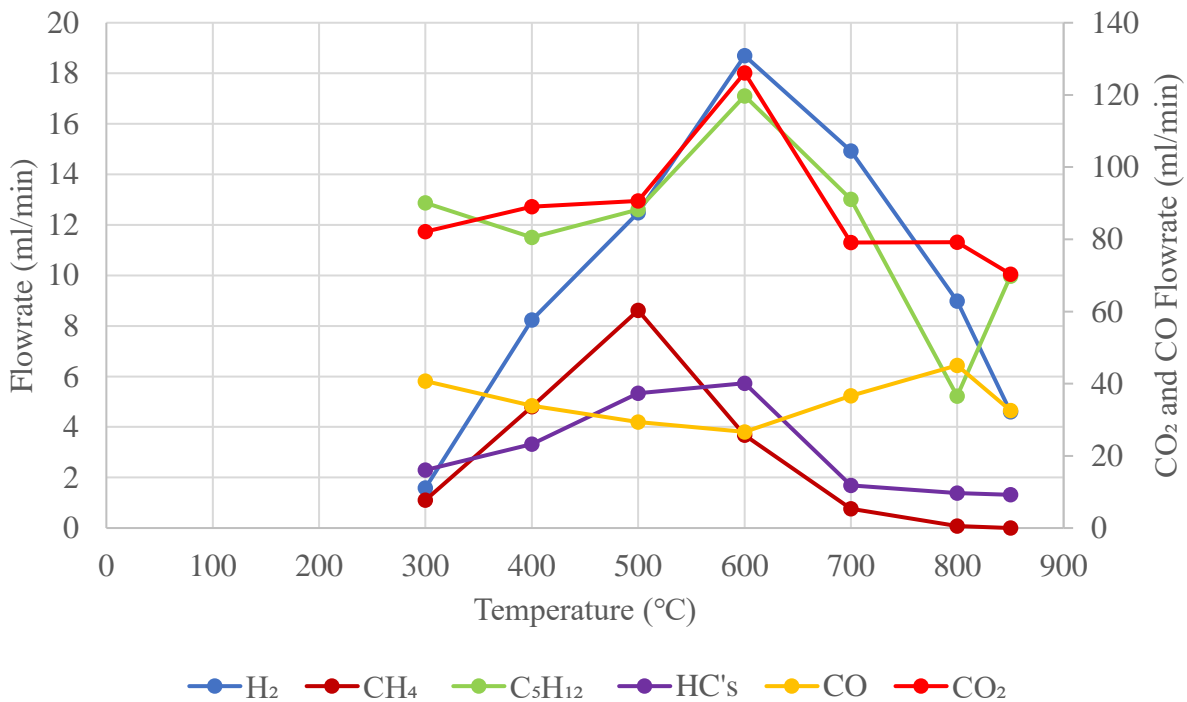


Figure 5-2: Evolution of gases with air and 10% CO₂ (ER 0.3)

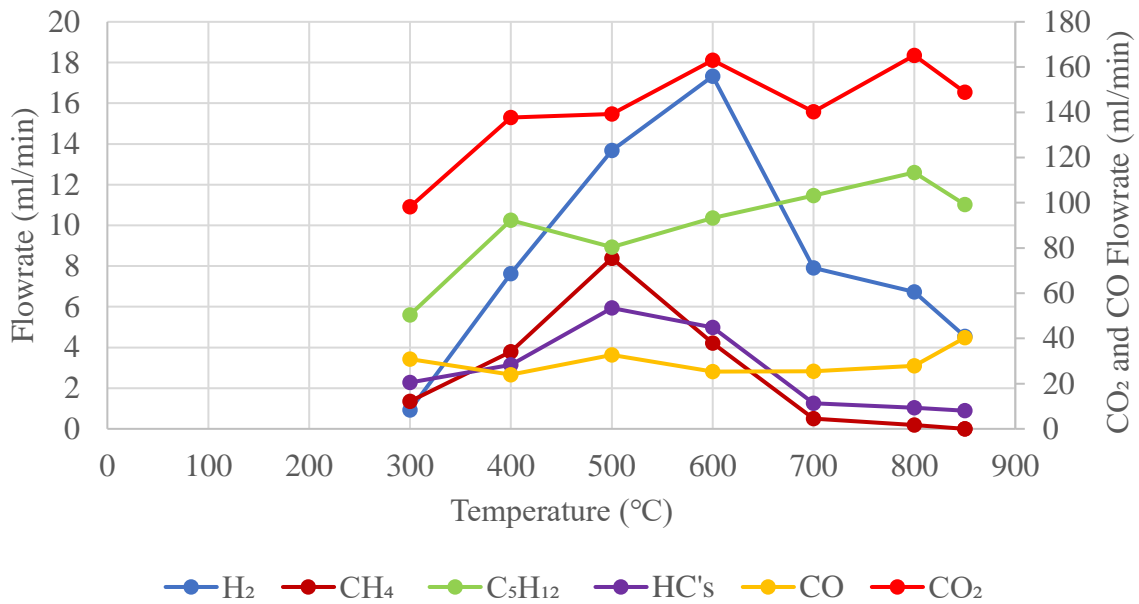


Figure 5-3: Evolution of gases with air and 20% CO₂ (ER 0.3)

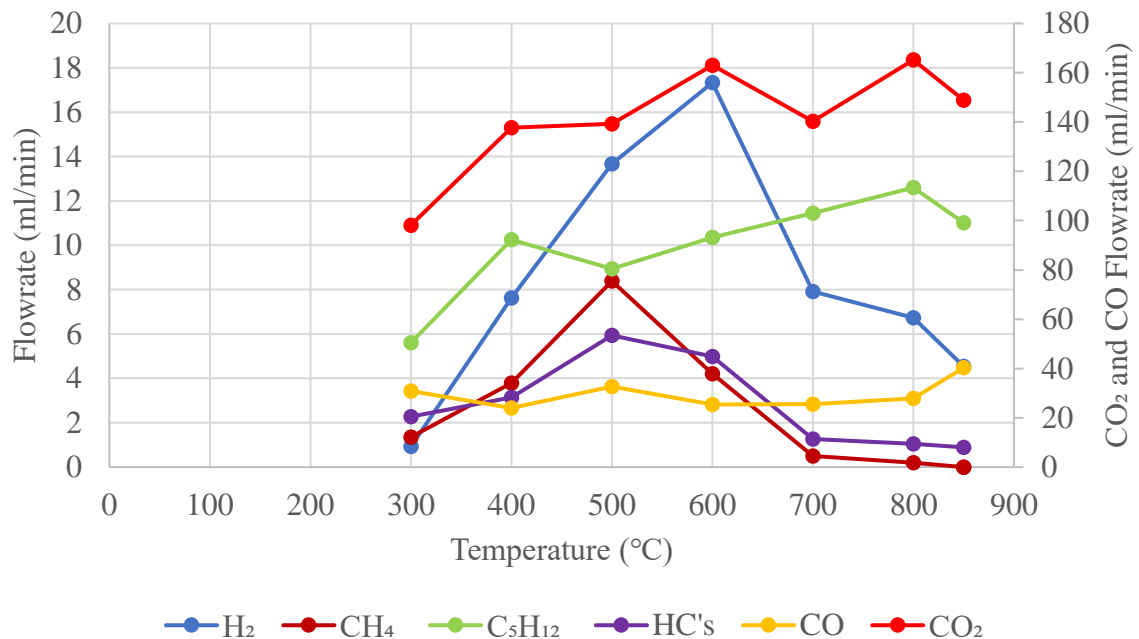


Figure 5-4: Evolution of gases with air and 40% CO₂ (ER 0.3)

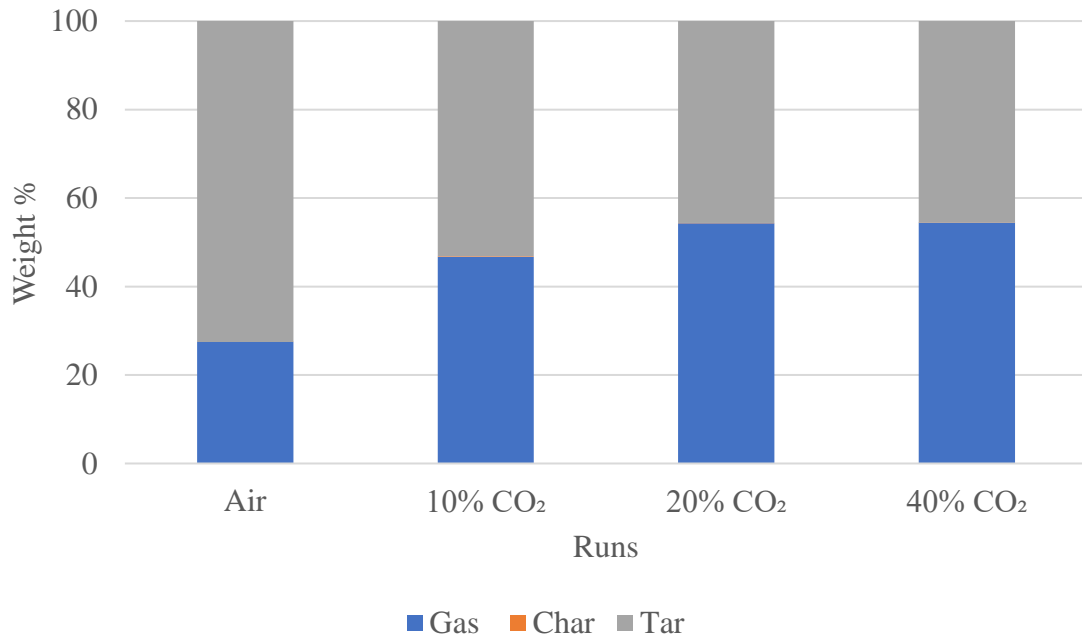


Figure 5-5: ER 0.3 carbon conversion chart with CO₂

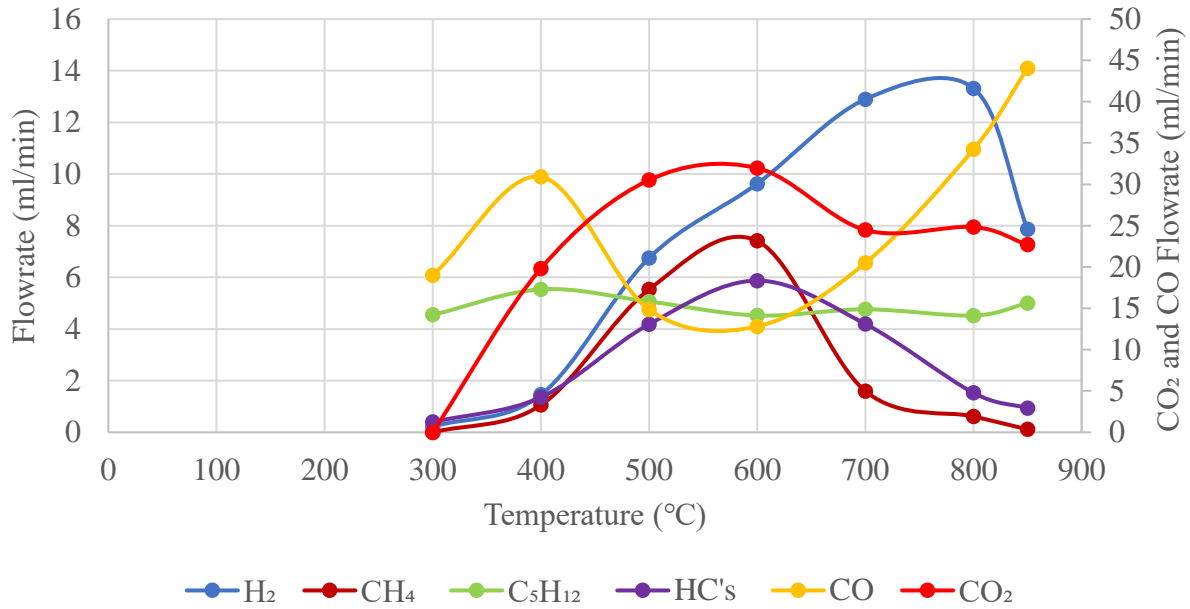


Figure 5-6: Evolution of gases with air (ER 0.2)

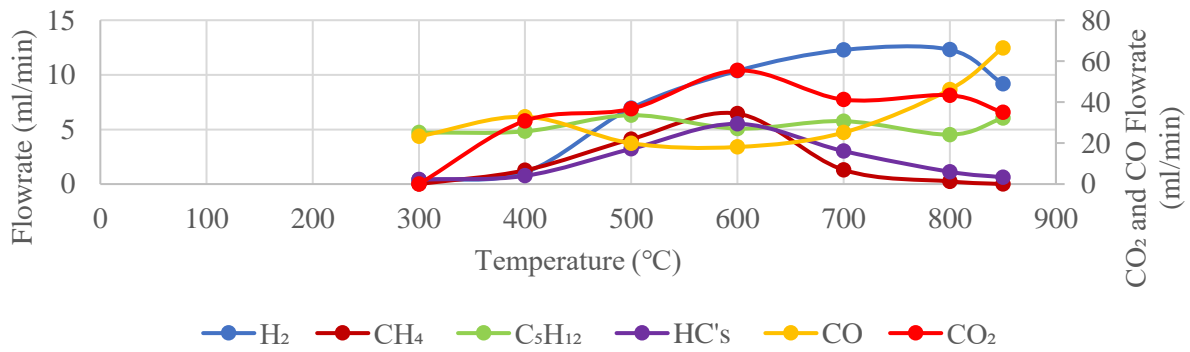


Figure 5-7: Evolution of gases with air and 10% CO₂ (ER 0.2)

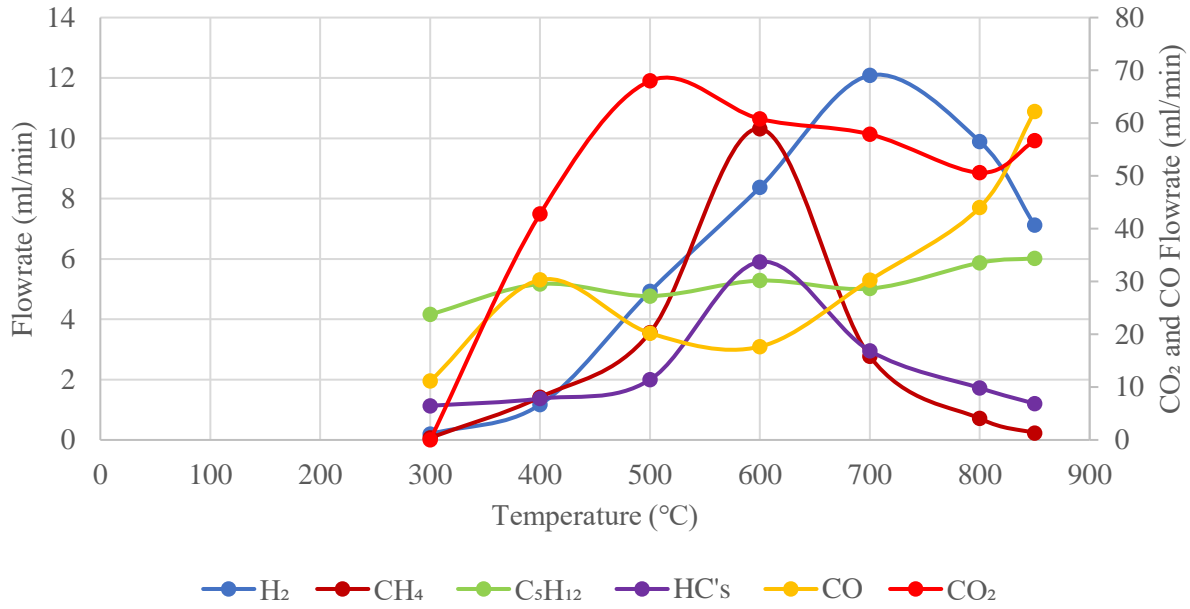


Figure 5-8: Evolution of gases with air and 20% CO₂ (ER 0.2)

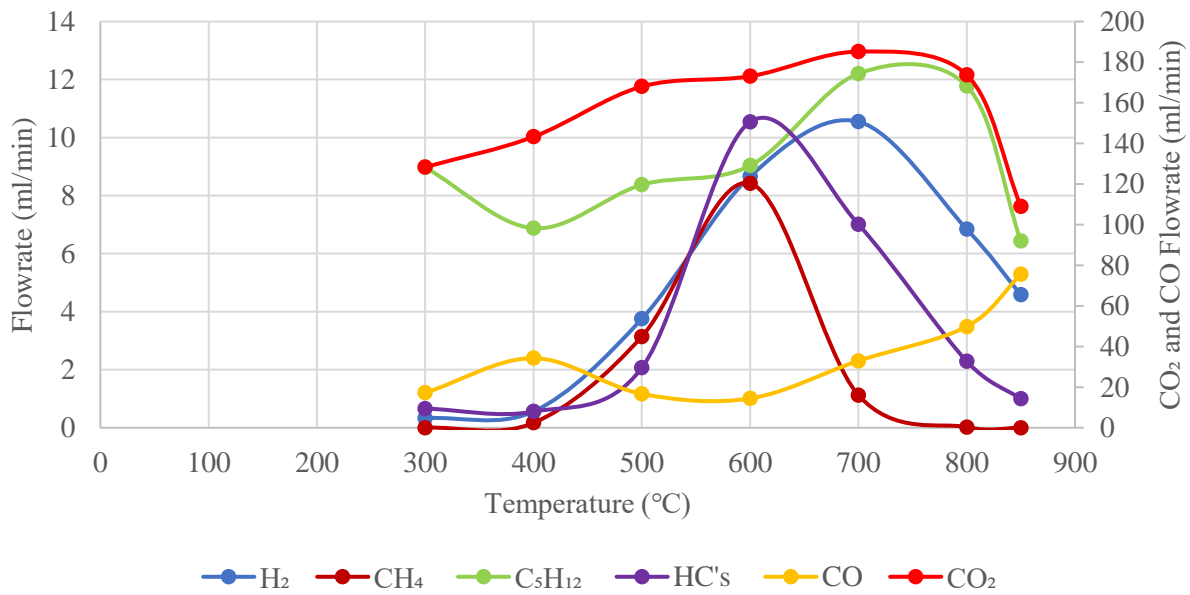


Figure 5-9: Evolution of gases with air and 40% CO₂ (ER 0.2)

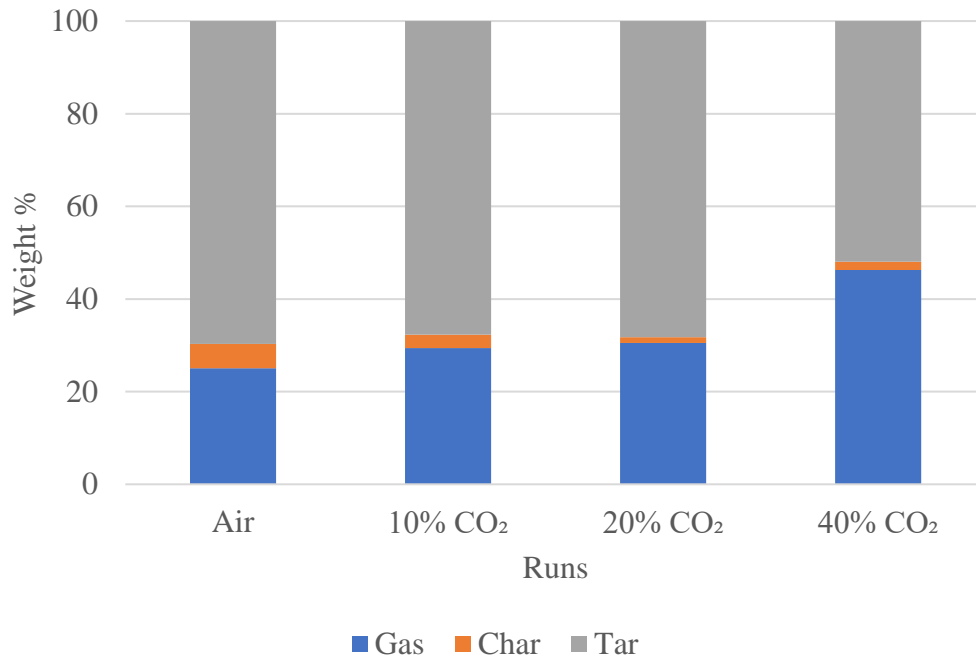


Figure 5-10: ER 0.2 carbon conversion chart with CO₂

Curriculum Vitae

Name: Joshua Cullen

Post-secondary Education and Degrees: Western University
London, Ontario, Canada
2016-2020 B.E.S.c

Honours and Awards: Dean's Honour List
2020

Related Work Experience Teaching Assistant
Western University
2020-2021